Impact of Windfarm Structures on a Region of Freshwater Influence

Thesis submitted in accordance with the requirements of the University of Liverpool for the degree of Doctor in Philosophy by

Daniel Eddon

School of Engineering

University of Liverpool

February 2017

Contents

Notations **xv**

Preface **xvii**

Abstract **xix**

Acknowledgements **xxi**

1 Introduction **1**
1.1 Background 1
1.1.1 Power and Energy 3
1.1.2 Fossil Fuels 5
1.1.3 Climate Change 6
1.1.4 Renewable Energy 8
1.2 Marine Environment and Energy Systems 9
1.2.1 Offshore Wind Farms 10
Wakes 13
1.2.2 Region of Freshwater influence 18
1.3 Project description, Methodology and Objectives 19
1.3.1 Objectives 21
1.4 Thesis Overview 21

2 Literature Review **23**
2.1 Introduction 23
2.2 Hydrodynamics 25
2.3 Turbulence Modelling 26
Mixing Length model 31
Turbulent and Kinetic Energy Models 32
$k-\omega$ model 33
$k-\varepsilon$ model 33
2.4 Models Techniques 34

3 Modelling Method **37**
3.1 POLCOMS-GOTM 38

3.1.1 POLCOMS . . . 41
3.1.2 GOTM . . . 43
3.2 Structure Module . . . 45
Momentum Equations . . . 45
Turbulence impacts . . . 49
3.3 Turbine Representation . . . 51
3.4 Liverpool Bay . . . 54
3.5 Model Set up . . . 57
3.6 Horizontal Turbulence Advection . . . 62
3.6.1 Results . . . 62

4 Impact of the Spatial Averaging Scale in Parameterisation of OWF's in Coastal Ocean Models 67
4.1 Two Spatial Averaging Schemes . . . 67
4.2 Validation of the Structure Model . . . 69
4.3 Comparison of the two methods . . . 76
4.3.1 Yearly time Series . . . 77
4.3.2 Velocity comparison . . . 81
4.3.3 Salinity Comparison . . . 90
4.3.4 Temperature Comparison . . . 95
4.3.5 Conclusions . . . 98

5 Parameterisation of OWF's in POLCOMS Governing Equations: The Influence of Turbulence Sources 101
5.1 Numerical Model Setup . . . 103
5.2 Yearly Time Series at Site A . . . 104
5.2.1 Surface Salinity Comparison . . . 112
5.2.2 Surface Temperature Comparison . . . 115
5.3 Temperature Fronts . . . 119
5.4 Conclusions . . . 121

6 Impacts of OWF's on Liverpool Bay Dynamics 123
6.1 Numerical simulation . . . 123
6.2 Results . . . 124
6.2.1 Yearly Time series comparison . . . 125
6.2.2 Speed and Turbulent Kinetic Energy Comparison . . . 131
6.2.3 Monthly Surface salinity . . . 136
6.2.4 Monthly Surface Temperature . . . 144
6.2.5 Monthly Temperature Fronts . . . 151
6.2.6 Site A comparison . . . 153
6.2.7 Conclusions . . . 158

7 Conclusion 161
7.1 Liverpool Bay Hydrodynamics . . . 161
7.2 Structure Module . . . 164

7.3 Further Work 165

References **169**

Illustrations

List of Figures

1.1 World Consumption (EIA 2013 Report, [26]), Btu $\times 10^{15}$ against year. Black represents the OECD countries and red represents the non-OECD countries. 2
1.2 Electricity Production by type (UK Energy Roadmap update, 2013, [28]) 3
1.3 Population Growth (Holtz, 2011 [37]) 4
1.4 World Electricity generation by fuel type (IEA, 2011 [3]) 6
1.5 CO_2 concentration, (Mackay,2008 [48]) 7
1.6 UK windfarm map, 2012, showing the sites of all windfarms deployed and in development on the UK continental shelf, shown by the light brown line, The Crown estate, [24] 11
1.7 An offshore wind turbine in situ, AnHolt Denmark, www.offshorewind.biz [78] 12
1.8 Picture of air wakes behind wind turbines, Horns Rev windfarm, Denmark. (www.noaanews.noaa.gov, 2011 [53], credit to Vattenfall) . 14
1.9 Offshore wind turbine wake trails, www.americansgeophysicalunion.tumblr.com, [50] 15

2.1 Energy cascade of eddies 28

3.1 3D B-grid arrangement 39
3.2 Example control volume for OWF representation in domain. Blue dots represent turbine structures, blue shading represents impacted cells 52
3.3 Example individual cell representation method. Blue dots represent turbine structures, blue shading represents impacted cells 53
3.4 Map of the United Kingdom, red square highlights Liverpool Bay. . . 55
3.5 Liverpool Bay windfarms, 2008, www.offshorewind.biz, 2015 56
3.6 Domain showing the freshwater input conditions, A) Conwy, B) Clywd, C) Dee, D) Mersey, E) Ribble. 57
3.7 River Dee input forcing for 2008. 58
3.8 River Mersey input forcing for 2008. 58
3.9 River Ribble input forcing for 2008. 59

3.10 Bathymetry domain, Liverpool Bay showing site A (small red cross) and centre of two wind farms, North Hoyle to the left and Burbo Bank in the right represented by the blue squares. 61
3.11 Comparison of u component at Site A, a) Elevation, b) u with Advection, c) u without Advection, d) u difference, $WA - CA$. Plot is the time series taken at the Site A located in Liverpool Bay. 63
3.12 Comparison of v component at Site A, a) Elevation, b) v with Advection, c) v without Advection, d) v difference, $WA - CA$. For plot description see 3.11 64
3.13 Comparison of Turbulent Kinetic Energy component at Site A, a) Elevation, b) TKE with Advection, c) TKE without Advection, d) TKE difference, $WA - CA$ 65

4.1 Salinity comparison; a) 5m below surface b) 10m below surface c) 0.5m above seabed, Site A, Blue is field data and red is the model data. 70
4.2 Temperature comparison; a) 5m below surface b) 10m below surface c) 0.5m above seabed, Site A, Blue is field data and red is the model data. 72
4.3 Density comparison time series; a) 5m below surface b) 10m below surface c) 0.5m above seabed, Site A, Blue is field data and red is the model data. 73
4.4 Density comparison time series, 25 hour filtering process; a) 5m below surface b) 10m below surface c) 0.5m above seabed, Site A, Blue is field data and red is the model data. 74
4.5 Time series of salinity comparison , at site A at different elevations in the water column a) 5m below surface, b) 10m below surface c) 0.5m above seabed. Dark blue is field data and red is model data (F) and light blue is model data (T). 77
4.6 Time series of temperature comparison, see Figure 4.5 for plot details. 78
4.7 Time series of density anomaly (ρ-1000), see Figure 4.5 for plot details. 79
4.8 Time series of density anomaly (ρ-1000) 25 hour filtering, see Figure 4.5 for plot details. 80
4.9 Liverpool Bay Surface u Component(West-East) Plot for March 2008 average, North Hoyle to the left and Burbo Bank to the right represented by blue squares positioned at the OWF centres 82
4.10 Liverpool Bay Surface u Component (West-East) Difference Plot for March 2008 average, North Hoyle to the left and Burbo Bank to the right represented by blue squares positioned at the OWF centres . . 84

4.11 Liverpool Bay Surface v component (North-South) Plot for March 2008 average, North Hoyle to the left and Burbo Bank to the right represented by blue squares positioned at the windfarm centres . . . 86
4.12 Liverpool Bay Surface U Velocity (East-West) Plot for March 2008 average, North Hoyle to the left and Burbo Bank to the right represented by blue squares positioned at the OWF centres 88
4.13 Liverpool Bay speed difference and direction (T-F) showing the change in speed due to the different representation methods. 89
4.14 Liverpool Bay surface Salinity average plots for March 2008, North Hoyle to the left and Burbo Bank to the right represented by blue squares positioned at the OWF centres, Site A is indicated by a blue cross 91
4.15 Liverpool Bay Surface Salinity average difference plots for March 2008, North Hoyle to the left and Burbo Bank to the right represented by blue squares positioned at the OWF centres, Site A is indicated by a blue cross 92
4.16 River Dee Surface Salinity Residual for March 2008, Zoomed in to focus on the river inflow errors 94
4.17 Liverpool Bay average surface temperature plots for March 2008, North Hoyle to the left and Burbo Bank to the right represented by blue squares positioned at the OWF centres, Site A is indicated by a blue cross 96
4.18 Liverpool Bay average surface temperature plots for March 2008, North Hoyle to the left and Burbo Bank to the right represented by blue squares positioned at the OWF centres, Site A is indicated by a blue cross 97

5.1 Salinity (PSU) yearly time series comparison at site A for F (light bule) and M (red) plotted against observational data Blue; A) 5m below sea level, B) 10m below sealevel, C) 0.5m above sea bed 106
5.2 Temperature (°C); see Figure 5.1 for plot details 107
5.3 Density (kg/m^3), calculated using the UNESCO equation of state, (POLCOMS Documentation, [46]); see Figure 5.1 for plot details . . 108
5.4 Locations of the investigation points 109
5.5 Surface tke differences (M-C) on the surface at 5 points within Liverpool Bay 110
5.6 Surface tke differences (F-M) on the surface at 5 points within Liverpool Bay 111

5.7 Surface Salinity difference, F - C. Plotted on a latitude/longitude domain with OWF centres represented with a blue box and site A represented by the red cross 113
5.8 Surface Salinity difference, M - C. See Figure 5.7 for plot details . . . 114
5.9 Temperature impacts due to Momentum and Turbulence model, M - C115
5.10 Temperature impacts due to the Momentum model, F - C. 116
5.11 Salinity TKE impacts for December calculated by F - M, Latitude/-Longitude Domain, Windfarms marked as squares, Site A and B marked as triangles 118
5.12 Temperature TKE impacts, see Figure 5.11 for details 119
5.13 7°C temperature front for December, Latitude/Longitude Domain, OWF's marked as squares 120

6.1 Time series of Salinity difference (PSU) between C and F, ($\Delta PSU = PSU_F - PSU_c$) at site A at different elevations in the water column a) 5m below surface, b) 10m below surface c) 0.5m above seabed. The shaded areas represent March and December which are the time periods used for the monthly averages. 125
6.2 Time series of temperature difference, see Figure 6.1 for caption details126
6.3 25 hour filtered time series difference, Density. See Figure 6.1 for details127
6.4 River Input forcing for 2008 with highlighted March and December . 129
6.7 Surface tke differences (F-C) on the surface at 5 points within Liverpool Bay 135
6.8 Surface Salinity Monthly residual for March, latitude/longitude Domain, OWF's marked as squares 137
6.9 Surface Salinity Differences, latitude/longitude Domain. OWF's marked as squares, March 138
6.10 Surface Salinity Gradient plotted on a Latitude/Longitude domain with OWFs marked as squares. 140
6.11 Surface salinity monthly residual for December, Latitude/Longitude Domain, OWFs marked as squares 142
6.12 Surface salinity residual difference for December, latitude/longitude Domain. OWFs marked as squares 143
6.13 Surface temperature monthly residual for March. Latitude/Longitude Domain, OWF's marked as squares 146
6.14 Surface temperature residual difference for March. Latitude/Longitude Domain. OWF's marked as squares 147

6.15 Surface temperature monthly residual for December.Latitude/Longitude Domain, OWFs marked as squares 149
6.16 Surface temperature residual difference for December. Latitude/Longitude Domain. OWFs marked as squares 150
6.17 7°C temperature front in March. OWFs marked as squares 152
6.18 7°C temperature front line for December, OWF's shown as squares . 153
6.19 Site A, March U component comparison, top panel (A); Elevation, Second Panel (B); Model with turbine F, Third panel (C); Model without Turbines C 154
6.20 Site A, March V component comparison, top panel (A); Elevation, Second Panel (B); Model with turbine F, Third panel (C); Model without Turbines C 155
6.21 Salinity time series at Site A, top panel (A); Elevation, Second Panel (B); Model with turbine F, Third panel (C); Model without Turbines C156
6.22 Temperature time series at Site A, top panel (A); Elevation, Second Panel (B); Model with turbine F, Third panel (C); Model without Turbines C 156
6.23 Density time series at Site A, top panel (A); Elevation, Second Panel (B); Model with turbine, Third panel (C); Model without Turbines . 157

7.1 2015 surface salinity, Liverpool Bay showing site A (small red cross) and centre of four wind farms, represented by the blue squares. from left to right; Rhyl Flats, 25 structures, Gwynt y Mor, 160 structures, North Hoyle, 30 structures, Burbo Bank, 25 structures 166

List of Tables

3.1 Initial POLCOMS parameters applied to all simulation runs. Salinity and temperature apply for spin up month, December 2007 41
3.2 Initial GOTM parameters applied to simulations, Rodi, 1980 [61], Umlauf and Burchard, 2005 [72] 44
3.3 Turbine module parameter input method 51
3.4 Source of boundary conditions and forcing 59

4.1 Sensitivity model set up shows model and parameters for T and F using representation methods discussed in section 3.3. 68
4.2 Offshore wind farm information in Liverpool Bay in 2008 used in this study 70
4.3 Skill Values (Willmott 1981, [76]) for C, M and F simulation runs at site A. U and V represent velocity components. rho5, rho10 and rhoB represent density at 5m below water level, 10m below water level and 0.5m above seabed respectively. T5, T10 and TB represent temperature at 5m below water level, 10m below water level and 0.5m above seabed respectively. S5, S10 and SB represent salinity at 5m below water level, 10m below water level and 0.5m above seabed respectively. 75

5.1 Skill Values (Willmott 1981, [76]) for C, M and F simulation runs at site A. U and V represent velocity components. rho5, rho10 and rhoB represent density at 5m below water level, 10m below water level and 0.5m above seabed respectively. T5, T10 and TB represent temperature at 5m below water level, 10m below water level and 0.5m above seabed respectively. S5, S10 and SB represent salinity at 5m below water level, 10m below water level and 0.5m above seabed respectively. 105

6.1 Yearly average density difference, (F-C) 128
6.2 Average River monthly discharge, ($\bar{x} = \frac{\sum_i x_i}{n}$) 130

Notations

The following notations and abbreviations are found throughout this thesis:

A_D	Drag Area
A_{cell}	Area of influence
$\mathcal{A}$	Horizontal Eddy viscosity
F , G	bed and surface shear stresses
H_d	total water depth
N	Brunt Vaisala frequency
P	Pressure
R	Radius of Earth
V	Volume
d	diameter
f	Coriolis parameter
g	Gravitation constant
h	Reference height
k	Turbulent kinetic energy
n	number of sigma layers
t	time
u, v	Horizontal velocity
w	Vertical velocity
x, y	Horizontal coordinates
z	vertical sigma coordinates
Ω	angular velocity
μ	molecular viscosity
ε	turbulent diffusivity
ρ	Density
ω	dissipation per unit Kinetic Energy
ζ	Elevation above sea level
χ, ϕ	spherical polar coordinates
G^d	Momentum impact
N_s	Number of structures in a cell

P_d	Turbulence impact
x_{cell}	horizontal cell size
t_e, t_s	start and finish time
f_*	reciprocal coriolis
u', v'	velocity fluctuations
l_m	Mixing length

Preface

This thesis is primarily my own work. The sources of other materials are identifed.

Abstract

To date, most offshore wind farms are deployed in coastal regions including both well-mixed regions and other areas where water-column stratification plays an important role such as regions of freshwater influence and seasonally stratified shelf seas. In the UK for example, a number of offshore wind farms have been commissioned and approved in Liverpool Bay, which is a key region of freshwater influence, and approved in regions of the North Sea where the water column can stratify seasonally. While there has been significant work on determining the local environmental impacts of offshore wind farms, in particular when they relate to the structural integrity of the turbines (e.g. scour), there has been far fewer studies focusing on the water column dynamics in complex regions such as regions of freshwater influence, even though they have a significant control on the ecosystem.

This project addresses both issues: assessment of the modelling techniques; and impact of offshore wind farms on the dynamics of regions of freshwater influence. This is achieved via a numerical modelling study in which a new module was developed to simulate the impacts of offshore structures in the Proudman Oceanographic Laboratory Coastal Ocean Modelling System (POLCOMS). The overall model was then applied to a case study in Liverpool Bay, which is a salinity driven, hyper-tidal region of freshwater influence with complex dynamics in the North West of the UK and where an increasing number of offshore windfarms have been deployed since 2003.

This new module is based on a modified drag force approach, which takes

both momentum and turbulence effects into account by introducing impact equations and additional terms to the governing equations of the momentum solver in POLCOMS and of the k-e turbulence model (General Ocean Turbulence Model, GOTM). The updated coupled model is then implemented for Liverpool Bay with numerical simulations covering the full year 2008 and with 55 turbines represented in the model. It is validated using mooring data over the same period at selected locations in Liverpool Bay. A yearly time series of temperature, salinity, velocity and density shows that the model predicts the hydrodynamics well, and that inclusion of the wind farms in the model results in a slight improvement of numerical predictions based on skill values. A number of sensitivity tests address the influence of the modelling techniques used on the numerical results. These include a model-model comparisons considered the relative effect of taking into account changes to momentum and turbulence equations. The results demonstrate that using only one equation change (either momentum or turbulence) overestimates the effects of a structure in the water column and that both momentum and turbulence should be considered when assessing the impacts of structures in a 3D model. Finally, numerical results from the best simulation are analysed to determine the impact of the offshore wind farms on the region of freshwater dynamics. The position of the wind farms controls the level of impacts in the region of freshwater influence. When the wind farm is positioned in an area were the ambient velocity is high, the velocity is affected. In contrast, where the velocity is lower, the salinity and temperature is more affected. The main conclusions are: even a small number of structures do have a discernible impact on the dynamics of a region of freshwater influence; the representation of offshore wind farms in the model, considering momentum and turbulence modifications to governing equations, is critical for predictions of the total impact on the water column in a 3D model.

Acknowledgements

I would firstly like to thank my supervisors; Laurent Amoudry, Ian Walkington and Alejandro Souza. Laurent for his constant help and willingness to share his knowledge without prejudice. Without that, this PhD would not have been what it is. Ian for the number of hours he spent with me in his office talking about everything from mathematics to porpoises and Alex for his advice throughout the four years, thank you all.

Secondly, I would like to thank my partner for her patience and understanding when things got tough. I probably would not have got through it without her encouragement, thank you very much. Finally I would like to thank my parents, whose unwavering support and positive comments have got me to where I am today.

Chapter 1

Introduction

1.1 Background

Society has been built on power and is reliant on a continuous, stable source of energy with various generation methods having been developed and used through history. As such, energy production has been a key research area for many centuries. With the booming global population exceeding 7 billion people, the demand for energy has never been higher. Old and new emerging global markets as well as increased demands on food and transport have given rise to energy consumption levels of 524×10^{15} Btu in 2013. The U.S Energy Information Administration produces the International Energy Outlook (IEO) report which presents historical values of global energy demand and produces a forecast up to 2040.

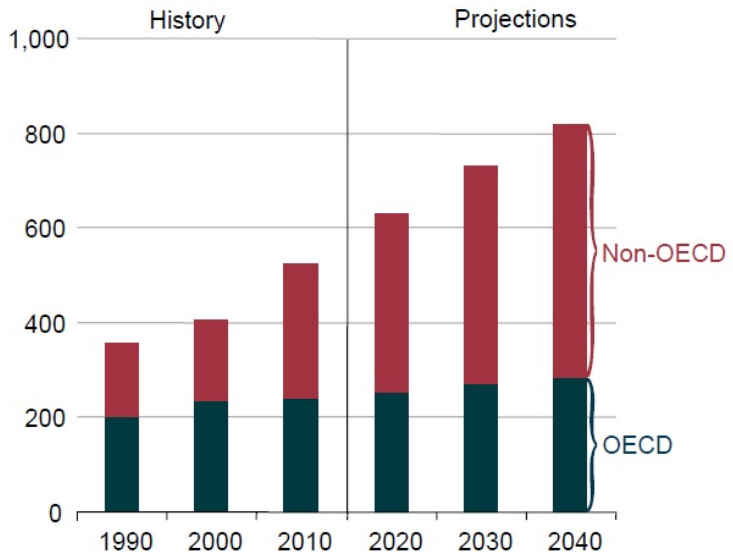

FIGURE 1.1: World Consumption (EIA 2013 Report, [26]), Btu $\times 10^{15}$ against year. Black represents the OECD countries and red represents the non-OECD countries.

Figure 1.1 splits both historical values and projections into Organisation for Economic Cooperation and Development (OECD) countries (black) and non-OECD countries (red). For information, the OECD (Organisation for Economic Cooperation and Development (www.oecd.org, 2016 [32]) include countries with generally mature economies, while non-OECD countries tend to have emerging economies. EIA IEO, 2013, [26] estimates a 58% increase in energy consumption by 2040, which is mostly driven by the increase in non-OECD countries.

There are many forms of energy used in modern society, however we will only focus on electricity generation methods in the United Kingdom. Figure 1.2 shows the energy production by generation methods in the UK in the second quarter of 2013. The Figure shows that electricity is predominately generated by so called fossil fuels, coal 35% and gas 28.5%. These are generally one of the cheapest and reliable methods of production and have been used for decades in the UK. However, when using fossil fuels, harmful by-products are released which can contribute to climate change.

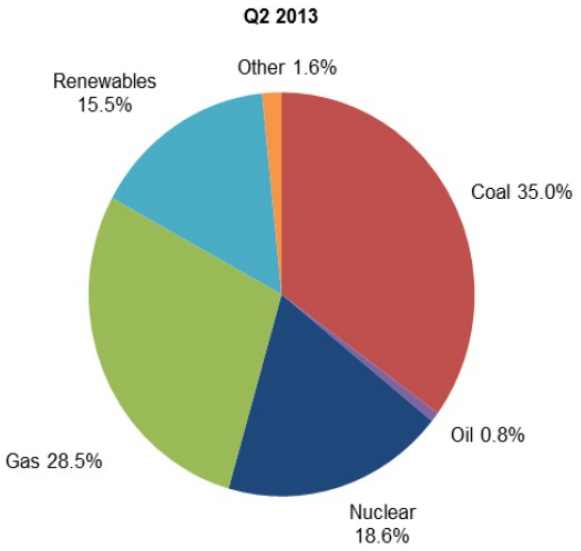

FIGURE 1.2: Electricity Production by type (UK Energy Roadmap update, 2013, [28])

While our main focus of this thesis is on the marine renewable sector, in this section we briefly discuss the background of energy production in the UK.

1.1.1 Power and Energy

In fundamental physics, power is a measure of the work used in time. The conservation of energy states; 'Energy cannot be created or destroyed, only converted from one form to another'. An example includes the conversion of calories in our food to energy used by our bodies to move. This principle can be seen throughout the universe, sunlight to heat and gravitational potential to kinetic energy are just a few simple examples.

Humans have become capable of using this conversion to their advantage. Throughout history, a range of methods for converting energy to forms that are useful to mankind were discovered and developed, for example water mills were used to power mill stones to produce flour, these used river flows to turn a wheel.

The steam engine was one of the largest leaps in history; the patent in 1769 of the first commercial engine which is widely credited for starting the industrial revolution in the UK. Over this period, the UK experienced unprecedented growth and provided the foundations for modern society (www.bbc.co.uk, 2014 [77]).

Human society is closely intertwined with energy availability, Figure 1.3 shows the population growth with predictions up to the year 2025. The population boost around the beginning of the 1800's was due to the start of the industrial revolution and increase of available energy. The graph shows the population levels over the last ten thousand years. What is very obvious is this jump from under one billion to over seven billion in 300 years. The energy has been used in many industries including farming, providing people with food and increases in medicine allowing people to live longer and healthier lives.

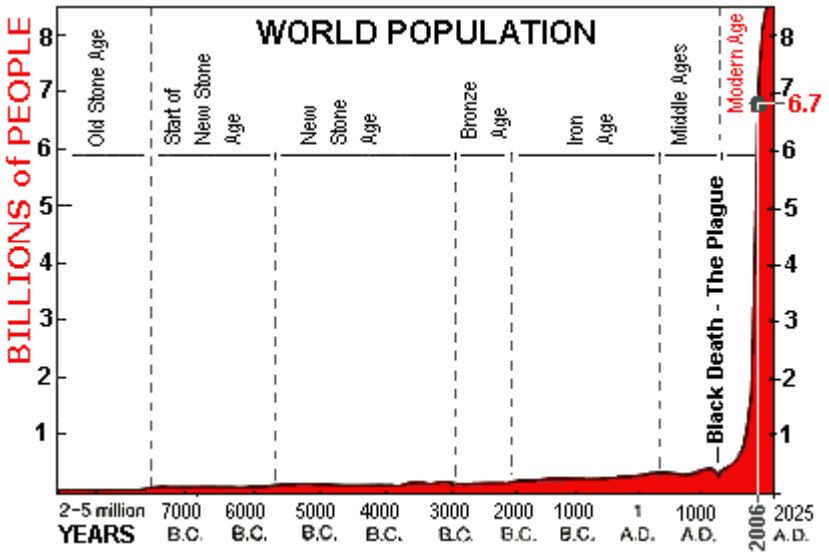

FIGURE 1.3: Population Growth (Holtz, 2011 [37])

Modern day society is entangled with the supply of energy. This is emphasized when countries go to war; much of the war effort is focused towards providing energy. The Arctic convoys in WW2 by the Merchant navy are considered one of the major reasons for winning the war which mainly comprised of fuel and

food. The average cost of living in the UK has increased steadily year on year the overarching reason for which can be linked to the cost of oil.

Finding new sources of energy is one of the most important tasks for many engineers and scientists all over the world. Renewable methods are one option, the advantage being renewable energy is continuously regenerating and has low environmental impacts. This could refer to sources such as sunlight, wave power, tidal power and geothermal energy, each provides a seemingly infinite energy source. There are other more advanced sources that also provide a stable energy supply however they have greater environmental impacts, the nuclear industry being one such method. Nuclear power is not a renewable energy because it uses uranium which is limited however the environmental impacts are low if the issue with nuclear waste is dealt with carefully. Nuclear waste and safety issues provide an issue for many people, nuclear disasters such as Chernobyl set public opinion against the nuclear industry even though the major events are rare (www.world-nuclear.org, 2016 [8]).

1.1.2 Fossil Fuels

Oil, gas and coal are used in various different technologies and industries around the world. Figure 1.2 shows the energy production by type, it shows 64.3% of electricity in the UK was generated by fossil fuels in 2013.

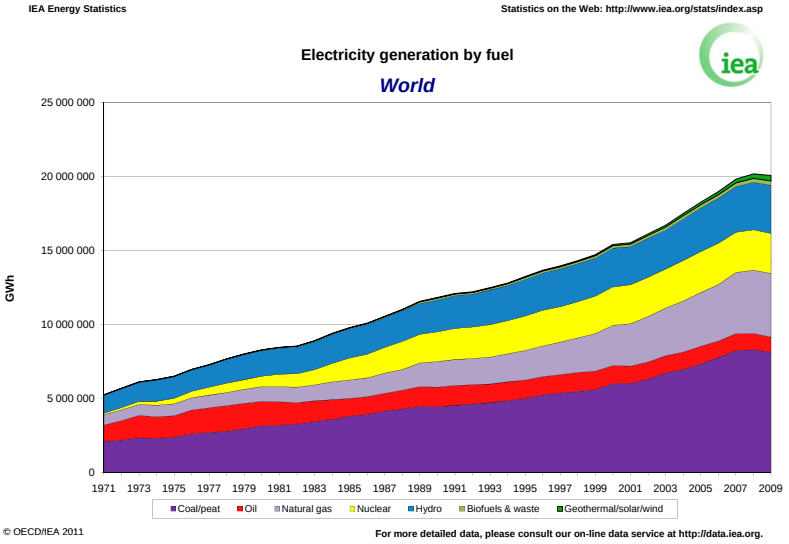

FIGURE 1.4: World Electricity generation by fuel type (IEA, 2011 [3])

Figure 1.4 shows the UK is consistent with the world average production which favours fossil fuels. There are two major issues with this, firstly the sources of fuel are depleting and secondly the process of converting the fuel into electricity creates greenhouse gases. The industrial revolution came about because the UK had vast amounts of coal in large seams. During the last 200 years, these seams have become less profitable to mine because of access becoming too difficult and as a result, expensive. There is debate within the industry about the levels of fossil fuels remaining and reports present conflicting ideas. However the general conclusions are that they will run out and new sources need to be found as soon as possible.

1.1.3 Climate Change

Climate change is one of the major issues for society in the 21st Century. A major side effect from the energy generation process is exhaust gases, predominately carbon dioxide (CO_2). CO_2 is a major contributor towards global warming due to its ability to reflect the heat, increasing the greenhouse effect between the Earth's surface and the atmosphere. The climate change conference in Doha,

Qatar 2011 revealed the CO_2 emissions had risen by 2.6% on 2010 levels to a total of 35.6 billion tonnes. It was also revealed that some 80% of the total increase was due to emerging markets (Non-OECD) (Gray, 2012 [30]).

Figure 1.5 shows the increase on CO_2 concentrations in the atmosphere using historical ice measurements and direct records from the 1960's. The graph clearly shows a correlation to the population graph (Figure 1.3), therefore there is a possible link between the industrial revolution and the increase in global population. In simple terms, more people, more energy required. When fossil fuels are burnt, a by-product is CO_2 therefore it is important to find methods of production that have limited greenhouse by-products.

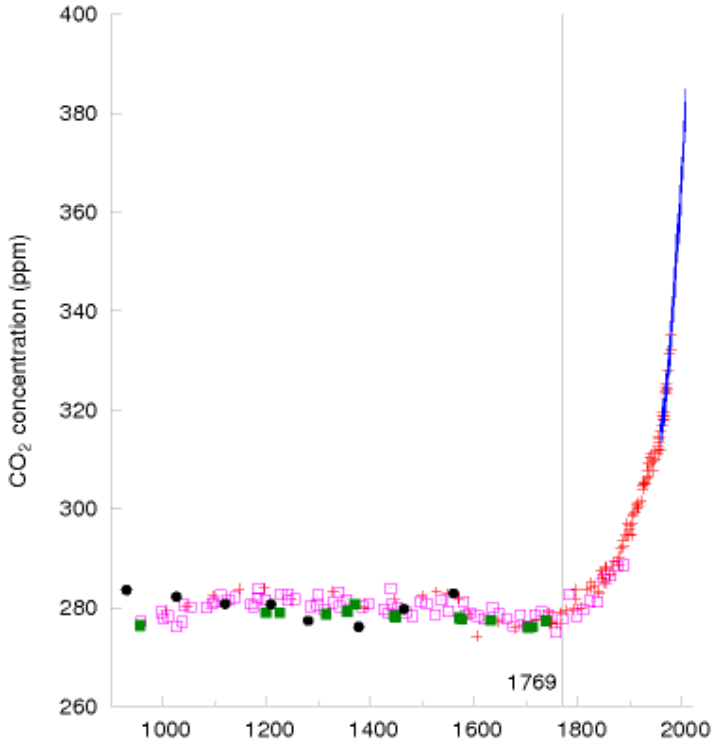

FIGURE 1.5: CO_2 concentration, (Mackay,2008 [48])

There is an obvious correlation between the patent of the James Watt steam engine (which burns coal, releasing CO_2 into the atmosphere) and the concentration increase of CO_2. The Watt steam engine permitted the mines to dig deeper and at a significantly lower cost than before meaning it became widely used.

Therefore as more engines and new methods such as steam driven turbines are used, the emissions increase. It can be concluded from this, that reducing the emissions from energy generation methods could decrease the global CO_2 output and help to decrease the rate of climate change.

1.1.4 Renewable Energy

Hydro power, which includes any system that uses a water head difference as the driving force is one of the oldest renewable sources known to man. Water wheels have been around for hundreds of years, the Hoover Dam, built during the depression in the USA at the end of the Grand Canyon provides energy into the grid. All these methods use the kinetic energy in the water to turn turbines. Other methods such as wind farms, solar and geothermal provide alternatives. This sector provides a whole new area for humans to continue developing into major sources of power. As the projects develop, the environmental consideration must be quantified, for example building a large concrete dam across a river produces large amounts of energy however it also fundamentally changes the local environment. Large areas of land upstream are flooded and the river downstream is then controlled by the flow through the dam. Balancing the need for energy and environmental concerns has become a large part of the planning process.

Many energy systems are available for use to produce renewable energy. Some of the more common, commercially viable methods include on and offshore wind farms, solar panels, geothermal techniques and hydroelectric dams. There are other methods in research and development stages which include tidal turbines and wave energy converters that have proven themselves at single device level and now being tested in array form to produce a commercially viable option in some locations where the water flows are large enough.

Europe is at the forefront of the renewable industry; we host some of the leading research institutes and have a geographical position which consists of

high wind speeds on and offshore, the second highest tidal range in the world and some of the fastest flowing tidal flows. Across the entire industry, the UK was able to generate 4% of all energy used by renewable sources (UK Energy Roadmap, 2013 [28]). Since 2003, the UK has had an offshore wind industry which has grown to become the largest in the world. Investment has led to a total of 3.5 GW capacity which can generate 9.7 TWh in 2013 (UK Energy roadmap, 2013 [28]).

1.2 Marine Environment and Energy Systems

As Britain is an island nation with some of the largest tides in the world, it is in a position to harvest tidal energy for all around its shores giving a strong position in the marine renewable energy market. Within the marine environment, the main source of energy is the kinetic energy of the tides, wind and the waves. Essentially, the energy systems exploit the kinetic energy in the fluid whether air or water. This can be achieved either directly by converting kinetic energy from fluid (wind turbines, tidal turbines) or indirectly by first storing the fluid and then releasing it to generate power, for example the proposed Swansea Lagoon in Wales. Many different methods have been proposed over the last 50 years, examples include tidal barrages, which are developed with particular sites in mind. Others such as wave energy converters that can be deployed where ever there are large enough waves. The wave energy converter creates electrical energy from the vertical motion of the waves. There are a number of concept machines in development, one such device was the Pelamis wave converter. This device was consists of a number of cylindrical modules connected by hydraulic rams.

Using the tides to generate power has been used for generations. Within the last 25 years, large investments in tidal energy converters have seen a full size tidal turbine installed in Strangford Lock in Northern Ireland. There are two types of turbines; the horizontal axis and the vertical axis turbines commercially

available. Typically the horizontal axis turbine is the preferred method because of the greater efficiency. Pentland firth in Scotland is the site of the first offshore tidal turbine array, which will provide electricity into the National Grid and vital research data for further development.

More experimental designs for TEC's include the oscillating paddle. When the water moves over an aerofoil an area of low pressure is created and lift is produced, causing a boom to rise and fall. This creates torque in a drive shaft to turn a generator. These devices have not been developed past academic assessments.

1.2.1 Offshore Wind Farms

Offshore wind has grown to become one of the major renewable energy sources used in the UK currently meeting around 5% of the UK electricity annual requirement (www.thecrownestate.co.uk, 2016, [24]) which equals almost 15 TWh generated. There are currently 1465 turbines across 28 projects with a total installed capacity of 6GW. A further 14.3 GW is in construction or planned approval stage and 3GW in planning. The UK currently has the largest offshore installed capacity anywhere in the world as of 2013 (UK Energy roadmap, 2013 [28]).

The UK offshore wind-farm industry is one of the fastest growing renewable energy sectors in the country. Government subsidies have lead to more than 20 fully commissioned or partially operational sites in UK waters. The sites were categorized in three rounds of planning. Round one were the first to be given permission, these were used as experimentation sites.

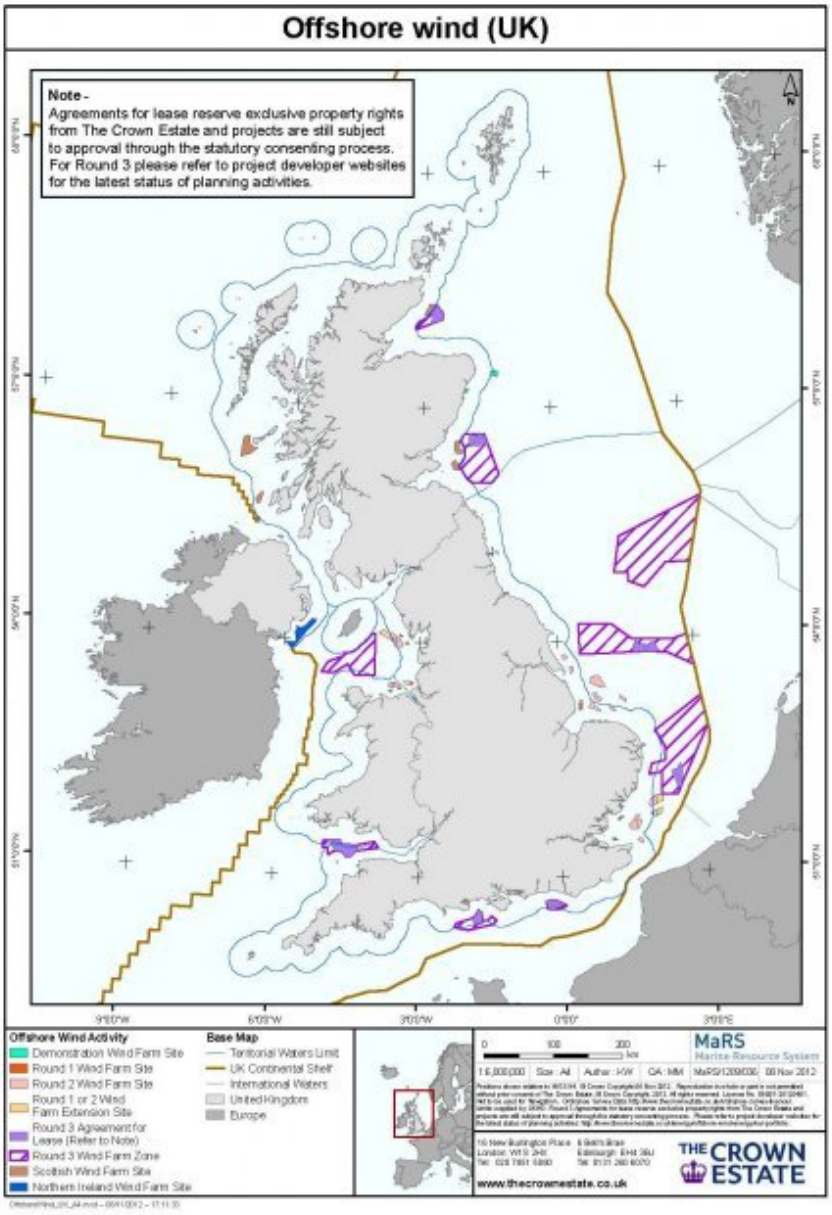

FIGURE 1.6: UK windfarm map, 2012, showing the sites of all windfarms deployed and in development on the UK continental shelf, shown by the light brown line, The Crown estate, [24]

Figure 1.6 shows the existing and planned OWF sites around the UK. The large purple areas represent the large round three developments planned. Smaller sites are plotted however the scale difference means that are not immediately obvious. Several of these sites have been cancelled in recent years, most notably the

large round 3 wind-farm in the Northern Irish Sea. Guidelines allowed a maximum of 30 turbines over a total area of 10km^2, this gave the industry a good indication of the limitations of the devices. The signs were promising, giving confidence to the Crown Estate to continue with the round two sites, which are much larger. Currently all round one farms are fully commissioned, many round two sites are partially constructed and round three are in the detailed planning stage. The Renewables Obligation (RO) was first set to 20% of electricity generation by 2020, then power was given to ministers to extend the RO. This was then increased to 30% of electricity generation by 2020 to help to provide the UK EU Renewable Directive of 15% of all energy by 2020 (Toke, 2010 [71]).

A wind turbine is a device that converts wind motion to electrical energy supported on a vertical support structure fixed to a foundation either in the seabed for offshore or concrete foundations for onshore applications.

FIGURE 1.7: An offshore wind turbine in situ, AnHolt Denmark, www.offshorewind.biz [78]

OWF are generally made of vertical cylindrical foundations piles which are anchored to the seabed. The construction costs are directly linked to the water

depth due to the amount of material needed to support the turbine above the water column. This can be seen on Figure 1.6 which shows OWF's are limited to the relatively shallow UK waters on the continent shelf (thin brown line).

Due to the size of the round one wind-farms (typically 3m-7m diameter monopiles) a small impact on the hydrodynamics in the water column could be seen on the hydrodynamics. Most of the computer models used to test the effects have either relied on 2D with a momentum reduction or 3D with a seabed momentum sink term. In this thesis we will test this theory by comparing a momentum sink method to the full effects model developed for this project.

Wind farms, naturally need to be in areas of high and consistent winds. This also means the wind will interact with the seas more than any other area, because of this the wind turbines need to be engineered to withstand the forces. This would usually mean larger foundations and as a direct result of this, more momentum will be lost from the water flow. This can cause the local environment to change dramatically as well as effecting the areas away from the site itself. This does not necessarily mean it changes the environment in a detrimental way, a news article by Mark Fischetti, [27] reports the work of Mark Jacobson who is suggesting that using wind turbines to reduce the momentum could result is them stalling hurricanes before they make landfall. However, to accomplish this, over 78000 turbines were needed. In theory, this could be a good thing, however the cost of development would far exceed any benefits. Not to mention, most of the turbines will barely produce any power when hurricanes force winds are not present due to necessary spacing between structures.

Wakes

Wakes behind OWF turbines are common place both above and below the water column. Wakes are generated by the interference in flow due to a structure. Wind turbine structures have foundation piles below the water and a spinning blade in the air flow which both cause wakes.

FIGURE 1.8: Picture of air wakes behind wind turbines, Horns Rev windfarm, Denmark. (www.noaanews.noaa.gov, 2011 [53], credit to Vattenfall)

Figure 1.8 shows the wakes of wind turbines in the air, a phenomenon usually invisible but caught on camera at the Horns Rev wind farm in Denmark. Air wakes generally are studied using computer simulation methods due to the difficulty in gaining in situ air flow measurements to fully test the wake. Air wake effects can be felt many diameters downstream of the turbine (Barthelmie et al, 2009 [11]) the direction of which is fully dependant of the direction of the flow speed at the time. Various studies have been conducted investigating flow patterns around offshore wind farms (Rethore, 2009, [63], Stovell et al, 2010, [68]) over the years.

Wind turbines rely on an unaffected air flow in order to generate the maximum possible power therefore array layout has a direct effect on the total power output. Several studies have been conducted to predict the most efficient layouts to ensure the best case scenario is used (Barthelmie, 2010, [12], Kusiak, 2010 [45]).

FIGURE 1.9: Offshore wind turbine wake trails, www.americansgeophysicalunion.tumblr.com, [50]

More recently, focus has changed towards the environmental impacts of renewable devices on the water column and bathymetry. Aerial photography can capture wakes behind turbine structures in the correct conditions. Figure 1.9 depicts darker wakes in water behind the turbines. These are attributed to the mixing in the water column caused by the turbine foundation which increases the amount of sediments through the water column. This is a common sight behind any man made structure in a marine environment making wakes that are visible to satellite imaging. Vanhellemont and Ruddick, 2014 [74] used Landsat 8 (Roy et al, 2014 [62]), a joint NASA and USGS collaboration satellite to compare the wakes behind offshore wind farms in the southern North Sea. This study looks at 7 placements totalling 2186 MW installed capacity and predominately focuses on the suspended particulate matter in the water column. The resolution of Landsat 8 (approximately 30m) means the darker matter filled wakes can be seen clearly behind the turbines, the direction of which is dependant on the tidal flow direction. The study reports plumes are 30m to 150m wide and typically extend 1km+ downstream.

Baeye and Fettweis, 2014 [10] used an experimental approach to confirm the hypothesis presented in Vanhellemont and Ruddick, 2014 [62]. The study utilizes an acoustic profiling method by using a Doppler current profiler (ADCP) to infer spatiotemporal sediment plume dynamics. The paper confirms a link between sediment plumage and turbines in the OWF. The planned increase of OWF's will lead to continuing effects on the hydrodynamics in coastal ocean systems. Turbine structures also effect the local wave field by redirecting the reflection and refraction (van der Molen et al, 2015 [73]).

The engineering aspects of the turbine have been studied for many years, to the point where the turbines are as efficient as is physically possible taking the Betz Limit into account and losses in the conversion process. The Betz Limit is a numerical limit stating the the maximum energy that can be extracted from a turbine is 59.3% in free flow/unrestricted water. This law is derived from the conservation of mass and momentum of a fluid stream flow and an idealised actuator disk. Typically, a turbine can achieve 10-30% conversion of kinetic energy. It is only recently that the impacts of putting very large structures into the marine environment been studied in any details. With the development of mathematical models, sediment flow around the foundations have been investigated. Harris et al, [32], use a mathematical model to chart the development of scour over a period of time and compare this to physical data collected at the site.

Scour pits develop when the structures change the flow dynamics, which causes sediment movement and creates the pits around the structures. This may then require intervention to stop scour exposing the foundations. Several options are available to the constructors however all are costly therefore the models are important to assess the correct level of scour protection needed on a case by case basis.

There is a lot of interest in the modelling community on structure impact in the coastal environment. This is because currently we are reliant on simulation techniques to predict the impacts of offshore structure due to the lack of large

scale arrays. This means there is a lack of field data surrounding any offshore array that can be used. The two common methods of modelling turbines are the momentum sink approach and the bottom friction method. The bottom friction method increases the bottom friction term to approximate the presence of a structure in the water column, the increase is averaged over the water column. This method is predominantly used in 2D simulations because of the average through the water column is suitable for this model type (Atwater and Lawrence, [9], Garrett and Cummings,[70] and Sutherland et al, [69]). The second approach, the momentum sink method which using a momentum sink/source term in the governing equations to simulate the presence in a water column. This can be an average throughout the water column or it can be calculated through the water column in a 3D model. The latter is the more comprehensive method, however requires greater computer power. Therefore depending on the application either method can be used.

As computer power has become cheaper, models are able to use ever more complicated techniques. There is work being carried out to update existing models with turbine inclusion modules, for example Yang and Wang, 2011 [82] have compared the bottom friction to the momentum sink method to represent tidal turbines in an enclosed bay for the purpose of analysing the effects on the hydrodynamics. The authors have developed a turbine module for FVCOM (finite volume coastal ocean model), quantifying the effects on the hydrodynamics and power outputs. This shows that hydraulic modelling can be an effective way of studying the impacts of structures in the coastal environment.

There is a distinct lack of research investigating the effects of structures on the hydrodynamics in the wakes. This work aims to address this gap in knowledge.

1.2.2 Region of Freshwater influence

A Region of Freshwater Influence (ROFI) is the name for an area of a coastal ocean with significant freshwater input. The name, first coined in the 1993 by J. Simpson, (Simpson et al, 1993 [66]) is the generalisation of river plume terminology. ROFI's are a vital link between the saline, coastal water and the fresh fluvial water from river estuaries which typically experience strong salinity gradients at the freshwater front.

ROFI's are an area of research that is in its infancy with only a small number of studies over the last 20 years that have quantified some of the physical processes which drive the flux of freshwater and in turn carbon, nutrients and pollutants from land to the ocean. Work such has been carried out to define the effects of vertical mixing and tidal straining (De Boer et al, 2006 [15], Simpson et al, 1990 [66]).

Strain Induced Periodic stratification (hereafter known as SIPS) (Simpson et al, 1990 [66]) was a key process in freshwater/saline water interaction in Liverpool Bay (a ROFI) conducted prior to the construction of any offshore structures. Classic theory assumed that the exchange flow was a gravity-driven circulation, However SIPS introduces the hypothesis that offshore and onshore flow directions change the stratification due to shear effects. When the flow is onshore, the shear in the tidal current structure interacts with the offshore salinity gradient which induces stratification, in contrast when the flow is offshore the shear acts as destabilising force destroying the stratification. In the context of this work, applying an additional obstruction at this sensitive salinity front may cause instabilities in the vertical structure. This is one of the questions this study aims to investigate.

The ability to measure turbulent kinetic energy in the marine environment has led to the evolution of the understanding of structure of dissipation in a ROFI (Rippeth et al, 2001 [60]). The evidence presented in this paper supports

the SIPS theory by showing enhanced dissipation levels on the flood phase of the tide by processing ADCP measurements in Liverpool Bay. These measurements counter the traditional theory that stratification is caused purely by density. SIPS has since been used to describe the freshwater interaction in other ROFI's and estuaries throughout the world (Simpson et al, 2005 [65], Palmer, 2010, [56], Burchard, 2009 [21], Monismith, 1996 [51]). Each of these papers concludes that SIPS must influence the vertical structure in the ROFI and has measurements that support this theory.

As the ROFI is an unexplored area of science with the exception of the physical processes discussed above, there are numerous knowledge gaps that require some research. One such gap is the effect of OWF's on the Hydrodynamics which will be affected. In a ROFI, physical processes are not always intuitive, as is the case with the SIPS theory therefore a study to assess the impacts of physical structures would be beneficial. This work therefore aims in part to fill the gap and attempts to identify the influence of the OWF's to the ROFI.

1.3 Project description, Methodology and Objectives

The aim of this project is two-fold; firstly we aim to develop a validated structure impact model which can be used to simulate any structure in the fixed grid ocean circulation model, POLCOMS. Secondly, we aim to comprehensively study the effects of the offshore renewable energy structures deployed in Liverpool bay in 2008. The Proudman Oceanography Laboratory Coastal Ocean Modelling System (POLCOMS) is a 3D Baroclinic, coastal ocean circulation model used extensively to study circulation on the European continental shelf. It has the origins in a paper by James, 1986[42] and has been in constant development leading to various improvements such as a piecewise parabolic advection scheme

(James 1996 ([43]). POLCOMS has also been coupled to other models such as the general ocean turbulence model (GOTM) (Holt and Umlauf [34]). We use the impact equations derived from the drag force equation for a structured grid (Rennau, 2012 [59]) which take into account the effects of structures on momentum and turbulence. We do this by modifying the equations for time split primitive momentum equations and we take advantage of the coupled GOTM model to include the turbulence impact equation in the governing equations for a $k - \varepsilon$ turbulence model. We intentionally use a generic coding technique which provides the user with flexibility and leaving further module development a possibility.

We then use the impact module and apply it to a case study in Liverpool Bay, a region of freshwater influence. Liverpool Bay is situated in the Northern Irish sea and has been subjected to major offshore renewable development leading to the area containing over 250 offshore wind turbines and been the focus of tidal turbine development off the northern coast of Anglesey and tidal barrage schemes in the Mersey. We will look at the impacts of a small number of turbine structures which is consistent with the total number deployed in 2008. The reason why this time period was chosen is we have access to validated inflow conditions for the time period which consist of atmospheric data, sea boundary forcing and freshwater inflow (details of this are discussed in section 3.5). In this time period we also have access to water column field data recorded in the bay at various different sites throughout the Bay. This data is used to validate the model with the structures included and comment on the effects the structures have on the model accuracy.

We complete a comprehensive study of the effects structures have on the hydrodynamics in Liverpool Bay. This is completed by simulating the total number of structures in Liverpool Bay and using surface plots to analysis the impacts. We also use the module to simulate the momentum and turbulence impacts of the 2008 set up and compare to a momentum sink model. We comment

on the overall effect on the accuracy of the hydrodynamic simulation and then on the contributions of the momentum and turbulence impacts individually.

1.3.1 Objectives

Specific objectives of this PhD are:

- Develop a module to be used with the POLCOMS ocean circulation model that has the capability to simulate any structure in the fixed grid which calculates the impacts to momentum and turbulence kinetic energy.
- Validate the module using the 2008 numerical model for Liverpool Bay with simulated Offshore Wind Farm (OWF) foundation structures.
- Perform a sensitivity analysis to investigate the different methods of using simulating the OWF's in the module equations
- Perform a comprehensive study of the hydrodynamic (velocity components, salinity, temperature and density) effects caused by the deployed structures using 2008 as a case study.
- To test the module against a momentum sink only simulation over the 2008 period and compare the model accuracy, hydrodynamic effects and make comments on the most appropriate method of the simulation of structures in Liverpool Bay.

1.4 Thesis Overview

This thesis represents the 4 year PhD, 'Impacts of Windfarm Structures on a Region of Freshwater Influence'. In the report we will introduce the new module written for POLCOMS-GOTM (chapter 3). We will describe the numerical model equations and show the development of the impact equations and where they are applied in the governing equations. We will go on to discuss Liverpool

Bay and apply the new module to simulate the impact of the simple vertical structures from the foundation piles of the offshore wind farms which are present in 2008. We will discuss the validation method using this set-up by comparing field data taken at various points across the full year 2008 using the salinity, temperature and density as a comparison.

Once the model is validated we move on to discuss the way we simulate the structures in the domain. The impact model equations are written to average the impact across a structured grid, using this method we initially represent the turbines on wind farm spatial scale. In this study we compare this wind farm spatial scale to a turbine scale which represents each structure individually allowing unrestricted water flow through the middle of the offshore wind farm.

We move on to compare the full structure model developed in this thesis to a momentum sink only model. This study is to compare another common approach to structure modelling. We look at the impacts on the typical month of December and compare salinity, temperature and density and make comments on the accuracy of each modelling method and look at the added impacts of turbulence kinetic energy.

Using the validated 2008 set up, we assess the impact of the wind farm structures in Liverpool Bay. We will discuss the impacts on velocity, temperature, salinity and density by comparing the impact model to a control model which has no structures. The 2008 set up has been shown to be a typical year therefore we make comments on potential past and future impacts.

Finally, we discuss an attempt at simulating the much larger number of turbines as of 2015 and make comments on the objectives of this study to describe how each has been met. We will also discuss future work and possibilities of this model.

The aim of this work is to address the knowledge gap specifically in the region of freshwater influence, Liverpool Bay.

Chapter 2

Literature Review

We are using the 3D Proudman Oceanography Laboratory Coastal Ocean Modelling System (POLCOMS) for a numerical study to investigate the impacts of offshore structures in a coastal ocean. In this chapter we briefly discuss the origins and development of coastal ocean models.

2.1 Introduction

Ocean modelling is the branch of fluid dynamics that focuses on studying the hydrodynamics of a large body of water which can range spatially for several miles to large global circulation models. These models all use variations of the Navier-Stakes equations, applied to fluids of varying density in a rotating frame of reference.

Consider a fluid in static equilibrium with horizontal homogeneity producing purely vertical stratification. It is fair to say, that when a heavier particle is above a lighter particle the fluid is unstable. If a particle at a reference height $\rho(z)$, in the fluid column, is displaced by $z + h$ where the density is $\rho(z + h)$ and taking only incompressible fluid into account, the fluid particle retains its original density resulting in a force equalling its weight minus buoyancy (Archimedes'

Buoyancy Principle). Hence the weight of the displaced fluid is:

$$g[\rho(z) - \rho(z+h)]V \tag{2.1}$$

where V is volume. Using Newton's second law, equation 2.1 can be written to equal:

$$\rho(z)V\frac{d^2h}{dt^2} = g[\rho(z) - \rho(z+h)]V \tag{2.2}$$

In geophysical flows the density differences are relatively small when compared to the reference densities. This is the basis of the Boussinesq approximation. A Taylor expansion can be used to approximate the density difference which equals:

$$\rho(z) - \rho(z+h) \simeq \frac{d\rho}{dz}h \tag{2.3}$$

Dividing through by V gives:

$$\frac{d^2h}{dt^2} + N^2 = 0 \tag{2.4}$$

where;

$$N^2 = -\frac{g}{\rho_0}\frac{d\rho}{dz}h \tag{2.5}$$

Equation 2.4 is an oscillatory character with frequency N, The Brunt-Vaisala Frequency. It causes the particles to be pulled towards a stable position in the fluid where the forces on the particle are balanced. However, as the particle approaches that position inertia causes it to overshoot. N^2 then changes sign and causes the particle to change direction and return back to the stable position.

The Coriolis force is the name given to the force generated by the Earth's rotation on a fluid and plays a part in many atmospheric/fluid models. As the oceans are the biggest volumes of water on the planet, the force will be of greater magnitude therefore it is an essential part of a Geophysical Model.

The Coriolis force, defined as:

$$f = 2\Omega sin\varphi \tag{2.6}$$

$$f_* = 2\Omega cos\varphi \tag{2.7}$$

where Ω is angular velocity.

f is the Coriolis force and f_* has no name so for this report it will be referred to as the reciprocal Coriolis force, similar to Cushman-Roison [25]. The Corolis force, f is positive, n the northern hemisphere, zero at the equator and negative in the southern hemisphere. Whereas f_* is positive in both hemispheres and zero at the poles however due to the importance of other terms in the governing equations, f_* is small and can be neglected.

2.2 Hydrodynamics

The introduction of the Coriolis force and stratification in the standard Navier-Stokes governing equations lead to the Boussinesq approximation fluid equations. In the Boussinesq approximations for the rate of change of momentum and mass, density variations are neglected unless they are coupled with the gravitational acceleration of the buoyancy force (Spiegel and Veronis, 1960, [52]). Computer models of geophysical systems are limited by the horizontal resolution. This means they are only capable of resolving the largest turbulence fluctuations and motions smaller than the mesh size are unresolved. A subgrid-scale parametrization must be used to simulate the unresolvable scales. Boussinesq proposed a method to replace the molecular viscosity μ with a much large eddy viscosity $\mathcal{A}$ in the horizontal and ν_E in the vertical. $\mathcal{A}$ covers a much larger span of unresolved motions and therefore needs to be significantly higher than the ν_E. The governing momentum equations that are used are:

x-component:

$$\begin{aligned} &\frac{\partial u}{\partial t} + u\frac{\partial u}{\partial x} + v\frac{\partial u}{\partial y} + w\frac{\partial u}{\partial z} - fv \\ &= \frac{1}{\rho_0}\frac{\partial p}{\partial y} + \frac{\partial}{\partial x}\left(\mathcal{A}\frac{\partial u}{\partial x}\right) + \frac{\partial}{\partial y}\left(\mathcal{A}\frac{\partial u}{\partial y}\right) + \frac{\partial}{\partial z}\left(\nu_E\frac{\partial u}{\partial z}\right) \end{aligned} \tag{2.8}$$

y-component:

$$\begin{aligned} &\frac{\partial v}{\partial t} + u\frac{\partial v}{\partial x} + v\frac{\partial v}{\partial y} + w\frac{\partial v}{\partial z} + fu \\ &= \frac{1}{\rho_0}\frac{\partial p}{\partial y} + \frac{\partial}{\partial x}\left(\mathcal{A}\frac{\partial v}{\partial x}\right) + \frac{\partial}{\partial y}\left(\mathcal{A}\frac{\partial v}{\partial y}\right) + \frac{\partial}{\partial z}\left(\nu_E\frac{\partial v}{\partial z}\right) \end{aligned} \tag{2.9}$$

Hydrostatic z-component:

$$0 = -\frac{\partial p}{\partial z} - \rho g \tag{2.10}$$

The continuity equation:

$$\frac{\partial u}{\partial x} + \frac{\partial v}{\partial y} + \frac{\partial w}{\partial z} = 0 \tag{2.11}$$

The Energy equation:

$$\frac{\partial \rho}{\partial t} + u\frac{\partial \rho}{\partial x} + v\frac{\partial \rho}{\partial y} + w\frac{\partial \rho}{\partial z} = \frac{\partial}{\partial x}\left(\mathcal{A}\frac{\partial \rho}{\partial y}\right) + \frac{\partial}{\partial y}\left(\mathcal{A}\frac{\partial \rho}{\partial y}\right) + \frac{\partial}{\partial z}\left(\kappa_E)\frac{\partial \rho}{\partial z}\right) \tag{2.12}$$

where u, v, and w are velocity components, $\mathcal{A}$ is the horizontal eddy viscosity,ν_E is the vertical eddy viscosity and ρ is the water density.

These equations form the primitive equations that are fundamentally the basis of all geophysical flow computer models.

2.3 Turbulence Modelling

While it remains extremely difficult to precisely define turbulence, we can list a number of important characteristics. In the Reynolds experiment, a coloured dye was introduced into a fluid flow. At low velocities, the dye formed in ordered layers. This was due to the viscous forces being more dominant over the inner

shear stresses, subduing the disturbances from the effects of the walls and pipe. At high velocities, the dye is mixed in a random manner. With the use of computers in turbulence research, this interaction is researched using a number of models that have been developed to investigate the effects of turbulence.

Some of the important features in turbulent flows allow for an understanding of how turbulence interacts with the water column.

- Randomness of parameters with respect to time and space.
- Strong mixing in the flow because of interaction of transport values
- Wide range on length and time scales, making modelling challenging.

In turbulent flow the basic entity is the eddy, a volume of rotating fluid. The eddies can be up to the size of the system, therefore these have the system length scale and can be as small as a molecular length scale. The largest eddies extract kinetic energy from the mean flow of the water and then pass it down to smaller and smaller eddies until the smallest eddy where the energy is taken due to the viscous dissipation, as shown in Figure 2.1. Large eddies cannot dissipate as the viscous forces are negligible due to high shear effects. As the energy cascades to smaller and smaller eddies, the high shear forces reduce until the smallest eddy size where the shear forces and the viscous forces are of the order of 1, therefore the forces are balanced. After this point, the energy of the eddy is dissipated due to the higher viscous forces.

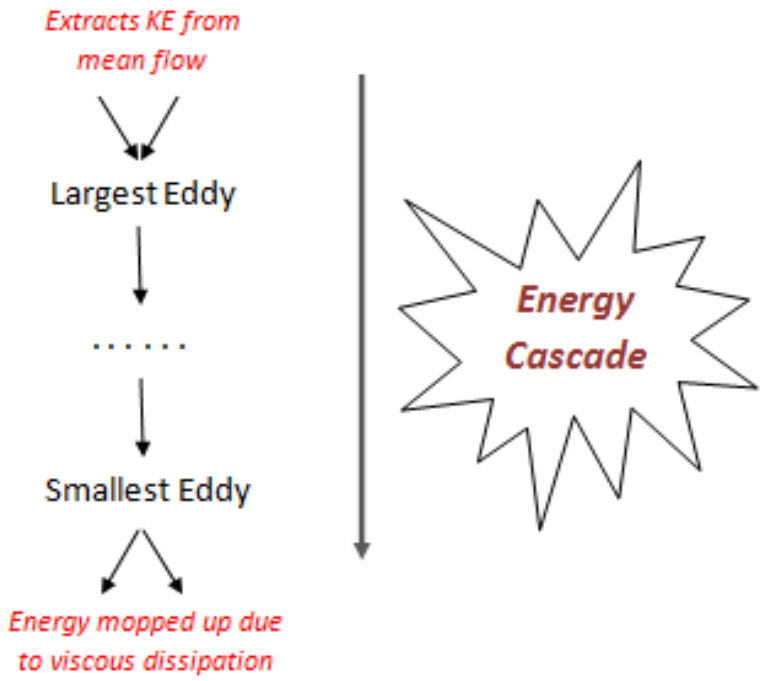

FIGURE 2.1: Energy cascade of eddies

investigating turbulence is impossible without the aide of computers and increasingly sophisticated simulation techniques within the ocean environment. When calculating the turbulence, the velocity, u is split into a mean component and fluctuating component:

$$u = \bar{u} + u' \tag{2.13}$$

In turbulence models the momentum and continuity equations need to be averaged. Starting with the continuity equation in the j direction;

$$\frac{\partial v}{\partial y} = 0; \tag{2.14}$$

Substituting 2.13 gives;

$$\frac{\partial \bar{v}}{\partial y} = 0; \tag{2.15}$$

for the continuity of the mean flow and;

$$\frac{\partial v'}{\partial y} = 0; \tag{2.16}$$

for the continuity of the fluctuating flow.

The Navier-Stokes equation;

$$\rho \left[\frac{\partial u}{\partial t} v \frac{\partial (uv)}{\partial y} \right] = -\frac{\partial p}{\partial x} + \frac{\partial}{\partial y} \left(\mu \frac{\partial u}{\partial y} \right) \tag{2.17}$$

Substituting in;

$$u_i = \bar{u} + u', v = \bar{v} + v', p = \bar{p} + p' \tag{2.18}$$

When substituting 2.18 into 2.17 and using simplifying rules the equation can be manipulated to;

$$\rho \left[\frac{\partial \bar{u}}{\partial t} + v \frac{\partial \overline{(uv)}}{\partial y} \right] = -\frac{\partial \bar{p}}{\partial x} + \frac{\partial}{\partial y} \left(\mu \frac{\partial \bar{u}}{\partial v} \right) - \frac{\partial}{\partial v} (\rho \overline{(u'v')}) \tag{2.19}$$

When the equation is averaged, an extra term emerges, $-\overline{\rho u'v'}$. This is know as the Reynolds stresses and cause the turbulence in the fluid flow. The Reynolds stresses can be written as a stress tensor;

$$-\overline{\rho u_i' u_j'} = \begin{pmatrix} \overline{u'^2} & \overline{u'v'} & \overline{u'w'} \\ \overline{u'v'} & \overline{v'^2} & \overline{v'w'} \\ \overline{u'w'} & \overline{v'w'} & \overline{w'^2} \end{pmatrix} \tag{2.20}$$

This shows that there are six different unknowns in the tensor, $\overline{u'^2}$, $\overline{v'^2}$, $\overline{w'^2}$, $\overline{u'v'}$, $\overline{u'w'}$ and $\overline{v'w'}$. This rises the closer problem where there are 10 unknowns

and only 4 equations. These are the focus of the turbulence models.

Two such methodologies that can be followed are;

- Eddy viscosity model;
- Reynolds stress transport model.

The commonly used eddy viscosity models include;

- Mixing Length
- Spalart-Allmaras model
- Standard $k-\varepsilon$ model
- RNG $k-\varepsilon$ model
- Realizable $k-\varepsilon$ model
- $k-\omega$ model

The Reynolds stress transport model tends to be too expensive because they solve the Reynolds stresses $-\overline{\rho u'v'}$ directly. In ocean model applications this is too computationally complex resulting in long run times therefore the eddy viscosity method is often the preferred method.

Eddy viscosity models split $-\overline{\rho u'v'}$ into two parts: isotropic and anisotropic.

$$-\overline{\rho u'v'} = -\frac{2\rho}{3}k\delta_{uv} + \mu_T\left(\frac{\partial\bar{v}}{\partial y} + \frac{\partial\bar{u}}{\partial x}\right) \tag{2.21}$$

Substituting equation 2.21 in the Navier-Stokes equations simplifies the right-hand side to;

$$-\bar{P}_{eff}\delta_{uv} + \mu_{eff}\left(\frac{\partial\bar{u}}{\partial\bar{y}} + \frac{\partial\bar{v}}{\partial x}\right) \tag{2.22}$$

Where $\bar{P}_{eff} = p + \frac{2}{3}\rho k$ and $\mu_{eff} = \mu + \mu_T$. This introduces k and μ_T which is the kinetic energy and eddy viscosity respectively. It is this that the eddy viscosity models calculate.

In addition to the above, several turbulence models have been specifically derived with ocean applications in mind, for example the general ocean turbulence model, GOTM (Umlauf and Burchard, 2005 [72]) which will be discussed later in chapter 3 .

Ocean models can use any turbulence model to simulate the effects of turbulence. Commonly used models types are a two equation models, for example; $k-\varepsilon$ or $k-\omega$ for studies that require more detail and the Mixing length model for simple representations because the computation time is shorter than its two equation counterparts.

Mixing Length model

This model attempts to link the characteristic velocity fluctuations with the mean flow properties because there is a strong connection between the mean flow and the behaviour of the larger eddies. Through a series of physical connections, $-\overline{\rho u'v'}$ can be written;

$$-\overline{\rho u'v'} = \rho l_m^2 \left|\frac{\partial \bar{u}}{\partial y}\right| \frac{\partial \bar{u}}{\partial y} = \mu_T \frac{\partial \bar{u}}{\partial y} \tag{2.23}$$

Where ρ is density, u' and v' are fluctuating velocity components and l_m is the mixing length. By manipulating equation 2.23 equations from μ_T and by extension ν_t';

$$\mu_T = \rho l_m^2 \left|\frac{\partial \bar{u}}{\partial y}\right| \tag{2.24}$$

$$\nu_t = l_m^2 \left|\frac{\partial \bar{u}}{\partial y}\right| \tag{2.25}$$

l_m has a k absorbed in because of the proportionality of u' and v'. Algebraic expressions can be used for simple flows and has several advantages include it being easy to implement, cheap on computation resources and can produce a good representation. However there are several disadvantages such as its inability to describe varying length scales and only calculates mean flow properties

and turbulent shear stresses, which are unsuitable for simulating flow around structures.

Turbulent and Kinetic Energy Models

The instantaneous kinetic energy $k(t)$ of a turbulent flow is the sum of the mean kinetic energy $\overline{k}$ and the turbulent energy k;

$$\overline{k} = \frac{1}{2}\left(\overline{u_1^2} + \overline{u_2^2} + \overline{u_3^2}\right) \tag{2.26}$$

$$k = \frac{1}{2}\left(\overline{u_1'^2} + \overline{u_2'^2} + \overline{u_3'^2}\right) \tag{2.27}$$

$$k(t) = \overline{k} + k \tag{2.28}$$

and the dissipation rate of k is equal to:

$$\varepsilon = v\overline{\frac{\partial u_i'}{\partial x_J}\frac{\partial u_i'}{\partial x_J}} \tag{2.29}$$

Equations need to be formulated for k and ε. The starting point comes from the Reynolds averaged Navier-Stokes equation (RANS). The objective is to get RANS in terms of u'. To do this, the RANS equations are subtracted from the Navier-Stokes:

$$\frac{\partial u_i'}{\partial t} + \frac{\partial}{\partial x_j}(\bar{u_i}u_j' + \bar{u_i}u_i' + u_i'u_j' - \overline{u_i'u_j'}) = -\frac{1}{\rho}\frac{\partial p'}{\partial x_i} + \frac{\partial}{\partial x_i}\left(u\frac{\partial u_i'}{\partial x_j}\right) \tag{2.30}$$

The next step is to write equation 2.30 in terms of kinetic energy. To do this, it is multiplied by u_j'. After manipulation an average is taken:

$$\frac{\partial k}{\partial t} + \bar{u_j}\frac{\partial k}{\partial x_j} = -\frac{\partial}{\partial x_j}\left(\frac{1}{2}\overline{u_j'u_i'u_i'} + \frac{1}{\rho}\overline{u_j'p'} - vu_i'\frac{\partial u'}{\partial x_j}\right) + \overline{u_i'u_j'}\frac{\partial \bar{u_i}}{\partial x_j} - v\overline{\frac{\partial u_i'\partial u_i'}{\partial x_j \partial x_j}} \tag{2.31}$$

Each term can be defined as: *Rate of change of k + Transport by advection = (Transport of k by stresses + Transport by pressure - Transport by viscous*

forces)+Turbulence production-Rate of dissipation of k.

The dissipation rate equation can also be written in a similar form and will be discussed in the later.

$k-\omega$ model

The $k-\omega$ model solves a modified equation for k and an equation for ω with is defined as the dissipation per unit kinetic energy, $\omega = \frac{\varepsilon}{k}$.

$$k = \frac{\partial k}{\partial t} + \bar{u}_j \frac{\partial k}{\partial x_j} = \frac{\partial}{\partial x_j}\left[\nu + \frac{\nu_t}{\sigma_k}\frac{\partial k}{\partial x_j}\right] + \nu_t\left(\frac{\partial \bar{u}_i}{\partial x_j} + \frac{\partial \bar{u}_i}{\partial x_i}\right)\frac{\partial \bar{u}_j}{\partial x_i} - \beta' k\omega \quad (2.32)$$

$$\omega = \frac{\partial \omega}{\partial t} + \bar{u}_j \frac{\partial \omega}{\partial x_j} = \frac{\partial}{\partial x_j}\left[\nu + \frac{\nu_t}{\sigma_\omega}\frac{\partial \omega}{\partial x_j}\right] + \alpha\nu_t\left(\frac{\partial \bar{u}_i}{\partial x_j} + \frac{\partial \bar{u}_i}{\partial x_i}\right)\frac{\partial \bar{u}_j}{\partial x_i} - \beta_2\omega^2 \quad (2.33)$$

The constants are:

Constant	Value
β_2	0.075
β'	0.09
u_t	0.533
σ_k	2
σ_ω	2

and the eddy viscosity is calculated by:

$$\mu_t = \rho\frac{k}{\omega} \quad (2.34)$$

$k-\varepsilon$ model

The $k-\varepsilon$ model uses equations for k and ε to calculate the μ_T. The model equation for turbulent kinetic energy k is:

$$\frac{Dk}{Dt} = \frac{\partial k}{\partial t} + \bar{u_i}\frac{\partial k}{\partial x_i} = \frac{\partial}{\partial x_j}\left[\frac{\nu_t}{\omega_k}\frac{\partial k}{\partial x_j}\right] + P - \varepsilon \quad (2.35)$$

and the equation for turbulent diffusion ε is:

$$\frac{D\varepsilon}{Dt} = \frac{\partial \varepsilon}{\partial t} + \bar{u_j}\frac{\partial \varepsilon}{\partial x_i} = \frac{\partial}{\partial x_j}\left[\frac{\nu_t}{\sigma_\varepsilon}\frac{\partial \varepsilon}{\partial x_j}\right] + C_{\varepsilon 1}\frac{P\varepsilon}{k} - C_{\varepsilon 2}\frac{\varepsilon^2}{k} \tag{2.36}$$

Where $C_{\varepsilon 1}$,$C_{\varepsilon 2}$,C_μ,σ_k and σ_ε are model stability constants. The Reynolds stresses are calculated using equation 2.21. Velocity and Length scales are represented for large scale turbulence, which are defined as:

Constant	Value
$C_{\varepsilon 1}$	1.44
$C_{\varepsilon 2}$	1.92
C_μ	0.09
σ_k	1.0
σ_ε	1.3

$$\vartheta \sim k^{\frac{1}{2}} \tag{2.37}$$

$$\ell \sim \frac{k^{\frac{3}{2}}}{\varepsilon} \tag{2.38}$$

$$\nu_t \sim \vartheta \ell \tag{2.39}$$

$$\mu_T = \rho C_\mu \frac{k^2}{\varepsilon} \tag{2.40}$$

The advantages of the $k-\varepsilon$ model include the relative simplicity to implement and has stable outputs. The other benefit of the $k-\varepsilon$ model is that it is widely used and therefore validated for many flow types.

2.4 Models Techniques

Through the years, many different ocean modelling techniques have been developed for a variety of applications and areas. In this section we discuss several ocean models and give examples of uses and studies for each. Computer models

require a discretization technique to split the domain into a grid pattern. Fundamentally, the computational power required to solve the equations increases as the number of mesh points increase. Therefore choosing the grid is essential to ensure accurate results. There are two kinds of grid pattern on which the equations are solved, structured and unstructured. A structured grid is one where the domain is split in to cells which all the same size. These grids are typically used for large scale circulation models in which very high horizontal resolutions are not required. Such a grid is typically used by a finite difference decretization method. The structured grid is generally very good at providing useful results for large coastal ocean circulations with realistic computational time. The major drawback using the structured method is the inability in resolving of fine detail in the flow where high detail is required. In most ocean circulation models, the grid size tends to be greater than 100m and therefore any flow characteristics with size smaller than that is not simulated.

Unstructured grids are split up into cells each potentially different number of neighbouring cells. This provides freedom for the user to specify areas within a domain where high spatial resolutions are required. Unlike structured grids which tend to be rectangles, unstructured grids can be either quadrilateral or triangular which allows different sized grid cells to fit together. Unstructured grids tend to be used in studies where fine detail in a particular area of the domain is required, allowing a fine resolution in the area of interest and a coarser one further away to save the overall computing power.

The Finite Volume Community Ocean Model (FVCOM) (Chen et al, 2003 [22]) uses an unstructured grid, finite volume method to solve primitive ocean circulation equations. FVCOM is well suited to simulate the circulation from global to estuarine scales and due to the unstructured nature is particularly capable at predicting complex areas such as coastlines, islands and inter-tidal zones. FVCOM was initially developed by the University of Massachusetts for the study of

estuarine wetting/drying processes and tidal, buoyancy and wind -driven circulation in coastal regions (FVCOM website, [80]). Further developments includes a sediment module, a biological module and a spherical coordinate system for basin and global applications. FVCOM has become a very competent ocean circulation model with is used for many ocean circulation models.

The Regional Ocean Modelling System (ROMS) is a free-surface, terrain following, primitive equations ocean model with is applied to a framework of regional ocean domains to simulate the ocean circulations (ROMS website, [41]). ROMS has been coupled with several models for biogeochemical, bio-optical, sediment and sea ice applications. The model uses a split-explicit time-stepping scheme on a structured grid domain. ROMS is generally used for large spatial scale models for example, sea-ice applications.

POLCOMS is a 3D fully baroclinic ocean model with the ability to simulate areas that include both deep and coastal ocean domains (POLCOMS Documentation, [46]). We are using POLCOMS as the base hydrodynamic solver for this work. The main advantages of using POLCOMS are the local expertise and the open access to all the source code so modification is easier. POLCOMS will be discussed in detail in chapter 3.

The modelling systems discussed above are all academic only methods which are open source software available for anyone to use for scientific purposes. There are also a multitude of commercial models available which are licensed for engineering and consultancy purposes such as TUFLOW (www.tuflow.com, 2016 [47]), MIKE suite (www.mikepoweredbydhi.com, 2016 [81]), Flood modeller (www.floodmodeller.com, 2016 [79]) for example which all use the primitive shallow water equations to provide engineering solutions to problems. These systems tend to be 'black box' type programs which are only developed by the owner of the software and cannot be modified without prior permission, therefore for academic study these models tend to be used less.

Chapter 3

Modelling Method

In this chapter, we present the new module developed for use in the Proudman Oceanographic Laboratory Coastal Ocean Modelling System (POLCOMS) to simulate the effects of any structure present in the water column. POLCOMS uses a fixed grid (Arakawa-B, Arakawa, 1972 [6]), finite difference method to solve the 3D momentum equations coupled with the General Ocean Turbulence Model (GOTM) for a selection of turbulence options (POLCOMS Documentation, [46]). In this chapter, we utilize a parametrization technique which represents the structures as an average impact across the numerical cell. The parametrization technique is used because it is appropriate when the model resolution is significantly greater than the structure (see chapter 4 for details). It has the added benefit of dramatically reducing computational resources needed when compared to a direct resolve method (Copping et al. 2014 [23], Yang et al. 2013 [83]).

We use the equations developed for structured coastal models (Rennau, 2012 [59]) which modifies the drag equation (Fluid Mechanics, Sixth Edition, White, [75]) and apply them to the incompressible, hydrostatic, Boussinesq equations of motion and k-ε governing equations. We take the impact equation as discussed in this chapter for momentum and turbulence, modify and include them in POLCOMS-GOTM model.

We present the POLCOMS model used in this study and a detailed plan of how the parametrization technique is applied to the model. We go into detail on how the equations are derived and how they are modified to be included in POLCOMS-GOTM. Finally the model with offshore wind farms (hereafter referred to as OWF's) is validated. To achieve this, the hydrodynamic effects by comparing a numerical simulation using a 2008 set up (section 4.2) to validation data (Polton et al, 2011 [57]) recorded over the same time period.

3.1 POLCOMS-GOTM

The POLCOMS-GOTM model is used in this thesis as the underlining hydrodynamic model for all the studies that are conducted. Here we discuss the origin and development of each model individually.

The Proudman Oceanographic Laboratory Coastal Ocean Modelling System (POLCOMS) is a 3D baroclinic ocean model with the ability to simulate areas that include both deep and coastal ocean domains (POLCOMS Documentation, [46]). POLCOMS has its origins in James, 1986 [42] where the model was developed as a simple eddy resolving model (POL3DB). This 3D model included a free surface and employed a simple hybrid advection scheme (also found in other stock models of that time); which had the ability to resolve tidal fronts (areas of sharp density changes). The hybrid advection scheme was then superseded in James 1996 ([43]) by a Piecewise Parabolic Method, which was found to resolve the tidal fronts more accurately (Proctor and James 1996 [58]). The 'horizontal' discretization is based on the Arakawa B-grid (Arakawa 1977, [6]). Both the B-grid(Figure 3.1)and C-grid arrangements were considered, however the C-grid was found to have a detrimental impact on the results, therefore the B-grid was selected (POLCOMS Documentation, [46]). The POLCOMS time step is limited by the Courant-Friedrichs-Lewy number (Courant et al, 1967, translated from 1928 [61]).

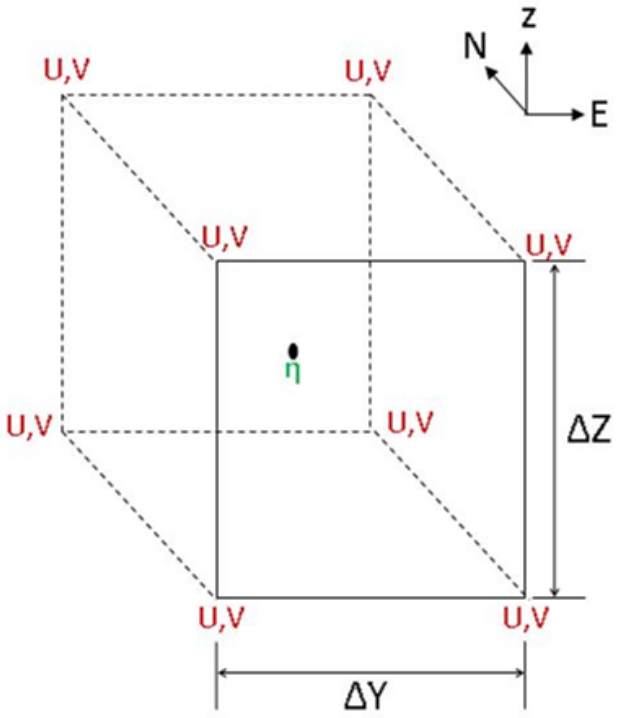

FIGURE 3.1: 3D B-grid arrangement

As a result, POLCOMS is solved by mode splitting the momentum equations are split in the baroclinic part and the remaining terms known as the barotropic part. The baroclinic part has the time step dt and barotropic part has a time step equal to the baroclinic part multiplied by a factor. The model uses a leapfrog finite difference scheme to resolve the momentum equations. Boundary conditions can be applied to any boundary which can either be set as fixed points or can be used to force the model using input data from a variety of sources. External forcing terms can be included which include freshwater inflow, atmospheric forcing and sea boundary inflows.

The modelling system has seen continuous development over a number of years. This includes coupling with various other models, WAM (Bender, 1996 [14]), GOTM (GOTM.net [31]), FABM (FABM Documentation [44]) and a sediment transport module (Amoudry and Souza 2011, [5]) which have all been used

for a variety of applications using the hydrodynamics from POLCOMS. Examples such as Howarth and Proctor, 2005 [40] discuss the use of POLCOMS to understand the coastal response in Liverpool Bay due to natural forcing and human activity in the area. The paper discusses the origins of the 3 model nesting system. The continental shelf model used to provide forcing for the Irish Sea, which in turn is used to force the boundaries in the Liverpool bay domain used in this thesis (section 3.5). The method is shown in this paper to be an effective way to model the coastal ocean area around Liverpool to get the detail required for the study. The paper also discusses the use of the nested POLCOMS model in collaboration with the Met Office providing daily runs for forecasting purposes. In that paper POLCOMS is coupled with WAM to provide the surface waves and ERSEM to provide nutrient transport through the domain. This paper shows the model capability when in use in the public sector and also highlights the flexibility when coupling to other models.

Holt et al, 2003, ([36]) discusses the use of POLCOMS in the MET Office's larger, deep ocean model FOAM and the subsequent use of the SST in the weather prediction models to forecast coastal ocean fog. This paper discusses the flexibility of the POLCOMS modelling system used in a variety of studies and the continued use in weather forecasting in and around the UK. Ashworth et al, 2004 ([7]) show the development of a multi-core code for use on clusters. This development has provided POLCOMS with the ability to solve the equations much faster, therefore allowing longer model runs within a practical time. This is an important development for future uses of the modelling system allowing more complicated and detailed results, as well as coupling modelling systems and calculating in a reasonable time, i.e. not real time or greater.

We intend to use POLCOMS as the hydrodynamic solver, as such the only parameters that will be changed are regarding the structures which are simulated. Below is a list of initial parameters that are used in all POLCOMS-GOTM simulations from here on.

Parameter	Value
Model grid, latitude (l)	576
Model grid, Longitude (m)	474
Model grid, Vertical (n)	22
Barotropic time step	1 second
Baroclinic time factor	3 seconds
Wetting and Drying	on
Initial Salinity	35.1 PSU
Initial Temperature	7 °C
Horizontal resolution	180m

TABLE 3.1: Initial POLCOMS parameters applied to all simulation runs. Salinity and temperature apply for spin up month, December 2007

POLCOMS uses sigma coordinate system in the vertical direction. The barotropic time step is set to 1 second and the baroclinic equations are solved at every three seconds. Table 3.1 shows the parameters used in the simulations, the initial set up refers to a spin up month of December 2007 which is used to provide forcing terms for the full year run (section 3.5). These parameters will be used in all simulations conducted in this study.

3.1.1 POLCOMS

Here we present the model equations solved in POLCOMS model. Firstly, POLCOMS solves the continuity equation:

$$\frac{\partial u}{\partial x} + \frac{\partial v}{\partial y} + \frac{\partial w}{\partial z} = 0 \tag{3.1}$$

where u, v, and w are velocity components, and x, y, x are the direction components.

The governing equations for momentum solved in POLCOMS are based on the Navier-Stokes equation with the Boussinesq Approximation (Cushman-Roisin and Jean-Marie, 2011 edition [25]). Navier-Stokes Equations are derived from Newton's second law of motion, $F = M/A$ and expressed in 3D Cartesian co-ordinates to calculate fluid flow. The Boussinesq Approximation equations were derived for large scale ocean flow by Joseph Boussinesq including terms for the coriolis and stratification (section 2.1). As discussed previously in the chapter, the momentum terms are split into Barotropic and Baroclinic equations,

Barotropic equations:

$$\frac{\partial \bar{u}}{\partial t} = f\bar{v} - (Rcos\phi)^{-1}\left[g\frac{\partial \zeta}{\partial \chi} + \rho_0^- 1\frac{\partial P_a}{\partial \chi}\right] + H_d^- 1[F_s - F_b] + NLB_\chi \tag{3.2}$$

$$\frac{\partial \bar{v}}{\partial t} = f\bar{u} - R^{-1}\left[g\frac{\partial \zeta}{\partial \phi} + \rho_0^- 1\frac{\partial P_a}{\partial \phi}\right] + H_d^- 1[G_s - G_b] + NLB_\phi \tag{3.3}$$

Depth varying, Baroclinic equations:

$$\frac{\partial u_r}{\partial t} = -L(u) - u_r - \frac{uvtan\phi}{R} - \Pi_\chi + D(u) - H_d^{-1}\left[F_s - F_b\right] - NLB_\chi \tag{3.4}$$

$$\frac{\partial v_r}{\partial t} = -L(v) - u_r - \frac{u^2 tan\phi}{R} - \Pi_\phi + D(v) - H_d^{-1}\left[G_s - G_b\right] - NLB_\phi \tag{3.5}$$

Where u and v are the horizontal velocity components, North-South and East-West respectively. u_r and v_r are the baroclinic velocity components, $\bar{u}$ and $\bar{v}$ are depth-average velocity components, f is the coriolis term, R is the radius of the Earth, g is the gravitational constant, ζ is the elevation above reference sea level, χ and ϕ are spherical polar coordinates (east and west respectively), ρ_o is reference density, H_d is total water depth, F and G are bed and surface shear stresses, D is the diffusive term and Π represents the buoyancy term (see Holt

and James [35] and POLCOMS documentation [46] for detailed description of equations). NLB is the non-linear and buoyancy terms;

$$NLB_{\chi} = \int_{-1}^{0} \left[-L(u) + \frac{uvtan\phi}{R} - \Pi_{\chi} \right] d\sigma \tag{3.6}$$

$$NLB_{\phi} = \int_{-1}^{0} \left[-L(v) + \frac{u^2 tan\phi}{R} - \Pi_{\phi} \right] d\sigma \tag{3.7}$$

Where L represents the advection terms and σ is the vertical spherical polar coordinate (See POLCOMS documentation for details). Equations 3.2, 3.3, 3.4, 3.5 are the fundamental equations along with the continuity equation are currently employed in POLCOMS as the basis of all solutions.

3.1.2 GOTM

Turbulence modelling in POLCOMS is limited to the Mellor-Yamada-Galperin 2.5 turbulence closure scheme (Mellor and Yamada 1974 [49], Galperin et al, 1988 [29]) with an algebraic mixing length (POLCOMS Documentation, [46]). The General Ocean Turbulence Model (GOTM) is a one-dimensional stand-alone ocean model which has been developed specifically to be coupled with 3D ocean models and provide higher order turbulence models for use when solving hydrodynamic model equations (GOTM.net, [31]). Based on Umlauf and Burchard, 2005 [72], GOTM has been developed to solve a variety of turbulence schemes including $k-\varepsilon$ and $k-\omega$ by inputting different parameters to the general equation case, as a standalone model or as a coupled model for turbulence modelling as is the case here.

POLCOMS was first coupled to GOTM in Holt and Umlauf [34] and has been used in various studies such as Brown et al, 2011 [20] and Bolaños et al. 2011 [16], showing the good validation against various field datasets, particularly in Liverpool Bay. In the present study, we use the $k-\varepsilon$ turbulence equations

in the GOTM code to simulate the structure impact through the water column for a number of reasons. Firstly, the two-equation turbulence models has been proven to provide a good approximation in previous studies (Brown et al, 2015, [19], Holt and Umlauf, 2008, [34]). We carried out an early analysis not included in this thesis which compared $k-\varepsilon$, $k-\omega$ and the mixing length models and concluded that the $k-\varepsilon$ and $k-\omega$ preformed better than the mixing length model. There were negligible differences between the model outputs $k-\varepsilon$ and $k-\omega$ from therefore when combined with the accuracy shown in the other uses of the POLCOMS-GOTM, the logical choice is to continue with the $k-\varepsilon$ turbulence model.

Parameter	Value
$C_\varepsilon 1$	1.44
$C_\varepsilon 2$	1.92
$C_\varepsilon 3-$	-0.4
$C_\varepsilon 3+$	1.0
σ_k	1.0
σ_ε	1.11

TABLE 3.2: Initial GOTM parameters applied to simulations, Rodi, 1980 [61], Umlauf and Burchard, 2005 [72]

Table 3.2 shows the turbulence options that apply to all model runs in this study and will not change.

POLCOMS has a heavy bias on the vertical component due to the horizontal spatial scales which is in line with other coastal ocean models. The model domain used for this study has a 180m horizontal resolution and vertical resolution of 22 equally space terrain following sigma layers. This leads to several neglected terms which do not warrant the increase in computer resources needed. Horizontal turbulence advection is a neglected term in the standard POLCOMS-GOTM

model, this simulates the horizontal movement of the turbulence through the water. In this study, we simulate the impacts on turbulence therefore this term is a necessary part of the simulation. We discuss this model development in section 3.6.

3.2 Structure Module

The purpose of this thesis is to develop the coding for POLCOMS-GOTM to simulate the impacts of any structure positioned in the water. Here we discuss the equations derived in Rennau et al, 2012, [59] and how they are modified to be applied into the POLCOMS and GOTM governing equations. Firstly, we focus on the momentum equations in POLCOMS because momentum loss is the first step in modelling the effects of offshore structures.

Momentum Equations

The levels of impact from the structure on fluid flow can be represented by using the drag force. The drag force equation takes into account the velocity and density of the surrounding fluid and the size of the object. Based on dimensional analysis, the drag force is found:

$$D = \frac{1}{2} C_D \rho A U^2 \tag{3.8}$$

Where A is the reference area of a structure, U is the velocity and ρ is density. C_d is the drag coefficient determined by experimentation taking skin friction and form drag into account. In this case, it is assumed that the marine structures present a solid orthographic projection perpendicular to the dominant flow of the water.

When applying the momentum loss equation to a structured ocean model and the horizontal resolution is greater than the size of structure, i.e. they are

not directly resolved, a spatial averaging method is needed. This means a force balance across the control volume to simulate the number of structures in any one grid is used.

Following the derived equations in Rennau 2012 [59], a drag equation modified for geophysical ocean models is obtained.

Starting with the standard drag equation;

$$D = \frac{1}{2} C_D \rho A_D u^2 \tag{3.9}$$

The mass of the water in the cell equals;

$$mass = \rho h A_s \tag{3.10}$$

Where h is height of the water column and A_D is area of drag and A_s is horizontal area of the cell.

$$\frac{mass}{unit\ height} = A_s \rho \tag{3.11}$$

$$G = \frac{\frac{1}{2} C_D \rho d U \sqrt{u^2 + v^2}}{A_s} \tag{3.12}$$

$$G = \frac{\frac{1}{2} C_D d U \sqrt{u^2 + v^2}}{A_s \rho} \tag{3.13}$$

Where G is total impact term, u and v are velocity components, east-west and north-south respectively, U is velocity. For multiple structures in one cell, equation 3.13 can be multiplied by the number of structures, N.

$$G_d = \frac{1}{2} C_D a U \sqrt{u^2 + v^2} \tag{3.14}$$

Where:

$$a = \frac{Nd}{A_s} \tag{3.15}$$

Where d is the diameter of the structures and A_s is the horizontal face area of the cells. The area of influence is the spatial area in which structures are impacting, for example given one structure in a POLCOMS grid cell, the area of influence would be the horizontal area of that grid ($180m \times 180m$). This equation can simulate the effects of structures present in the water column by considering a force balance over a control volume corresponding to the grid size. As a result, a structure that is relatively small compared to the cell size can be represented without the need to reduce the grid size.

The method used to implement the equations into the model has been intentionally kept simple to reduce computational time. In the first time step of the model simulation we create a global C_D map. This map is the size of the domain and contains C_D values where structures are present and zero elsewhere. This eliminates the need for if statements for every calculation step to determine where the structures are and allows the user to input individual C_D terms at each sigma level giving maximum flexibility. A large part of the momentum reduction equations are the same in both directions, therefore this part can be calculated only once for each time step.

$$G_{d(partial)} = \frac{1}{2} C_D a \sqrt{u^2 + v^2} \tag{3.16}$$

Equation 3.16 represents the part of the modified drag equation that is solved only once for each cell at the time step. This leads to equation 3.17 which represents the full equation, simply multiply $G_{d(partial)}$ by the appropriate velocity component, v_{ij} or u_{ij}.

$$G_d^u = u \times G_{d(partial)}, G_d^v = v \times G_{d(partial)} \tag{3.17}$$

This method is the most efficient method of calculation of the drag effects. The FORTRAN subroutine calculates this for each cell and subtracts it in the governing equations to produce the momentum loss effects for the structures.

$$G_d^u = \frac{1}{2} C_D a u \sqrt{u^2 + v^2} \tag{3.18}$$

$$G_d^v = \frac{1}{2} C_D a v \sqrt{u^2 + v^2} \tag{3.19}$$

These equations are applied directly into the geophysical momentum equations as a sink term.

$$\frac{Du}{Dt} - fv + G_d^u = -\frac{1}{\rho_0}\frac{\partial p}{\partial x} + \frac{\partial}{\partial x}\left(A\frac{\partial u}{\partial x}\right) + \frac{\partial}{\partial y}\left(A\frac{\partial u}{\partial y}\right) + \frac{\partial}{\partial z}\left(\nu_E\frac{\partial u}{\partial y}\right) \tag{3.20}$$

$$\frac{Dv}{Dt} - fu + G_d^u = -\frac{1}{\rho_0}\frac{\partial p}{\partial x} + \frac{\partial}{\partial x}\left(A\frac{\partial v}{\partial x}\right) + \frac{\partial}{\partial y}\left(A\frac{\partial v}{\partial y}\right) + \frac{\partial}{\partial z}\left(\nu_E\frac{\partial v}{\partial y}\right) \tag{3.21}$$

By mode splitting 3.18 and 3.19 and applying directly in the momentum equations in POLCOMS for u and v, the structures are simulated in the momentum across all sigma levels. Barotropic equations:

$$\frac{\partial \bar{u}}{\partial t} = f\bar{v} - (Rcos\phi)^{-1}\left[g\frac{\partial \zeta}{\partial \chi} + \rho_0^- 1\frac{\partial P_a}{\partial \chi}\right] + H^- 1[F_s - F_b] + NLB_\chi \tag{3.22}$$

$$\frac{\partial \bar{v}}{\partial t} = f\bar{u} - R^{-1}\left[g\frac{\partial \zeta}{\partial \phi} + \rho_0^- 1\frac{\partial P_a}{\partial \phi}\right] + H^- 1[G_s - G_b] + NLB_\phi \tag{3.23}$$

Depth varying, Baroclinic equations:

$$\frac{\partial u_r}{\partial t} = -L(u) - u_r - \frac{uvtan\phi}{R} - \Pi_\chi + D(u) - H^{-1}\left[F_s - F_b\right] - NLB_\chi - G_d^u \quad (3.24)$$

$$\frac{\partial v_r}{\partial t} = -L(v) - u_r - \frac{u^2tan\phi}{R} - \Pi_\phi + D(v) - H^{-1}\left[G_s - G_b\right] - NLB_\phi - G_d^v \quad (3.25)$$

$$NLB_\chi = \int_{-1}^{0}\left[-L(u) + \frac{uvtan\phi}{R} - \Pi_\chi + G_d^u\right] d\sigma \quad (3.26)$$

$$NLB_\phi = \int_{-1}^{0}\left[-L(v) + \frac{u^2tan\phi}{R} - \Pi_\phi + G_d^v\right] d\sigma \quad (3.27)$$

Where NLB is the term dealing with mode splitting of non-linear terms such as the advection, L term. The impact term, G_d (equation 3.18 and 3.19) are non-linear terms, therefore we utilize this method in POLCOMS to mode split the equations. At this stage, POLCOMS can simulate the impacts of structures in the momentum governing equations at all water levels. The next step is to look at the GOTM k $-$ ε equations and include the structures effect on the turbulence.

Turbulence impacts

The balance equation for TKE impact in the turbulence model can be derived from the momentum equations, Additional terms in the momentum equations will thus result in additional terms in the turbulence balance (k and ε for the k $-$ ε model).

To simulate the impact of structures in GOTM we include a production term P_d (equation 3.28) directly into the turbulence equations. The term is obtained when the k equation is derived from the momentum equations (3.20), (3.21) and P_d is constituted from the components which are included to simulate the momentum loss.

$$P_d = \frac{1}{2} C_D a \left(u^2 + v^2\right)^{\frac{3}{2}} \tag{3.28}$$

This equation is applied directly into the production term in the turbulent equations in GOTM by applying equation 3.28 into the turbulent kinetic energy and dissipation equation:

$$\frac{\partial k}{\partial t} + u\frac{\partial k}{\partial x} + v\frac{\partial k}{\partial y} + w\frac{\partial k}{\partial z} - \frac{\partial}{\partial z}\left(\frac{A_v}{\sigma_k}\frac{\partial k}{\partial z}\right) = P + P_d + B - \varepsilon \tag{3.29}$$

$$\frac{\partial \varepsilon}{\partial t} + u\frac{\partial \varepsilon}{\partial x} + v\frac{\partial k\varepsilon}{\partial y} + w\frac{\partial \varepsilon}{\partial z} - \frac{\partial}{\partial z}\left(\frac{A_v}{\sigma_\varepsilon}\frac{\partial \varepsilon}{\partial z}\right) = \frac{\varepsilon}{k}\left(c_1 P + c_4 P_d + c_3 B - c_2 \varepsilon\right) \tag{3.30}$$

P is extra production term and B is the buoyancy production. Using this method, the effects are simulated through the water column.

Rennau 2012, [59] uses a calibration method to determine the value of c_4 in stratified flow which includes simulating a range of froude numbers and a range of c_4 values which resulted in using 0.6 for the high mixing scenario and 1.4 as the low mixing scenario. A high mixing environment is generally considered to be an area of high vertical instabilities such as a ROFI. This method uses the assumption that the mean kinetic energy transfers directly into mean turbulence kinetic energy ignoring the energy cascade process. As a direct result we assume that the wake recovery is less than the horizontal representation. This is a reasonable assumption because typical wake recovery lengths behind a device are less than 10 diameters of the cylinder (Batten et al, 2013 [13]). The coefficient c_4 is taken as 0.6 as the high turbulence case (Rennau 2012, [59]) for the remainder of this project, this is because Liverpool Bay is an area of high mixing.

This module has been specifically designed to be as generic as possible allowing us to use the module for as many different scenarios as necessary. There

are several parameters that are required for the simulations to work. Table 3.3 provides details of those parameters and which are hard coded and which are input parameters for the model run with OWF present.

Parameter	Input method
Diameter of OWF	Hard coded (input system in place)
Area of influence	Retrieved from coding
Number of Turbines	User input
Drag coefficient	hard coded (input system in place)
Cells with structures	User input
Number of Turbines	User Input

TABLE 3.3: Turbine module parameter input method

Table 3.3 shows the list of input conditions and how they are submitted in the module used in this study. User input refers to terms that can be specified in the 'turb.dat' file which controls the number of arrays and the position in terms of i,j points in the domain. Hard coded terms have to be changed before the program is compiled. There is scope to replace these hard coded terms as user inputs in the future. The input file structure used is such that we can specify any number of impacted cells in the domain allowing the user to create several arrays containing a differing number of structures of the same type, for example two separate wind farm placements (section 3.5). As such we now have a flexible analysis tool which is used in the Liverpool Bay region of freshwater influence.

3.3 Turbine Representation

The parameterization technique used here means the structure being simulated is averaged across the horizontal grid (in this study 180m x 180m). We use a 4m diameter cylinder through the water column as the representation for the

structures in this study, this size is a typical size of OWF foundations, but very small compared to the grid size. This is a reasonable size to simulate as OWF foundation structures range from 4m to 7m depending on size of turbine and size restraints. However turbines are positioned further apart to accommodate the swept areas which are between 100m-200m in diameter and wake recovery, taking this into consideration two methods of simulating an array in the domain have become possible.

A so-called control volume method uses the spatial area of the OWF and averages the total impacts of all the turbines across the area of influence.

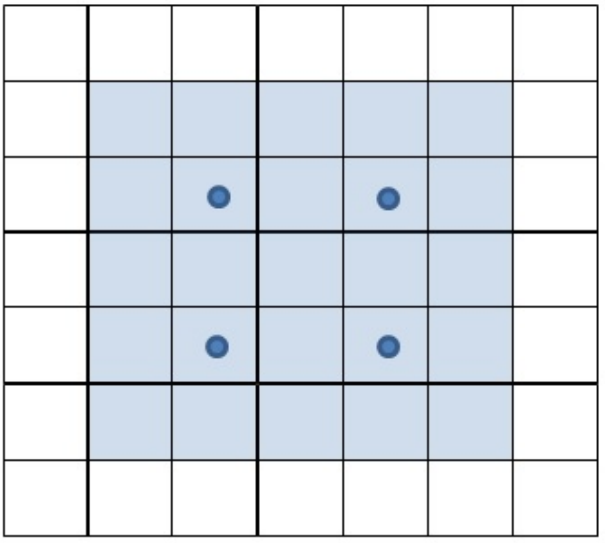

FIGURE 3.2: Example control volume for OWF representation in domain. Blue dots represent turbine structures, blue shading represents impacted cells

Figure 3.2 shows the control volume method, where the blue shaded area represents the impacted cells and structures are blue dots. This method has many benefits including this being the simplest to represent an OWF. Using this method the OWF becomes the smallest unit of impact. Another added benefit is that this method reduces the shock generated in the governing equations particularly in the early simulation run, which is particularly important at the beginning of a simulation where the gradient increases significantly due to the

sudden change in momentum and turbulent kinetic energy. Using this method the impacts from all the turbines are averaged across a larger spatial area, therefore reducing the gradients involved.

The second method is to represent each turbine individually, this means there are free un-impacted flow cells through the OWF.

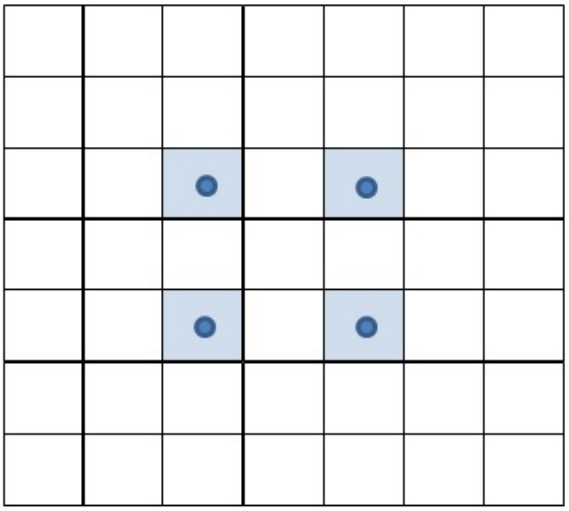

FIGURE 3.3: Example individual cell representation method. Blue dots represent turbine structures, blue shading represents impacted cells

Figure 3.3 is a pictorial representation of the individual volume method, impacted cells are represented by a blue shade and the structures are represented as a blue dot. This method represents the OWF in greater resolution by having one turbine per cell. In the Liverpool Bay domain used in this study the mesh resolution is 180m, which means we can simulate two clear cells between turbines and the flow within the arrays can be modelled. This method simulates the hydrodynamic impacts on the same resolution of the model. This removes the assumption that all cells within the OWF footprint are affected. However, it has great effects on the model stability.

In this study we will do a sensitivity analysis (Chapter 4) to assess the hydrodynamic effects of both methods of parametrization and give reasons for carrying on with one method.

3.4 Liverpool Bay

We now discuss the study area that will form the basis of this study. Liverpool Bay is a semi-enclosed hyper tidal (spring tidal amplitude in excess of 10m) coastal sea located in the eastern Irish Sea (Figure 3.4). The area is surrounded by land on two sides, North West England to the east and the North Wales coast to the south and has two open sea boundaries to the west and north. The area is a salinity driven region of freshwater influence (ROFI) which gives rise to a sharp salinity front resulting from the freshwater inflow from The Mersey, Dee, Ribble, Conwy and Clywd and several smaller rivers (Hopkins and Polton, 2012 [38]. There have been previous studies on the dynamics of Liverpool Bay for a number of years. Strain-induced Periodic Stratification (SIPS) was initially tested using Liverpool Bay as the test case (Simpson et al, 1993, [66]) which proves to be an ideal case for the theory. Experimental measurements (Sharples and Simpson, 1995 [64], Bolanos and Souza, 2010 [17]) have been used to analyse the ocean circulation by either mobile CTD instruments towed behind ships or stationary acoustic rigs used to measure a variety of hydrodynamic properties. These datasets have been used to make observations of the ocean circulation in the region, which have ultimately led to a detailed understanding of the processes contributing to the flow patterns in Liverpool Bay.

FIGURE 3.4: Map of the United Kingdom, red square highlights Liverpool Bay.

The tide in the bay is a near-perfect standing wave resulting from a Kelvin wave reflecting on the Sefton coast (Rippeth et al, 2001 [60]). The tidal ellipse is almost completely rectilinear with a dominant east-west component (Simpson et al, 1990 [67]) and a horizontal salinity gradient flows through the area due to the freshwater influence.

Recently, Liverpool Bay has seen significant development of offshore wind-farms. North Hoyle was the first OWF commissioned in UK waters; it has 30 deployed turbines situated north-west of the Dee estuary (Figure 3.5). Burbo Bank was commissioned later in 2007 containing 25 structures situated in the Mersey freshwater plume close to the deep water shipping channel from the Port of Liverpool (Figure 3.10). Both sites were part of the first round of leasing (www.renewableuk.com [2]) which limited OWF's to 90 MW capacity spread over a 10 km^2 spatial area.

Up to date, there are over 250 installed OWF in Liverpool Bay spread over four OWF sites to date with further extensions at various stages of planning (www.4coffshore.com, 2014 [1]). At a simple conceptual level, OWF's may have an effect on the dynamics simply because they will obstruct the water flow, and the flow-structure interaction will generate drag and turbulence. In 2008, North Hoyle and Burbo Bank were the only OWF's constructed in the area and they are situated near the outflow of the Dee and Mersey estuaries and close to the freshwater front. Using this arrangement allows us to simplify the set-up and enables a rigorous assessment of the model's ability to study OWF's impacts. Year 2008 is understood to be a typical year, atmospheric and hydrodynamic inputs prove to be consistent with the 7-year average (Norman et al. 2014 ([54])) and thus provides a valuable background for extrapolating the analysis of model results to other years. This study employs the simple set up in order to understand the baseline impacts a number of structures has on hydrodynamics and testing our conceptual understanding that such structures do have an effect on environmental dynamics in coastal and shelf seas. Figure 3.5 shows the positions of the OWF's in 2008 which were at various stages of development.

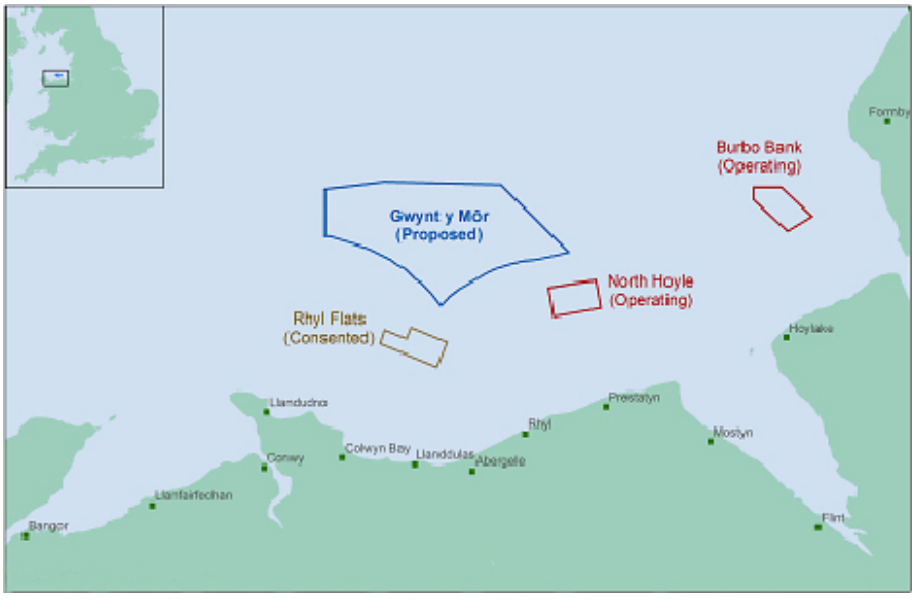

FIGURE 3.5: Liverpool Bay windfarms, 2008, www.offshorewind.biz, 2015

3.5 Model Set up

We now discuss the model domain used in POLCOMS. The freshwater is applied at a single point as daily averages, Figure 3.6 shows the positions for the five major sources in the domain.

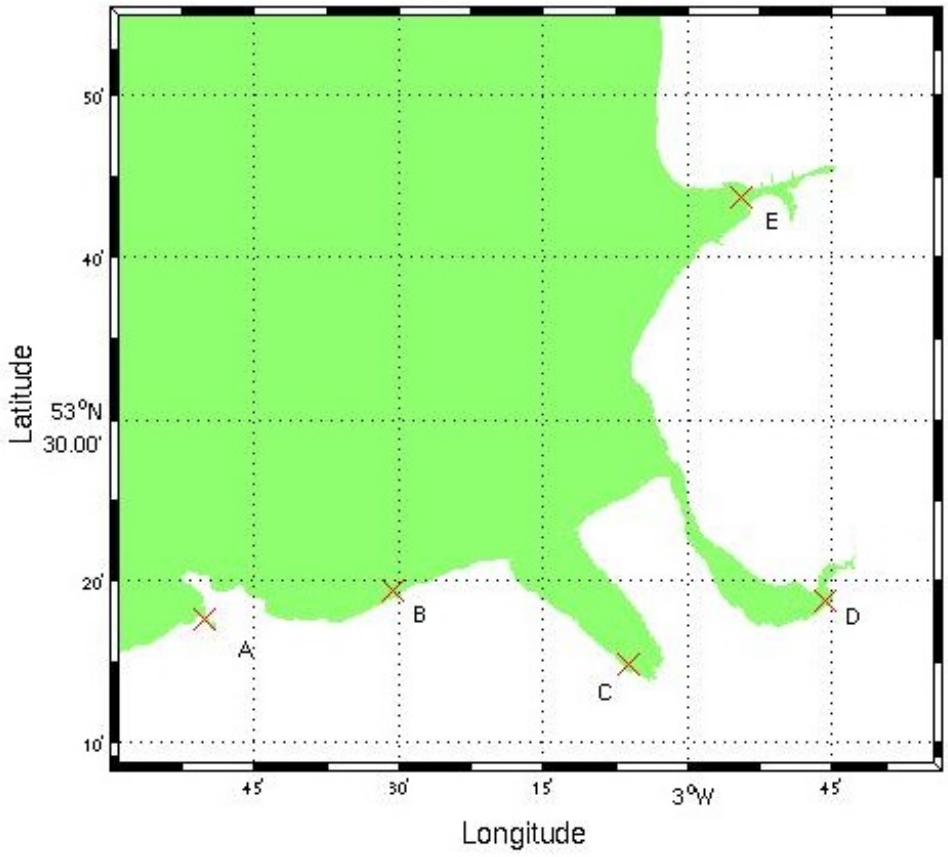

FIGURE 3.6: Domain showing the freshwater input conditions, A) Conwy, B) Clywd, C) Dee, D) Mersey, E) Ribble.

To represent the ROFI process, its crucial to get accurate input of fresh water in the domain. The freshwater input is provided by the Environmental agency, via CEH at daily averaged intervals (Brown et al [19]) . Below the yearly inflow is plotted for the large estuary systems which provide the greatest proportion of freshwater into the bay in Figure 3.7 to 3.9.

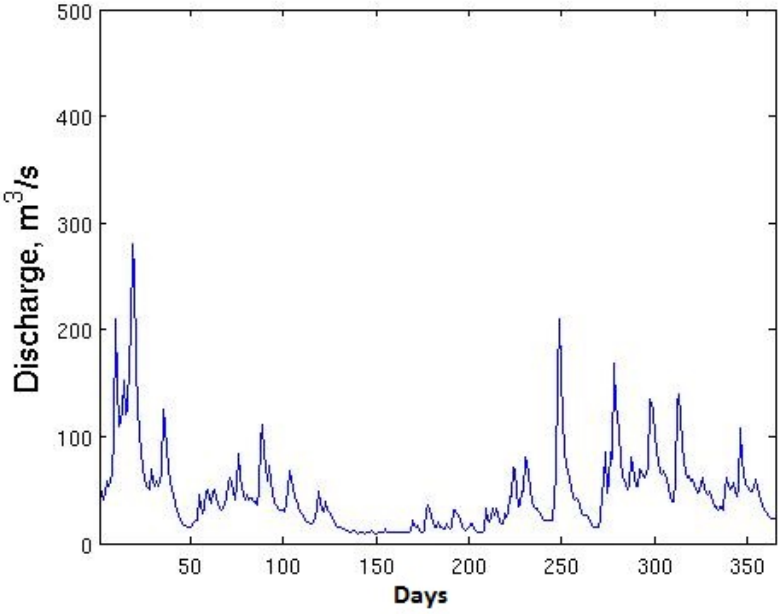

FIGURE 3.7: River Dee input forcing for 2008.

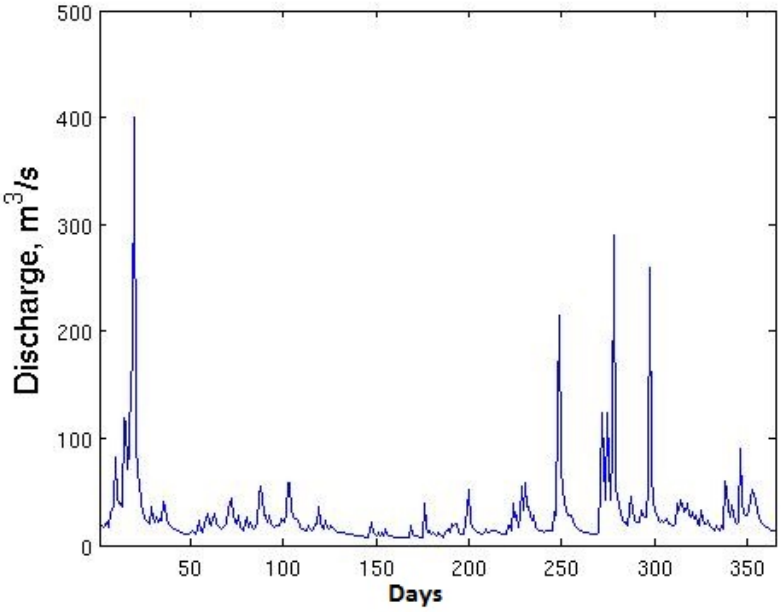

FIGURE 3.8: River Mersey input forcing for 2008.

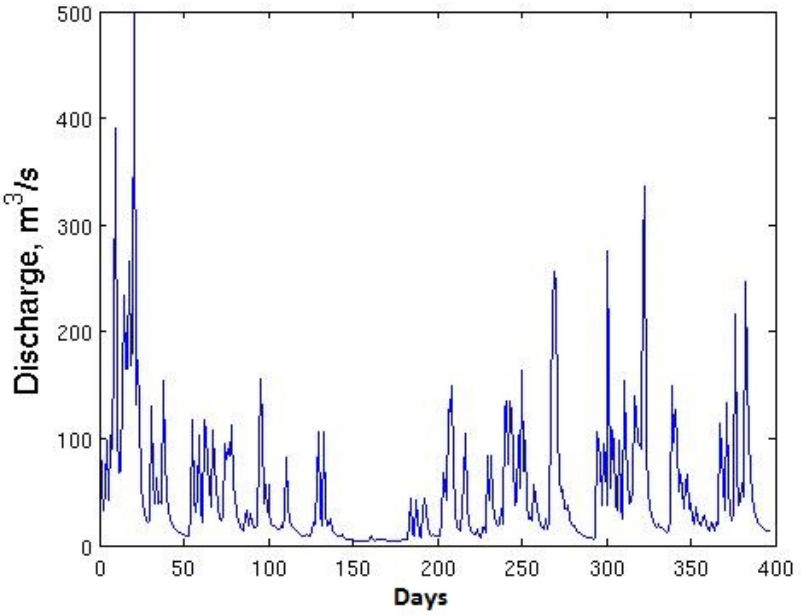

FIGURE 3.9: River Ribble input forcing for 2008.

Due to the wetting and dry element of the code that simulates inter-tidal flats along the coast, the freshwater is introduced as a timeseries in an area that is permanently wet. The point is fixed at 0 PSU which mixes very quickly to form estuarine brackish waters over a few horizontal grid cells, Brown et al, (2015) [19]. The freshwater is included under the assumption that the river temperature is equal to the inland atmospheric temperature at the river source. Which leads to the possibility to include a seasonal river temperature.

Parameter	Source
Atmospheric Forcing	3 hourly intervals from the UK Met Office
Sea boundaries (water levels and velocities)	Atlantic Margin Model
River boundaries	Environmental Agency

TABLE 3.4: Source of boundary conditions and forcing

Table 3.4 shows the sources of the boundary condtions. Atmospheric forcing is provided at 3 hourly intervals from the UK Met Office operational Mesoscale model hindcast at 12km horizontal resolution (Brown et al. 2015 [19]). Water level and flow velocities along the open sea boundaries are provided following a one-way nesting method (e.g. Howarth et al. 2005 [39]) in the Irish sea model which is forced using hourly inflow data for velocity, salinity and temperature from the pre-operational Coastal Observatory (COBS) Atlantic Margin Model (Neil et al. 2012 [55]) and in turn provides the sea boundary forcing for Liverpool Bay model used in this study.

The calculation is spun up from initial conditions generated from the COBS pre-operational modelling suite and ran from November 2007 using the climatological rivers across the Irish sea (Brown et al, 2015 [19]). Then the Liverpool Bay model is spun up in December 2007, to reach a new equilibrium with the more realistic river inflows and the structure inclusions.

To reduce the mathematical shock induced by the structures, we use a parameter ramping method which over the period of December 2007 gradually introduces the structure sink term so by the end of the month the model reached equilibrium with full structure effects activated.

We make one assumption in this study that there is no effects from the structure in airflow. In reality wind turbine foundations have a wind turbine structure above the water which will have impacts of the wind. However, on order to fully represent such effects, POLCOMS would need to be two way coupled with an atmospheric model, itself with modifications to simulate the structures above the sea surface. In the present state POLCOMS-GOTM uses the 12km resolution atmospheric model using a one way coupling method Developing a two way couple atmospheric-hydrodynamic model with structure impact from wind turbines is beyond the scope of this project.

The Liverpool bay domain we use here has a horizontal resolution of $180m \times 180m$ and uses vertical terrain following sigma layers to simulate the vertical

flow characteristics, we use 22 layers for this study. The horizontal resolution is based on the approximate rosby radius (200m) and the vertical resolution is a balance between vertical resolution and computational efficient. Figure 3.10 shows the bathymetry domain map used in this study which was obtained using depth measurements and ranges from $3.8°W$ to $3°W$ horizontally and $53.25°N$ to $53.65°N$ vertically. In total there are 576 in the eastern and 474 in the northern direction.

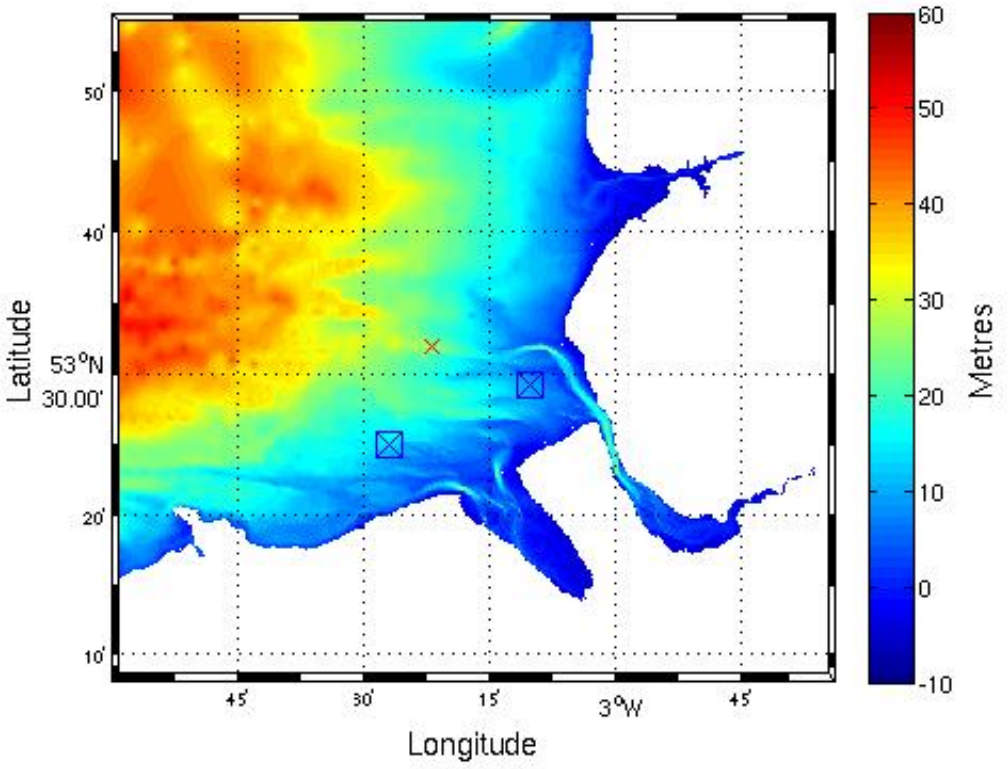

FIGURE 3.10: Bathymetry domain, Liverpool Bay showing site A (small red cross) and centre of two wind farms, North Hoyle to the left and Burbo Bank in the right represented by the blue squares.

3.6 Horizontal Turbulence Advection

As part of the initial set up for this thesis, we need to develop POLCOMS to include the horizontal turbulence advection term. This is used to simulate the horizontal turbulence transport which is vital to show the turbulence impacts in the wake of the offshore structures. As such, we utilized the piecewise parabolic method (PPM) (James 1996, [43]) used to solve the momentum advection and applied that here. The following results show a simple comparison between two models, one with horizontal turbulence advection (hereafter known as WA) and a control model containing no horizontal advection (hereafter known are CA). All other parameters are as described in table 3.1 for POLCOMS and 3.2 for GOTM, wind forcing and freshwater inflow are as described above. This study was used to assess the impacts in numerical results due to the horizontal turbulence advection..

The model results has been obtained using the model set-up for 2008 (section 3.5) in Liverpool Bay for the advection and non-advection model. We focus on the time series in March of the vertical profiles of Velocity and Turbulence Kinetic Energy (TKE) taken at the location of Site A where mooring was deployed (Polton et al, 2011 [57]).

3.6.1 Results

All figures present water elevation in the top panel, simulation with advection in the second panel, simulation without advection of turbulence in the third panel and the differences induced by the addition of the turbulence advection term in the bottom panel. Each panel is plotted against time in days. We have selected a period of time in March ranging for a spring tide to neap tide. This was selected because it was the period of time where the results are at maximum effects for the study period.

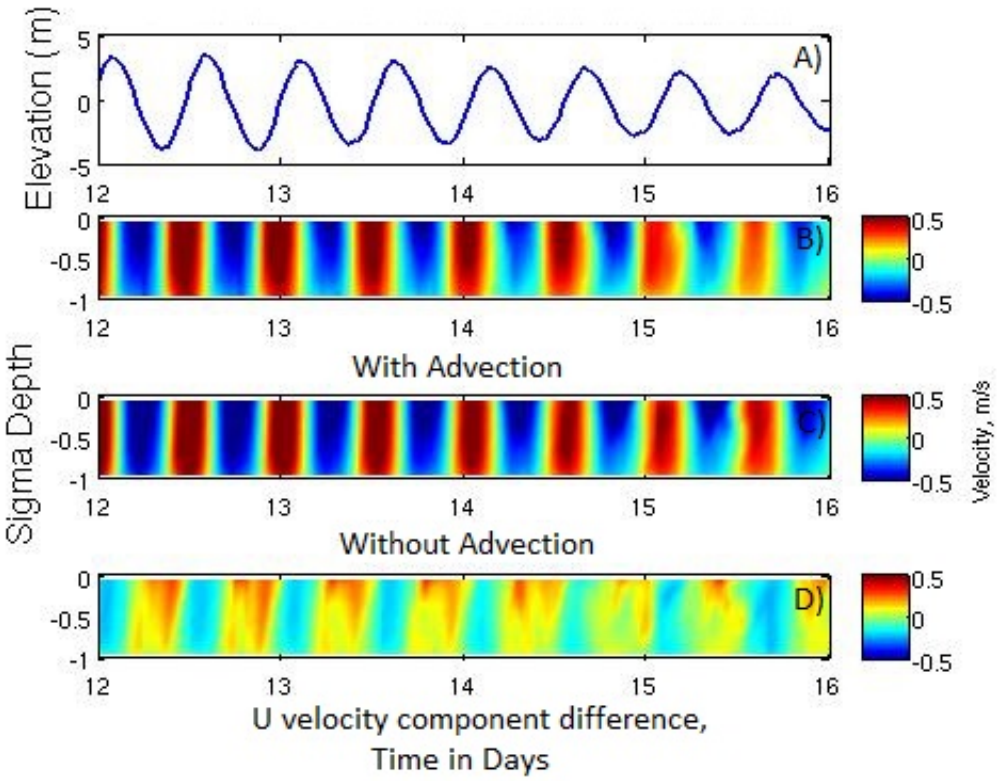

FIGURE 3.11: Comparison of u component at Site A, a) Elevation, b) u with Advection, c) u without Advection, d) u difference, $WA - CA$. Plot is the time series taken at the Site A located in Liverpool Bay.

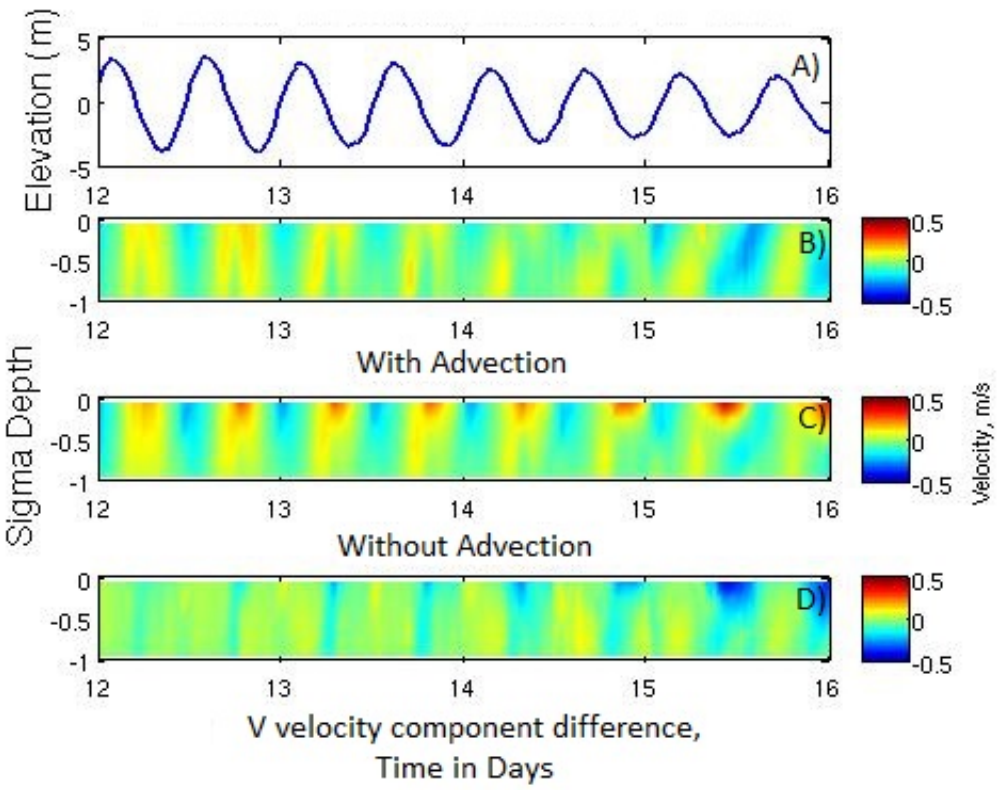

FIGURE 3.12: Comparison of v component at Site A, a) Elevation, b) v with Advection, c) v without Advection, d) v difference, $WA - CA$. For plot description see 3.11

Figures 3.11 and 3.12 shows the u and v velocity components respectively at Site A over a 4 day time period. The difference plot on Figure 3.11 shows WA-CA which shows a decrease in u during surface ebb and a slight change in timing phase due to the inclusion of advection. The early flood and ebb stratifications are intensified in contrast to the late flood and ebbs which are weakened. Towards the neap tide the velocity differences between the models decrease. Figure 3.12 shows the V component changes are small, the only obvious effects can be found near the surface towards the neap tide. A reason for this is that the u velocity component (East-West current) is the tidally dominant component and as such

the largest changes can be found due to the inclusion of horizontal turbulence advection.

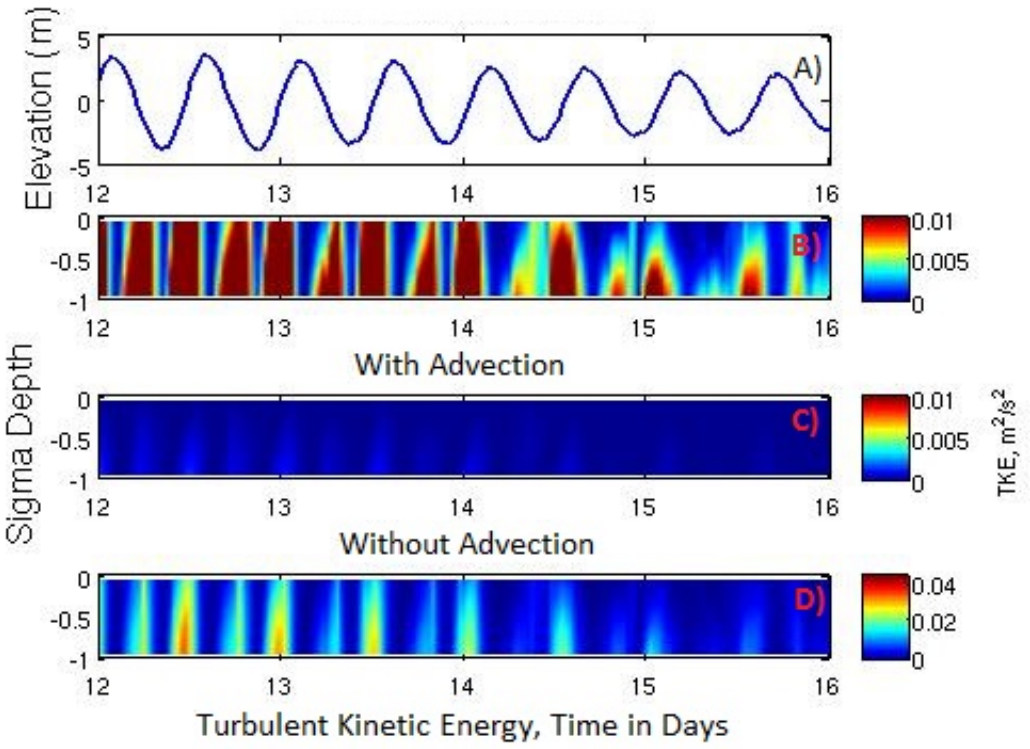

FIGURE 3.13: Comparison of Turbulent Kinetic Energy component at Site A, a) Elevation, b) TKE with Advection, c) TKE without Advection, d) TKE difference, $WA - CA$

Figure 3.13 shows the comparison of TKE for with and without advection term as previous. The bottom plot on the Figure shows the difference between WA and CA. Horizontal turbulence advection has caused a higher level of TKE through the point at the monthly high spring tide. This shows the horizontal turbulence advection does have an impact on the TKE therefore it will be included from now on.

We have shown here that although there are changes in computed velocities and tke, the amount of change has a minimal impact on the domain in this

model. However, it is essential to consider the full impacts on turbulence from any structure therefore the inclusion of this term in the hydrological calculations is paramount to fully consider the effects of the local source of turbulence generated by the structure.

Chapter 4

Impact of the Spatial Averaging Scale in Parameterisation of OWF's in Coastal Ocean Models

Two parameterisation approaches are presented, a so-called 'farm-averaged' parameterisation and an 'intra-tidal resolving' approach, each of which has its advantages and disadvantages. We will now provide a comprehensive comparison of these two modelling approaches, with the aim to determine which method enables the best compromise between result accuracy and model stability. To that end, we will investigate the impacts obtained using each method following the model setup described in section 3.5.

Specifically, this comparison will enable testing whether having unaffected grid cells within the wind farm without sufficient resolution to fully resolve the structure flow patterns around structures will lead to erroneous numerical results.

4.1 Two Spatial Averaging Schemes

We use the Liverpool domain described in section 3.4. We will simulate the OWF's, North Hoyle and Burbo bank in the domain using the two methods

introduced in section 3.3.

Model	Representation	No. of OWF's	No. of impacted cells
F	Farm (wide spatial) averaged	2	578
T	Single turbine (spatial) average	2	55

TABLE 4.1: Sensitivity model set up shows model and parameters for T and F using representation methods discussed in section 3.3.

The main difference between the two methods is the scale of the implied spatial averaging. The Farm Average method calculates an average value over the cells within the OWF boundary, whereas the Single Turbine Average method applied the impact of each structure in the cell where it is situated (for further details see section 3.3).

First we will discuss the advantages and disadvantages of the Farm Average method. The main advantage of this method when compared to the 'Single Turbine Average' method is it preserves some continuity through the spatial discretization. While this would also be satisfied with a fully resolved model ie sufficient resolution to resolve intra-tidal farm motions, the Single Turbine Average approach at sufficient resolution may introduce errors in the and thus generate numerical error and instabilities.

The total number of physical structures is the same in both models, the difference between the methods comes in the number of cells the impact is spread across, which leads to a second advantage. The farm average method has 578 cells with the impacts from 55 turbines involved, across allowing the horizontal gradient between the affected cells and unaffected cells at the OWF boundary to be minimised. Another advantage is that this method is more appropriate when the horizontal scales are very large. In particular, using the farm average

method would be have to be used where the horizontal grid is greater than the gap between the two turbines.

The single structure method in the Liverpool Bay domain represents each structure in the cell where the turbine is placed. This method can also create the correct pattern of the OWF and can use the resolution to potentially see fine details of the flow. There are several drawbacks to apply this method in Liverpool Bay. The main drawback revolves around the potential errors discussed above that this method can potentially create. The gradients between unaffected cells and impacted cells are amplified in comparison to the farm average method. In the following section, we will provide a comprehensive validation of the structure model used in this study.

4.2 Validation of the Structure Model

The model domain contains two wind farms, North Hoyle and Burbo Bank (table 4.2) which is in line with the total number of turbines present in 2008. North Hoyle contains 30 turbines and Burbo Bank contains 25 turbines. We have set the diameter at 4m for all the structures with drag coefficients (C_D) of 0.63 which is the coefficient for a 3D cylindrical structure. The coefficient the engineering drag coefficient for a 3D cylinder. Freshwater from the Environmental Agency (EA) and UK Met Office atmospheric forcing are used as described in 3.5. We parametrize the OWF using the Farm Averaged method for this validation by comparing a vertical profile at site A (Figure 3.10) from experimental data (Polton et al, 2011 [57]) water profile data from a mooring recording in the water column. Salinity and temperature were recorded by CTD probes and velocity measured by ADCP's. There is data for most of the year, however due to the nature of Liverpool Bay the experiment fails at several times for the bottom hydrodynamics. Site A is a useful site due to its proximity to both OWF's

placements and the freshwater plumes from the Mersey, Dee and Ribble estuaries. As a consequence the site data are used on numerous occasions in the study to investigate the vertical intertidal response.

OWF	Centre Position	Number of Structures	Footprint
North Hoyle	-3.448°N, 53.417°W	30	$10km^2$
Burbo Bank	-3.187°N, 53.488°W	25	$10km^2$

TABLE 4.2: Offshore wind farm information in Liverpool Bay in 2008 used in this study

We use the set up for the full impacts (discussed in section 3.5) for the turbine structures to validate the new module. In the Figures below we plot the salinity, temperature and density model data and field data at three levels in the water column, 5m below the surface, 10m below the surface and 0.5m above the seabed.

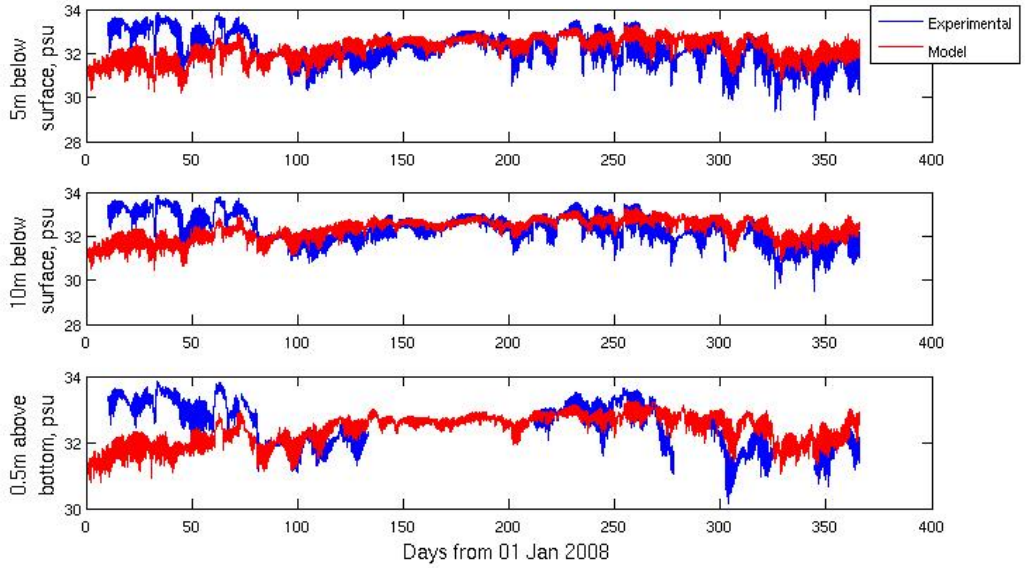

FIGURE 4.1: Salinity comparison; a) 5m below surface b) 10m below surface c) 0.5m above seabed, Site A, Blue is field data and red is the model data.

Figure 4.1 shows the salinity time series profile at site A. The blue line is the field data and the red line is the model data at the locations in the water column. The model initially fails to predict the salinity, this is in line with other studies using the POLCOMS-GOTM modelling system over this period of time (Bolaños et al, 2011 [16], Brown et al, 2015 [19]) and is probably due to imperfect initial conditions. There are a variety of ways this could be caused most revolving around initial conditions and forcing. Solving this issue is not the focus of this study therefore for the remainder of this project we discount the first two months of the year. March through to December yearly trend of salinity at site A is predicted very well all throughout the water column. Some tidal fluctuations in the autumn months are not modelled well, this is could be due to the meteorological forcing terms or the inability for the model to replicate the such large changes because of some unforeseen condition. This could be a large storm event that is not simulated in the atmospheric model hence is not replicated.

.

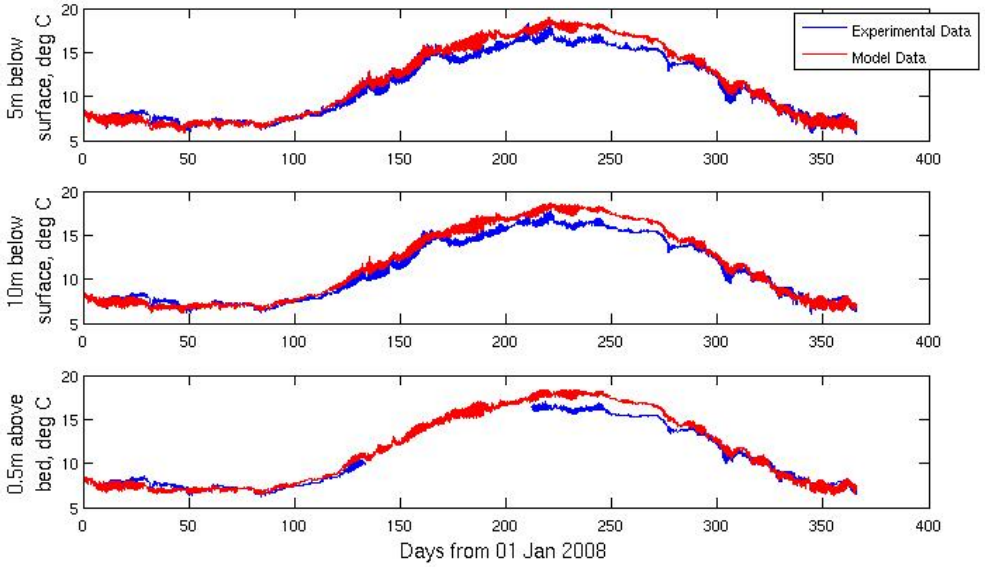

FIGURE 4.2: Temperature comparison; a) 5m below surface b) 10m below surface c) 0.5m above seabed, Site A, Blue is field data and red is the model data.

Figure 4.2 shows the temperature time series profile at site A. As in Figure 4.1 the blue time series is field data and the red time series is the model data. The model data predicts the temperature very well through the entire water column. There is a slight over prediction during the summer period however this is very small.

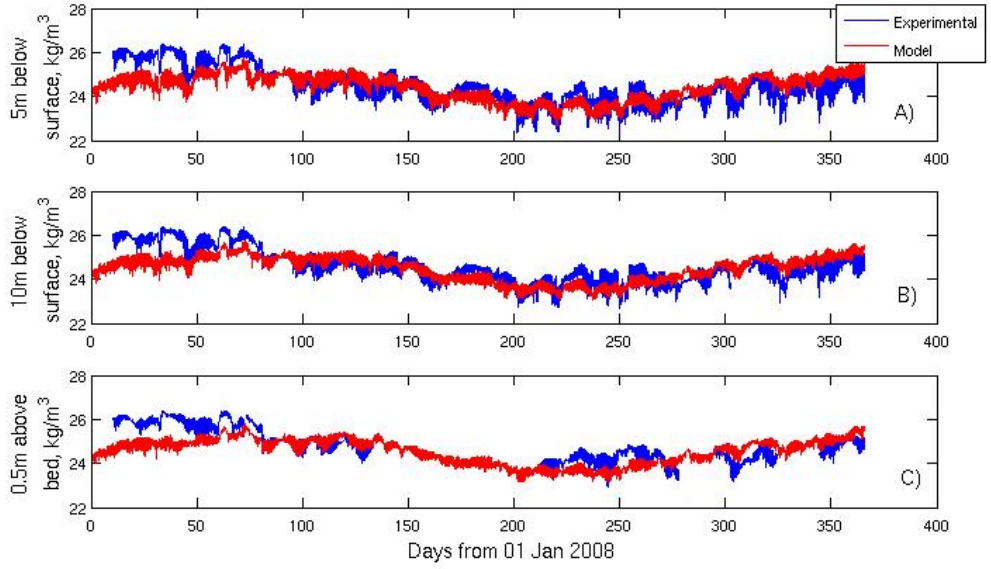

FIGURE 4.3: Density comparison time series; a) 5m below surface b) 10m below surface c) 0.5m above seabed, Site A, Blue is field data and red is the model data.

Figure 4.3 plots the density profiles through the water column calculated from the salinity and temperature using the UNESCO equation of state (POLCOMS Documentation, [46]). The initial period in the year are under predicted, this is due to the salinity contribution which is under-predicted across the same time period early in the year. Liverpool Bay is salinity driven region of freshwater influence therefore salinity does have a larger effect on the density. The density predictions recover to levels that can be used at the beginning of March, as with the salinity case, we consider the data from March through December. Over this period the model predicts the density profile reasonably well. We plot here the 25-hour moving average to filter density to show the effects without the tidal differences.

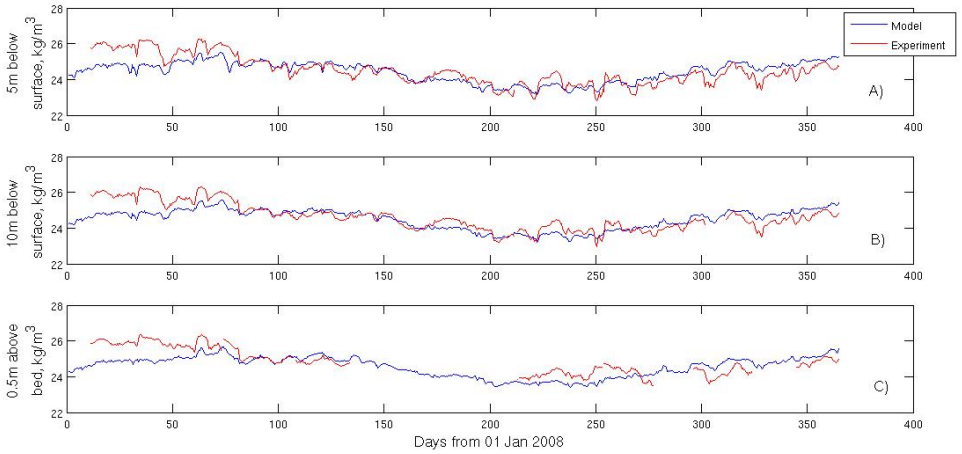

FIGURE 4.4: Density comparison time series, 25 hour filtering process; a) 5m below surface b) 10m below surface c) 0.5m above seabed, Site A, Blue is field data and red is the model data.

Figure 4.4 confirms the argument that POLCOMS-GOTM with structures does predict the density well with only a few fluctuations that are missed.

Figure 4.1, 4.2, 4.3 and 4.4 presents a graphical representation of the ability of the POLCOMS-GOTM model to predict the hydrodynamics. Now we consider a statistical analysis comparison using the skill values (Willmott 1981, [76]). This provides a statistical comparison on which to evaluate the ability of the models and to see which is more statistically accurate. We chose Skill values to compare because they were specifically designed for tidal analysis.

$$1 - \frac{\sum |X_{model} - Xobs|}{\sum \left(|X_{model} - \overline{X_{obs}}| + |X_{obs} - \overline{X_{obs}}| \right)} \tag{4.1}$$

Where X_obs is equal to observational data, $\overline{X_{obs}}$ is the associated time mean and X_{model} is the model data. A Skill value of 1 is a perfect match and complete disagreement is 0.

Parameter	Control	Full
U	0.97	0.97
V	0.79	0.80
rho5	0.82	0.83
rho10	0.84	0.76
rhoB	0.76	0.76
T5	0.99	0.99
T10	0.99	0.99
TB	0.99	0.99
S5	0.54	0.55
S10	0.54	0.55
SB	0.47	0.49

TABLE 4.3: Skill Values (Willmott 1981, [76]) for C, M and F simulation runs at site A. U and V represent velocity components. rho5, rho10 and rhoB represent density at 5m below water level, 10m below water level and 0.5m above seabed respectively. T5, T10 and TB represent temperature at 5m below water level, 10m below water level and 0.5m above seabed respectively. S5, S10 and SB represent salinity at 5m below water level, 10m below water level and 0.5m above seabed respectively.

Table 4.3 shows the skill values calculated using equation 4.1 for different parameters for a control model and the full impact model. The control model has the identical set-up as the full model described in section 3.5 however there are no structures present. This is a numerical comparison between two models, comparing each to the field data. A skill value of 1 is considered to be identical therefore the closer to 1 the value is that better the prediction. In most of the parameters we can see a slight improvement in skill values in the Full model

result in comparison with those from the control results. This shows the full impact model does in fact slightly improve the accuracy of the prediction.

In the various hydrodynamics and statistical analysis using skill values we have carried out, we can conclude that the 2008 POLCOMS model that contains the turbine representation predicts the hydrodynamics reasonably well in the months March to December. When using the skill values to compare to a control model which has been previously validated we show that the turbines do not make the simulation worse. In fact it is possible to say it improves the model slightly. Once the initial issues in the early months of 2008 are resolved, the model started to predict the hydrodynamics with sufficient accuracy to be able to use the model in further work.

4.3 Comparison of the two methods

The relative performance of each method is assessed via model-model comparisons. Additional comparison to field data (Polton et al, 2011 [57]) is used to determine the effect at up to the yearly scale. We then plot the impacts for the velocities in March, giving particular attention to the U and V velocity components. March is chosen in this study because it is a period of time when the average monthly river inflows for the Dee ($45.8m^3/s$) is closest in value to the average for the year ($47.2m^3/s$). The OWF's impacts are particularly sensitive to the Dee freshwater inflow so using a representative month gives a good understanding of the impacts on average year (Norman et al, 2014 ([54]).

We also compare the monthly-averaged surface salinity and temperature in March to December using the following equation 4.2.

$$\phi_{residual} = \frac{1}{(t_e - t_s)} \int_{t_s}^{t_e} \phi(t) dt \tag{4.2}$$

Where ϕ_{residual} is average value, t_e and t_s are the start time and end time and ϕ is the hourly value. December provides a comparison with a monthly inflow which is higher than average Dee river flow rate ($53.2m^3/s$). Using these comparison salinity and temperature impacts of simulations T and F can be discussed in terms of greater freshwater inflow.

4.3.1 Yearly time Series

We first show the yearly time series salinity, temperature and density anomaly. Each plot shows a time series of data at site A (see Figure 3.10) at 3 positions in the water column. Field data is represented in all plots by the dark blue line, Red represents simulation F and blue represents simulation T.

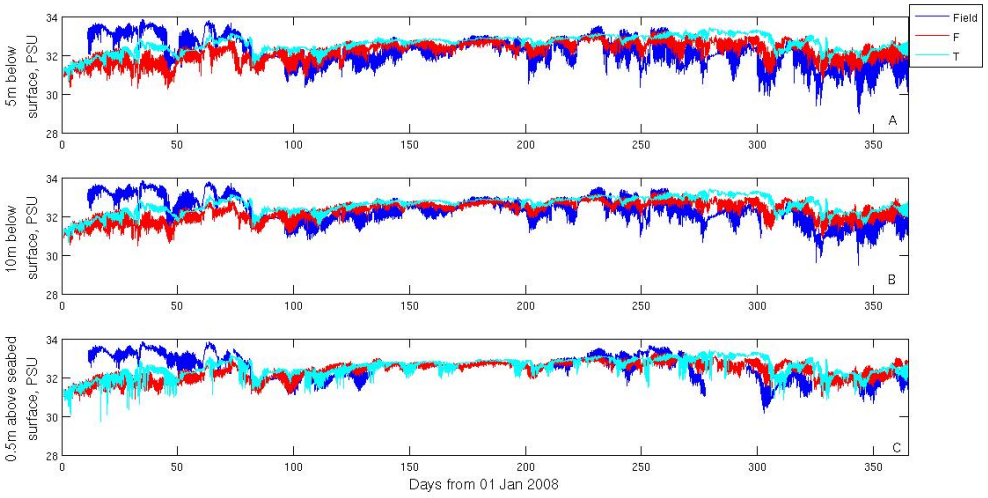

FIGURE 4.5: Time series of salinity comparison , at site A at different elevations in the water column a) 5m below surface, b) 10m below surface c) 0.5m above seabed. Dark blue is field data and red is model data (F) and light blue is model data (T).

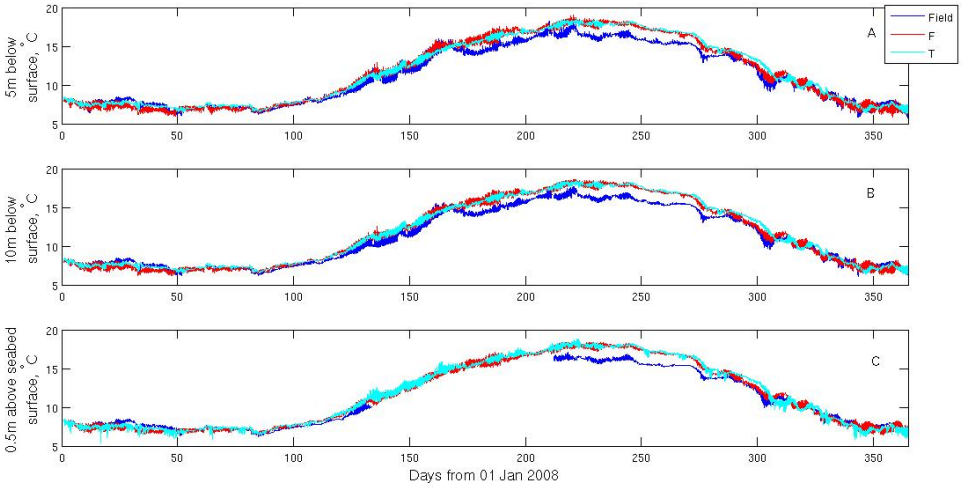

FIGURE 4.6: Time series of temperature comparison, see Figure 4.5 for plot details.

Figure 4.5 shows the yearly salinity plots at Site A for the two numerical simulations (F in red and T in light blue) and the observations in dark blue. T trends to slightly over predict the salinity over the year when compared to F and in plots showing salinity at the surface and in the water column (A and B), T tends to under predict most of the tidal fluctuations that appear in the observational data. In 4.5 C, showing the seabed salinity, both F and T struggle to predict the tidal fluctuations in the early months, where the salinity is dramatically reduced. This can be attributed to the model equalizing to the impacts from the OWF's which in T creates larger gradients than F. Throughout the year, T captures the overall trend of the salinity at the bottom of the water column well, however there are sudden fluctuations in PSU which isn't consistent with the field data. The initial three months show erroneous data prediction consistent with the validation section 4.2, T slightly out performs F in these early months by returning to the general trend faster however this is most likely due to the wrong reasons as the overall yearly prediction is slightly worse.

Figure 4.6 shows the yearly temperature plots at Site A for the two numerical simulations (F in red and T in light blue) and the observations in dark blue. The temperature trend is generally predicted well at all levels in both models. The main comparison that can be drawn in similar to salinity in that T is under predicting fluctuations at the sea surface and in the middle of the water column and at the seabed, T tends over predict fluctuations at site A.

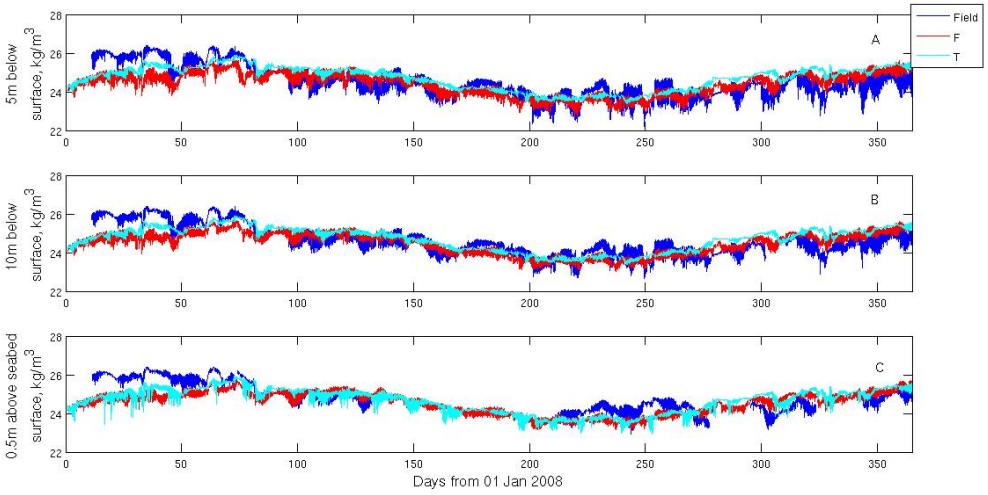

FIGURE 4.7: Time series of density anomaly (ρ-1000), see Figure 4.5 for plot details.

Figure 4.7 shows the density anomaly, calculated as $\rho - 1000$ at Site A for the two numerical simulations (F in red and T in light blue) and the observations in dark blue. The density is calculated using the UNESCO equation of state with uses salinity, temperature and pressure. Liverpool Bay is a salinity driven ROFI (section 1.2.2), the density time evolution follows closely that of salinity. The density at the sea surface and in the middle of the water column (Figure 4.7 A and B) shows T (light blue) barely picks up the fluctuations throughout the year when compared to F (red). This is seen in salinity and temperature, however it is possible that because of the combined effect on density, the errors in salinity and temperature compensate to give a good density.

In the salinity, temperature and density plots, we can see many localised areas of fluctuation caused by T representation of OWF's. Figure 4.8 shows the yearly time series for the density after applying a 25-hour moving average, which aims to filter out intra-tidal fluctuations.

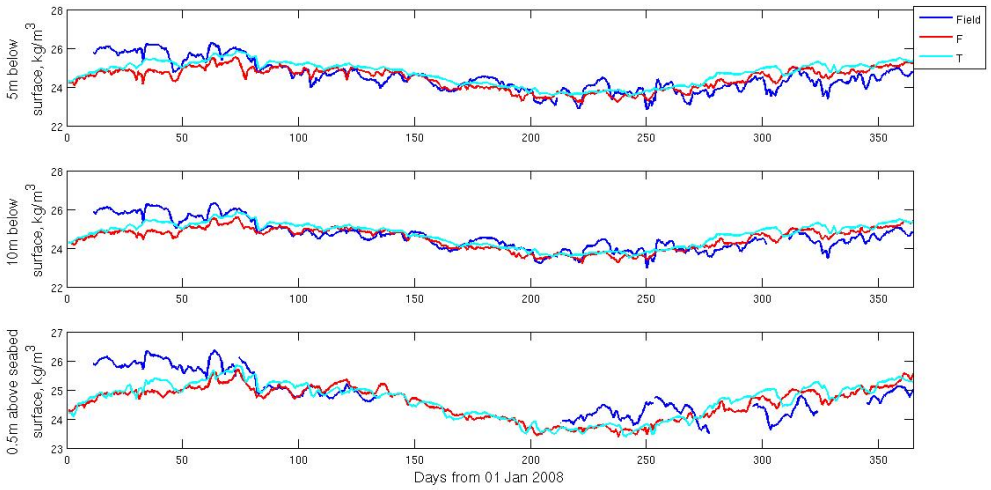

FIGURE 4.8: Time series of density anomaly (ρ-1000) 25 hour filtering, see Figure 4.5 for plot details.

We plot the 25 hour density anomaly, Figure 4.8 for F (red) and T (light blue). Removing the tidal fluctuations shows that both models predict the observational data fairly well. T tends to recover for the initial salinity under prediction, reaching equilibrium around day 60 where as F is slightly under predicting over this period but is picking up the pattern more accurately through all the water column. In contrast, at the end of the year F is predicting the density more accurately than T. It appears that T tends to reach the density values faster than F but cannot simulate the details as well as F at site A.

4.3.2 Velocity comparison

We have looked at the computed salinity, temperature and density on yearly temporal scales at site A. We now take a shorter temporal period and examine monthly average velocity at the surface, we use March as it is close to yearly average river inflows from the Dee. Monthly averages are calculated using equation 4.2 and plotted in Figure 4.9.

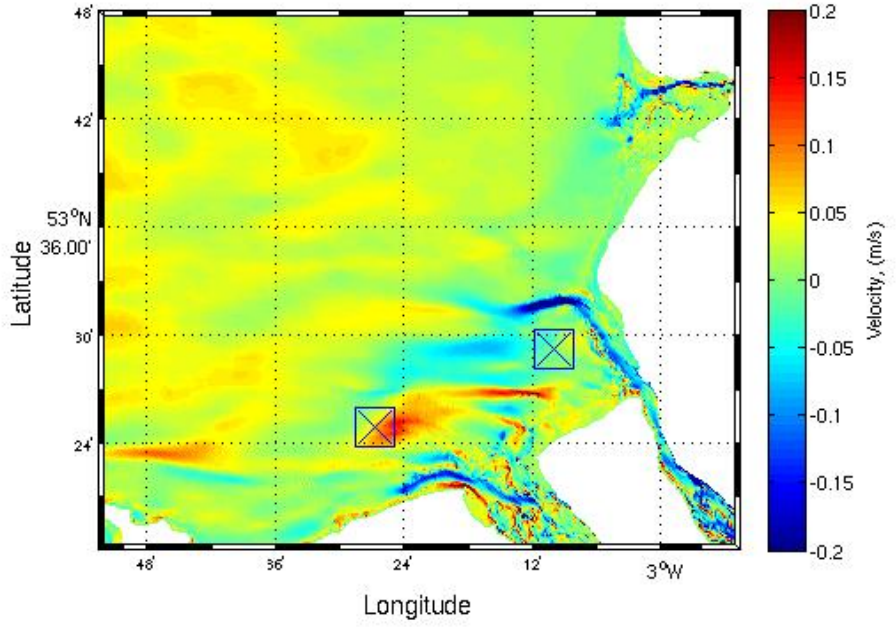

(a) F simulation

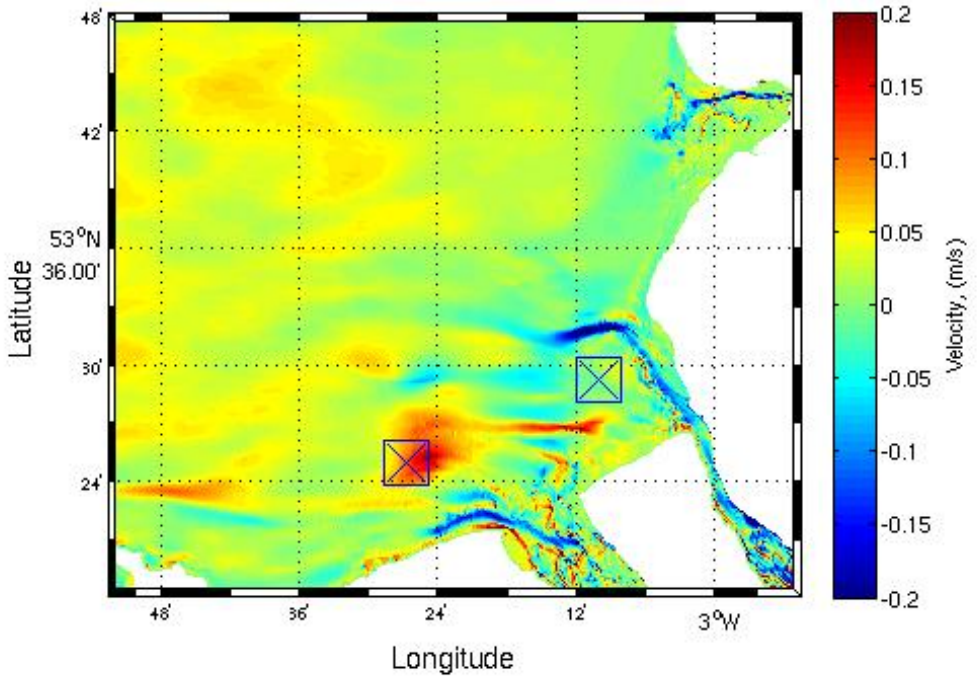

(b) T simulation

FIGURE 4.9: Liverpool Bay Surface u Component(West-East) Plot for March 2008 average, North Hoyle to the left and Burbo Bank to the right represented by blue squares positioned at the OWF centres

Figure 4.9(a) and 4.9(b) shows the U component for F and T respectively. U is positive West to East and as such where red is plotted shows a West-East flow. Figure 4.9(a) shows a flow structure emulating from the North Hoyle (western OWF). There is a circulation near North Hoyle with the water travelling in two directions. The deep water Mersey channel which exits the Mersey estuary and travels north of Burbo Bank (Eastern OWF) is clearly visible, magnitudes of 0.2m/s are visible near OWF's and in the Mersey channel. North Hoyle in particular shows the impact at the centre of the OWF. In Figure 4.9(b) with shows the U component for T, this shows the impacts extend further into the bay in comparison to F (Figure 4.9(a)).

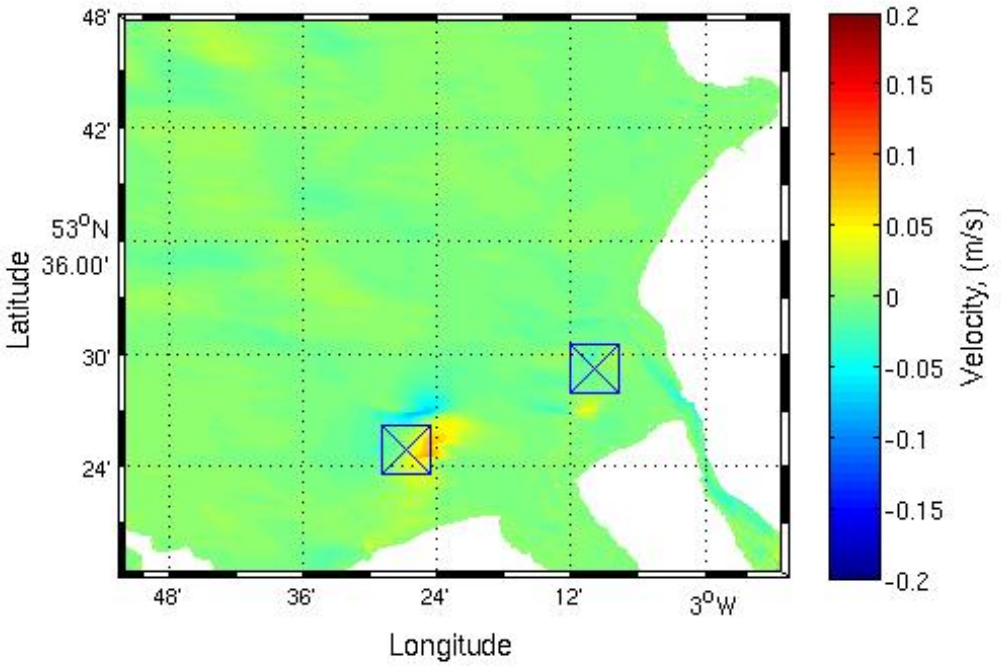

(a) F - control model

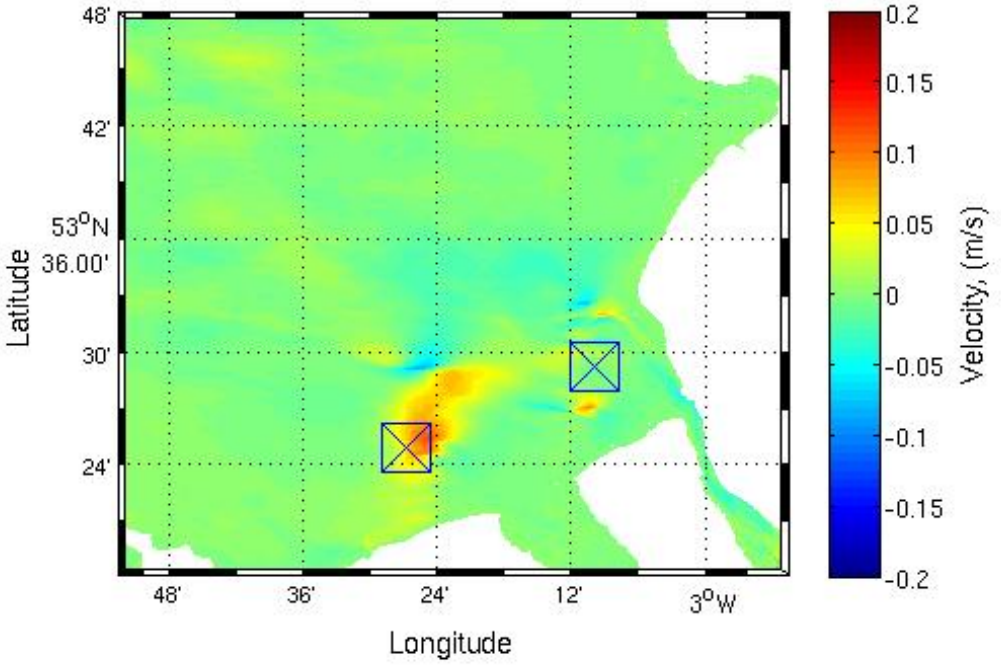

(b) T - control model

FIGURE 4.10: Liverpool Bay Surface u Component (West-East) Difference Plot for March 2008 average, North Hoyle to the left and Burbo Bank to the right represented by blue squares positioned at the OWF centres

Figure 4.10(a) and 4.10(b) show the magnitude in u component differences using a model with no turbine structures as a control. First, the velocity magnitude shows that the single structure method has the same magnitudes of impact on the U velocity. This is likely to be because the total number of structures are the same hence the numerical impact is equal in both models. When we compare the two models, the major difference is the spatial area over which the impact can be seen in T compared to F. This is likely due to strong flow between unaffected cells within the OWF in T simulation, which advecting any influence further away. Numerical errors may also cause these differences because the individual wakes are not resolved completely due to the assumption that all wakes are resolved in the grid distance.

Next we consider the v component of the velocity by plotting surface v velocities on Latitude/Longitude domain. The freshwater flow from the Dee is predominately in the North-South and as such using the v velocity direction plot we can highlight the local impacts on the freshwater.

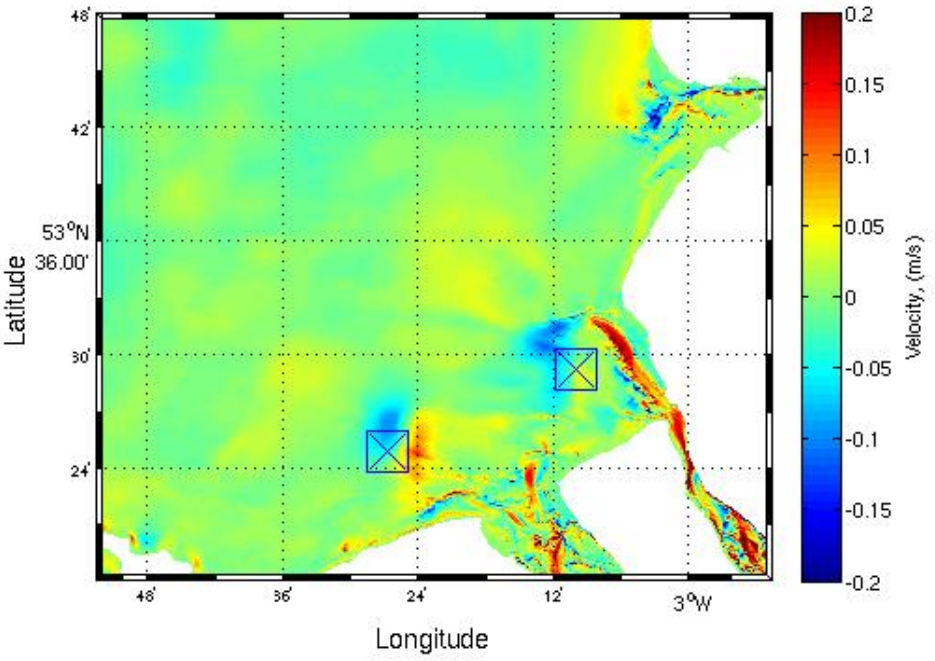

(a) F simulation

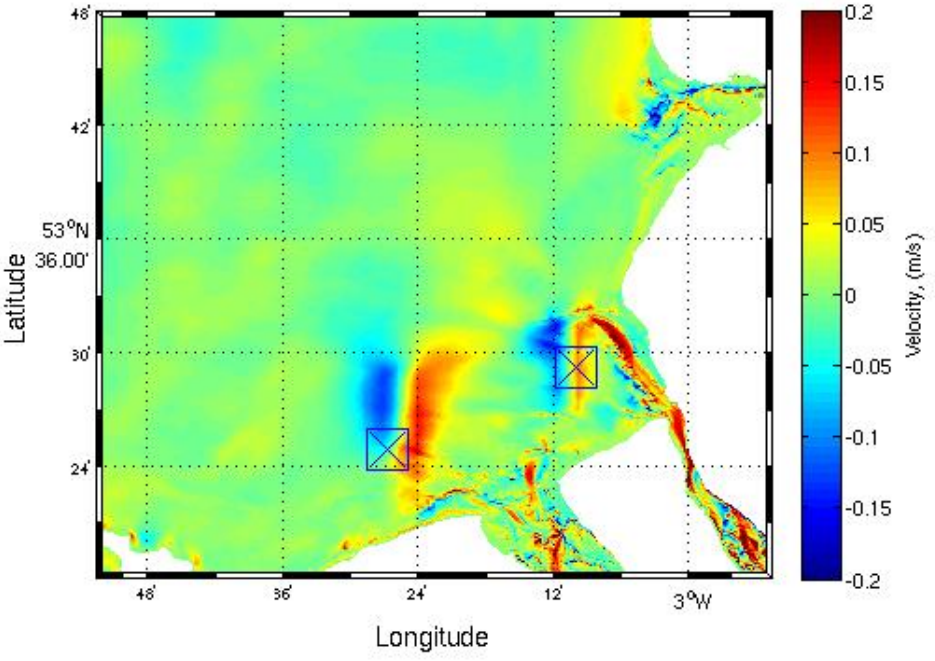

(b) T simulation

FIGURE 4.11: Liverpool Bay Surface v component (North-South) Plot for March 2008 average, North Hoyle to the left and Burbo Bank to the right represented by blue squares positioned at the windfarm centres

Figure 4.11(a) and 4.11(b) shows the V component contribution for F and T respectively. While the time-varying East-West current component is dominant as being the main tidal component, the North-South component results show significant (time-averaged) residuals due to baroclinic effects in the Bay (Palmer, 2010 [56]). Our numerical results suggest that the "Single turbine (spatial) average" generates a larger area of influence North of the OWF.

As with Figure 4.9(a), the magnitudes of impact are similar when comparing F and T. As the total number of structures is the same, the total impact is no difference therefore it is unlikely for the magnitude to change.

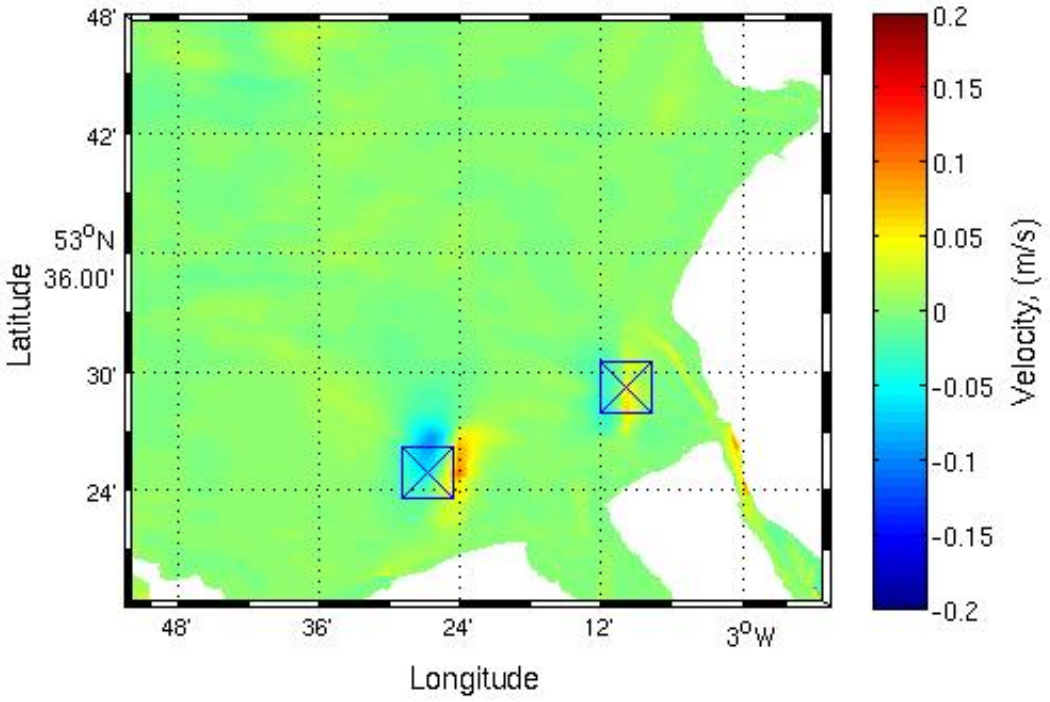

(a) F - control model

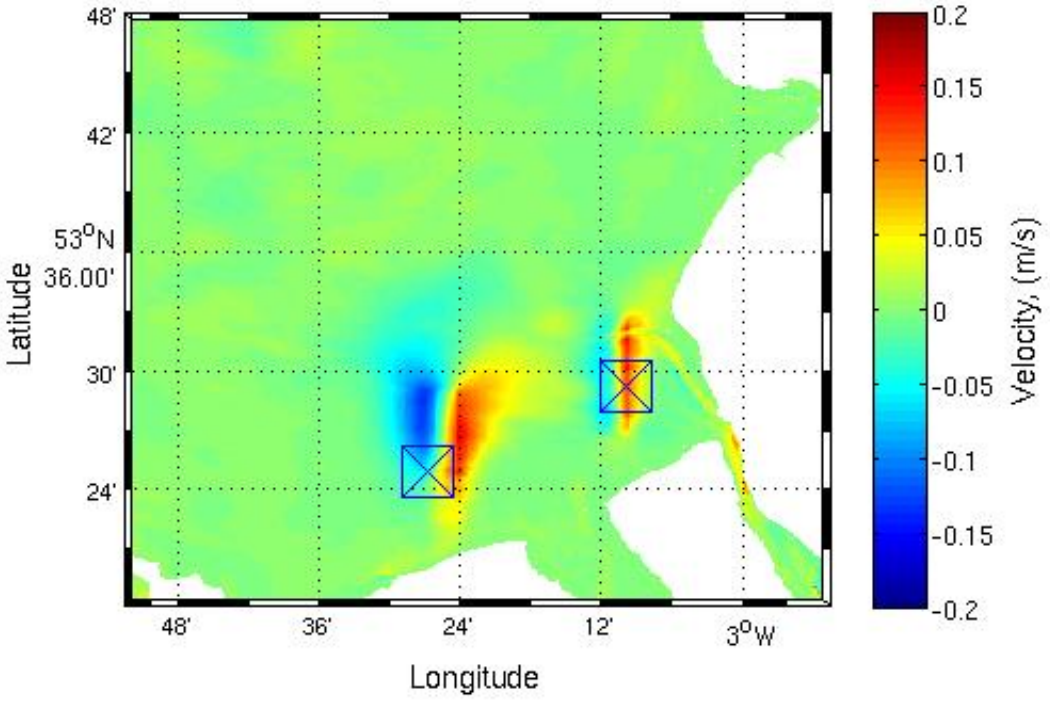

(b) T - control model

FIGURE 4.12: Liverpool Bay Surface U Velocity (East-West) Plot for March 2008 average, North Hoyle to the left and Burbo Bank to the right represented by blue squares positioned at the OWF centres

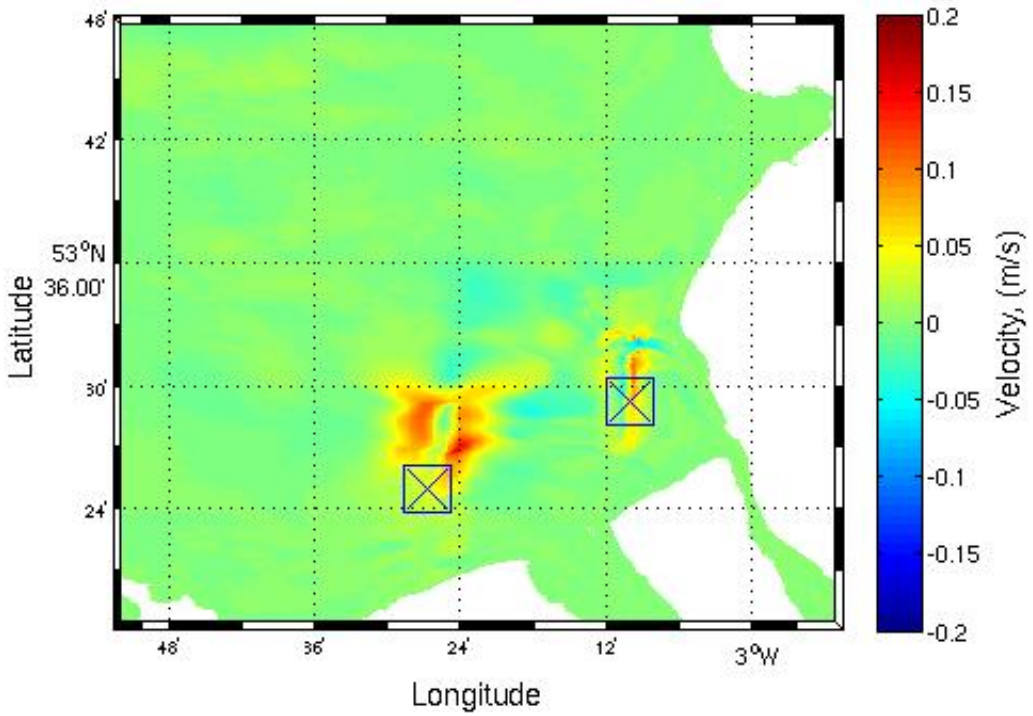

(a) T-F

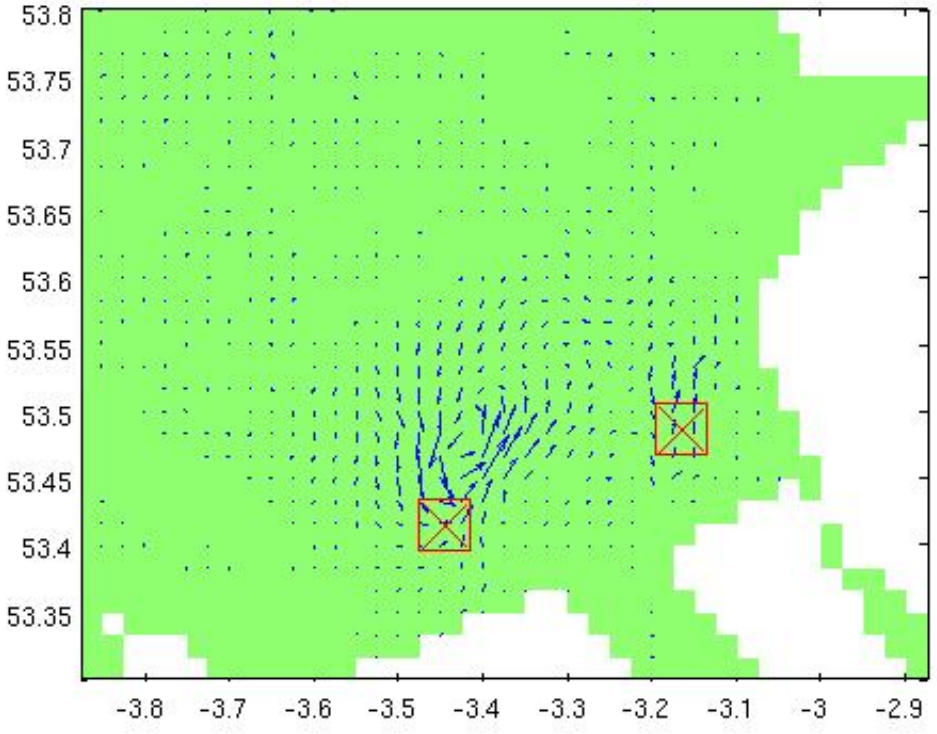

(b) T-F

FIGURE 4.13: Liverpool Bay speed difference and direction (T-F) showing the change in speed due to the different representation methods.

Figure 4.12(a) and 4.12(b) show the U component absolute difference using a model with no turbine structures as a control. Figure 4.13(a) shows the clear increase in speed near North Hoyle. This shows that the single structure method causes velocity effects further from the OWF centres when comparing to F. This shows again that the single turbine method causes effects on the residual velocity further from the OWF when compared to F. Even though the instantaneous velocity in unaffected cells is increased, there is little impact on residuals within the OWF. There is, however, a clear impact on the extent of the affected spatial area due to the velocity increase in unaffected cells in the OWF. A consequence is that the eddy generated near North Hoyle is larger (Figure 4.13(b)). The scalar transport (salt, nutrients etc) is also likely to be affected therefore we now consider the salinity and temperature average surface plots.

4.3.3 Salinity Comparison

Here we introduce the surface salinity average which is plotted on a latitude/longitude domain with OWF centres. As discussed above Liverpool bay is a salinity driven ROFI therefore it is particularly sensitive to changes in salinity.

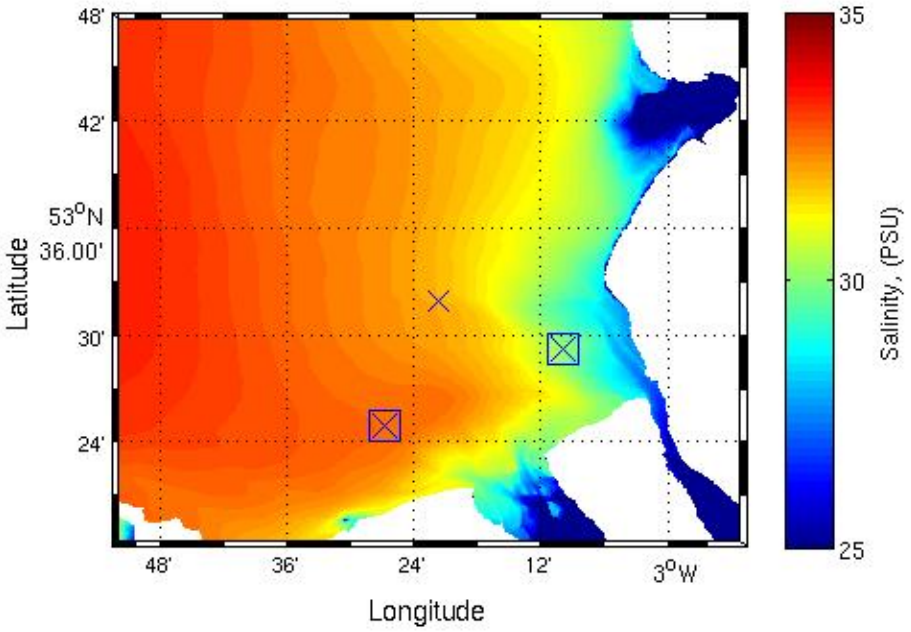

(a) F simulation

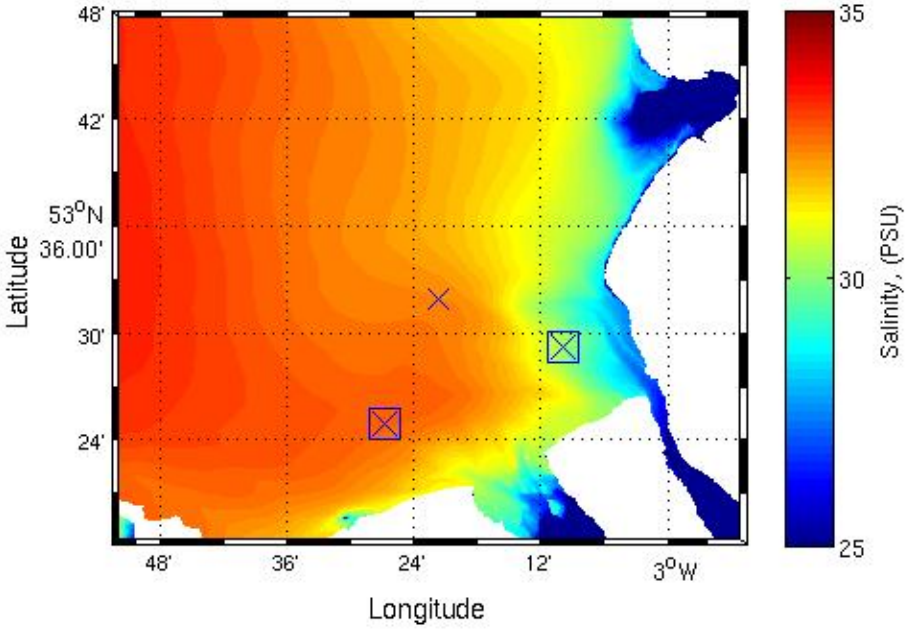

(b) T simulation

FIGURE 4.14: Liverpool Bay surface Salinity average plots for March 2008, North Hoyle to the left and Burbo Bank to the right represented by blue squares positioned at the OWF centres, Site A is indicated by a blue cross

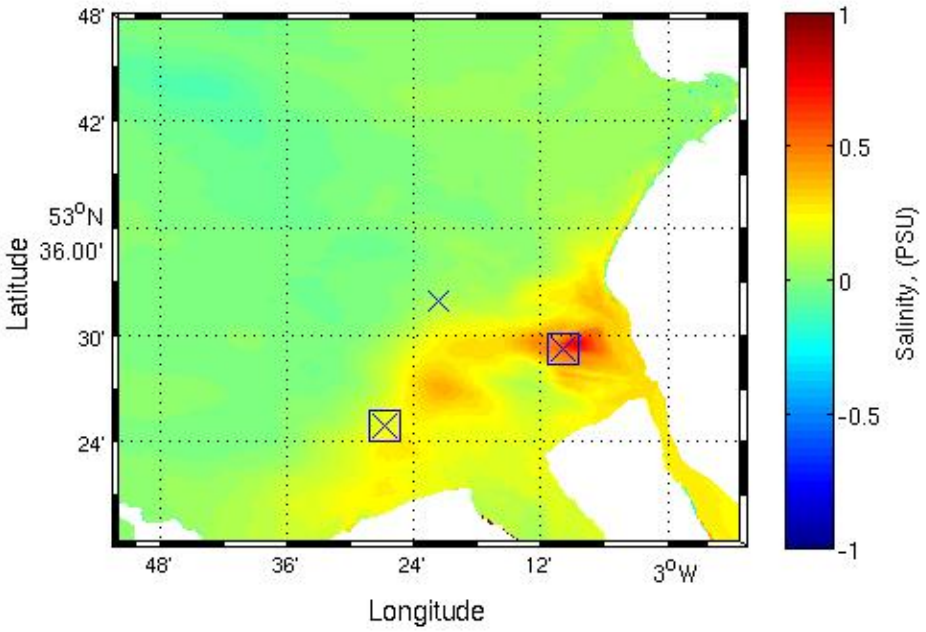

(a) F - control model

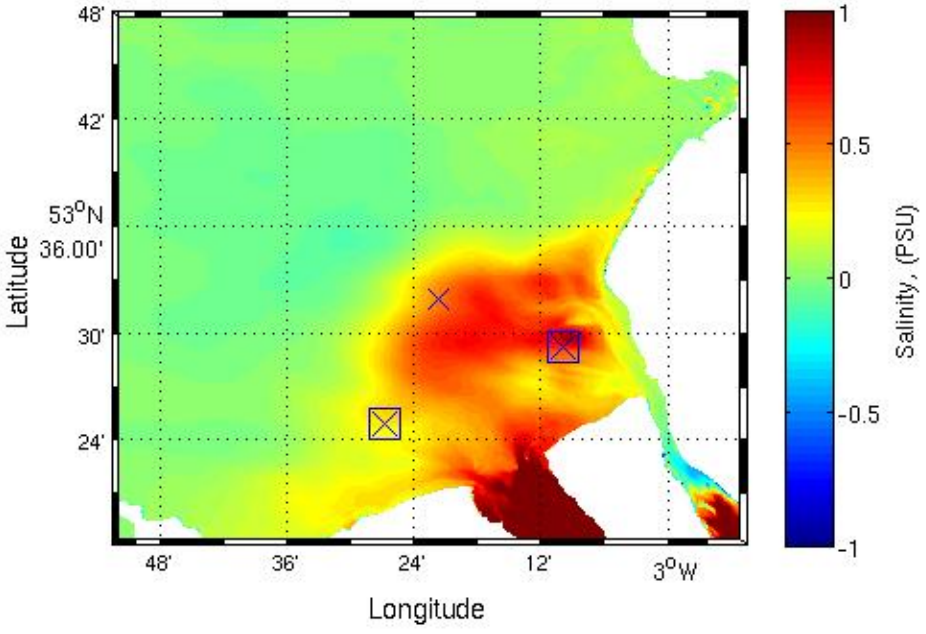

(b) T - control model

FIGURE 4.15: Liverpool Bay Surface Salinity average difference plots for March 2008, North Hoyle to the left and Burbo Bank to the right represented by blue squares positioned at the OWF centres, Site A is indicated by a blue cross

Figure 4.14(a) and 4.14(b) show the surface salinity for F and T respectively. The Figures also show the positions of the OWFs, and this confirms that Burbo Bank (eastern OWF) is close to the salinity front from the Mersey and Dee outflows.

Figure 4.15(a) and 4.15(b) shows F - control and T - control for average monthly surface salinity. There are several areas that have been affected due to the parameterisation method, firstly the area around site A. There is an increase in average salinity across this area. This is consistent with what is seen in Figure 4.5 which shows at site A, the salinity over March is higher in T than in F, this also is closer to the observational data at this time. This effect is likely to be a consequence of the increased velocity impacts seen in Figure 4.13(a) which allows the saline water to be blocked from moving near the estuary. We can see the Dee estuary has a large increase in surface salinity in T, there could be several reasons for this. It could be due to the blockage of the OWF's which have allowed saline water in on the flood tide which fails to flush out on the ebb tide because of the blockage. The more likely reason for this increase considering the magnitude of the increase (5 PSU, Figure 4.16) is an error with the coupling from the initial conditions and the increased gradients caused by the structure impacts.

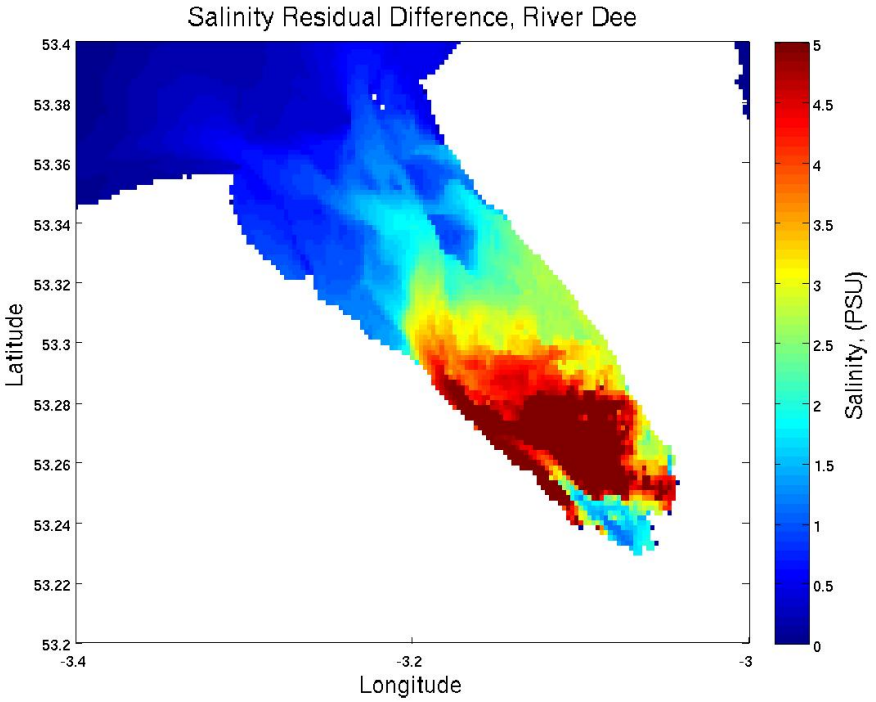

FIGURE 4.16: River Dee Surface Salinity Residual for March 2008, Zoomed in to focus on the river inflow errors

Figure 4.16 shows a zoomed plot of the Dee estuary. THe POLCOMS Liverpool Bay setup has been extensively used to study the dynamics and processes of the Dee Estuary (Bolanos et al, 2011 [16], Amoudry et al, 2014 [4]). In particular, the model has been validated against observational data for hydrodymanics, turbulence and sedimetn transport. The large increase in salinity in T (see Figure 4.16 zooming on the Dee estuary) due to the presence of 'single structure' highlights some of the erroneous results generated.

The approach, T seems to over predict the Dee estuary when compared to F approach, as a result using the farm average method seems to be able to provide the better results in the estuaries.

4.3.4 Temperature Comparison

Here we consider the surface temperature average for March using the latitude/-longitude domain used to represent the salinity. Each plot has the OWF centres and site A marked.

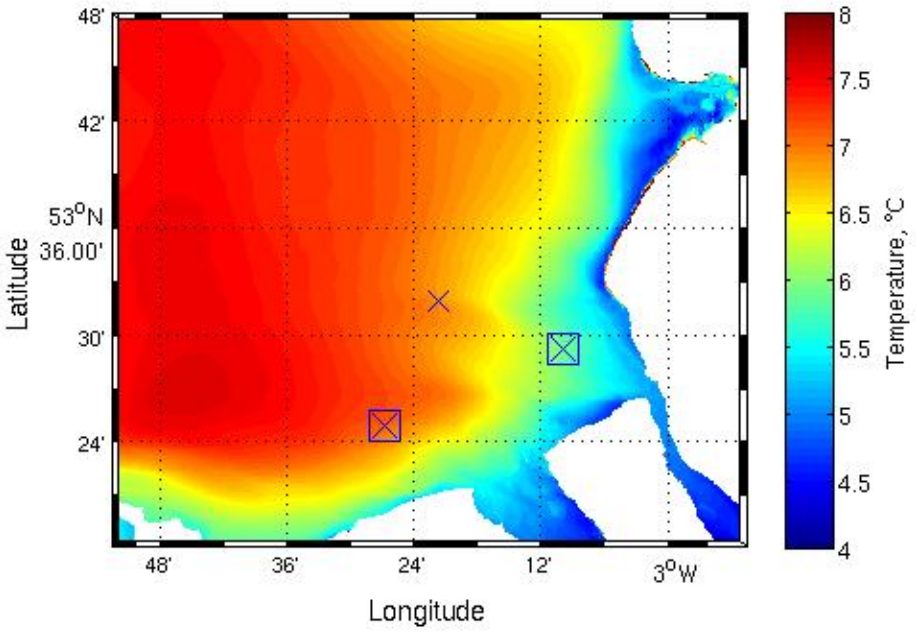

(a) F simulation

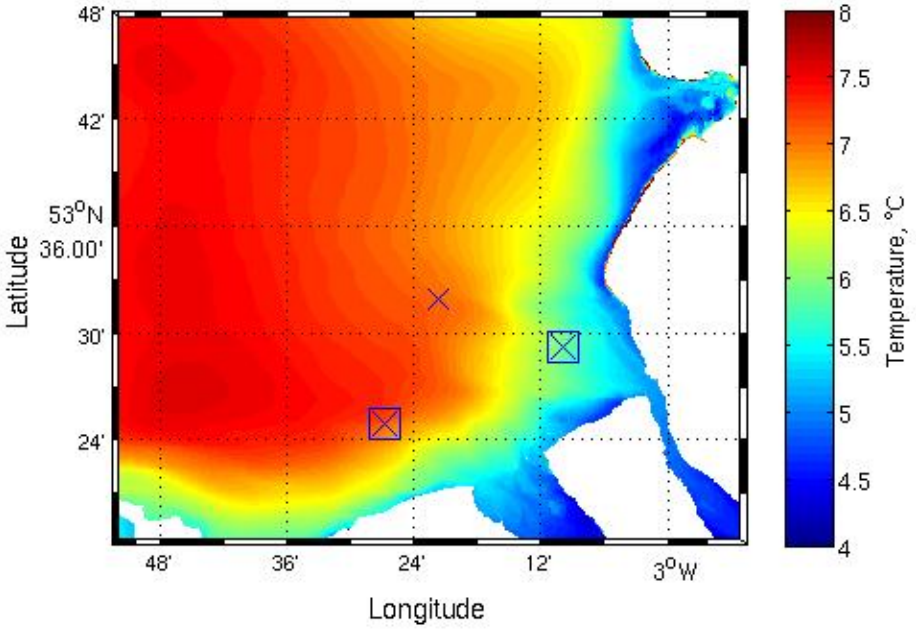

(b) T simulation

FIGURE 4.17: Liverpool Bay average surface temperature plots for March 2008, North Hoyle to the left and Burbo Bank to the right represented by blue squares positioned at the OWF centres, Site A is indicated by a blue cross

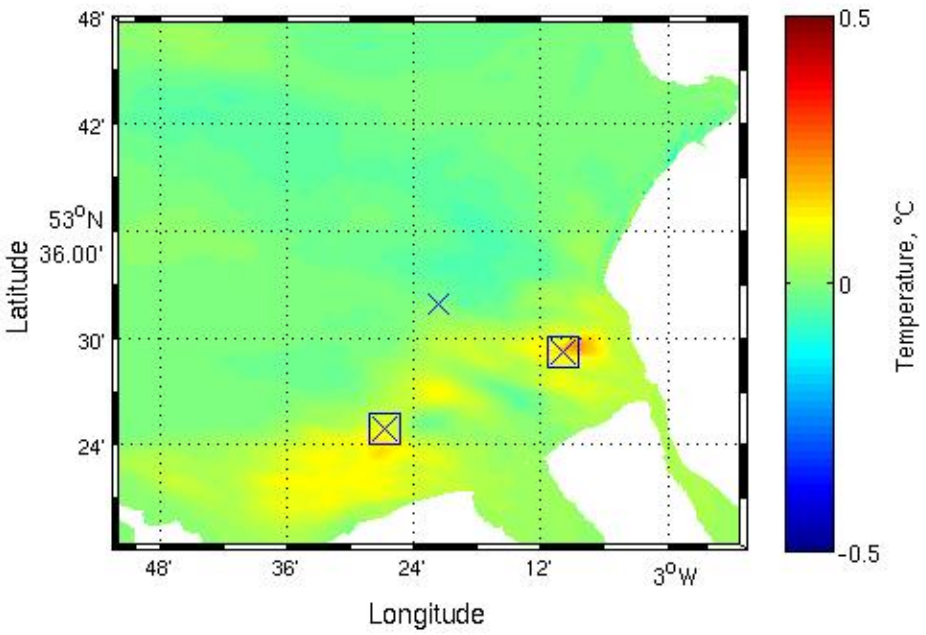

(a) F - control model

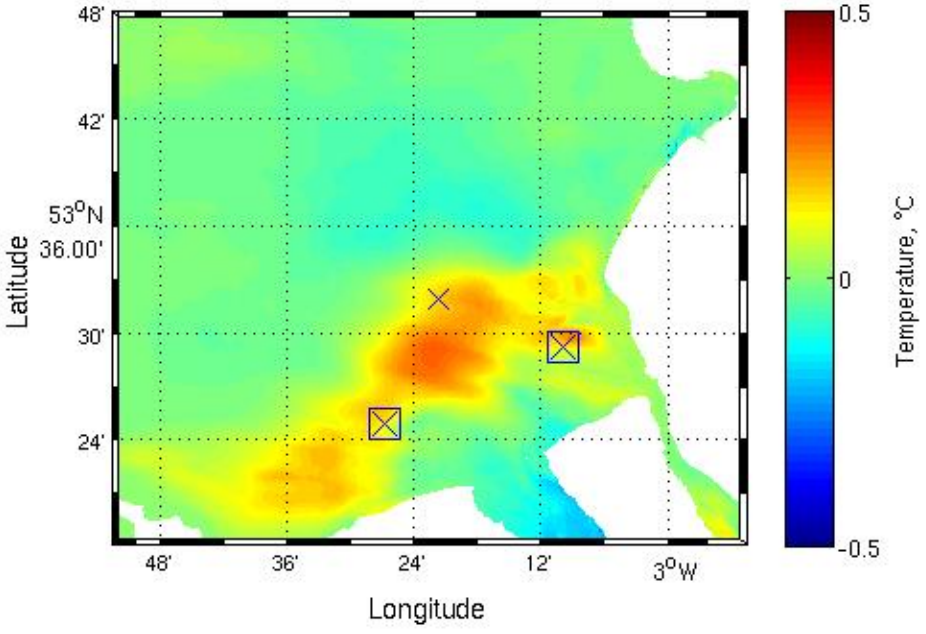

(b) T - control model

FIGURE 4.18: Liverpool Bay average surface temperature plots for March 2008, North Hoyle to the left and Burbo Bank to the right represented by blue squares positioned at the OWF centres, Site A is indicated by a blue cross

Figure 4.17(a) and 4.17(b) shows the monthly average temperature for F and T respectively. The OWF's are close to the temperature front which is consistent with the salinity plots, particularly Burbo Bank which is in the freshwater plume from the Mersey. Due the scale of the temperature profile, a better understanding can be obtained from the difference plots.

Figure 4.15(a) and 4.15(b) shows F - control and T - control for average monthly temperature salinity. Temperature is shown to increase around site A, this is consistent with the finding in 4.6 which shows T tends to over predict the temperature. This is likely due to the blockage of freshwater to these areas because of the increase in velocities near North Hoyle. This effect can also be seen in the salinity plots in section 4.3.3.

4.3.5 Conclusions

In this study, we have compared the numerical results from a simulation using two different parameterisation techniques, the Farm Average method and the Single Structure method. The Farm Average method represents OWF's as one area of influence in the shape of the spatial area covered by the whole array. This method leads to a smoother transition between affected and unaffected cells because the total impact from the structures is averaged across a large number of cells. This method is also appropriate for use in models with horizontal resolutions greater than the distance between the individual structures such as for a full European Continental Shelf model. The single structure method simulates the structures within the OWF as individual areas of influence, this leads to localised cells with larger impacts when compared to the farm average method and cells within the OWF that are simulated with no impact terms. As such this leads to the possibility to accurately model the structure positions within the domain depending on the horizontal grid resolution.

We found that Single Structure method tends to over predict the hydrodynamics at site A when compared to Farm Average method which is corroborated in the analysis of the March monthly average where an area of increased salinity and temperature can be clearly seen. This is likely due to the increased velocities seen in the velocity and speed plots which provides greater scalar transport through Site A in Single Structure method. We also found that Single Structure method dramatically increases the flow in the Dee estuary. We have attributed this to the continuity errors caused due to the high localised changes at the OWF sites with the input conditions and as such leading to saltier, warmer water pooling in the estuary.

In the analysis we conclude that for this set up in Liverpool bay the best and most appropriate method to carry forward into a full comprehensive study of the impacts in Liverpool bay is the Farm Average method.

Chapter 5

Parameterisation of OWF's in POLCOMS Governing Equations: The Influence of Turbulence Sources

Momentum only methods are commonly used to simulate offshore structures in ocean models. An example of this is can be seen in Wang and Yang, 2011 [82] and Wang et al, 2013 [83] which uses the FVCOM modelling system with a momentum sink to simulate energy extraction. Built in land points are employed to represent the offshore structures. These land points in FVCOM effectively are any points within the domain that do not get wet. When simulating a structure the elevation is set to be higher than the water surface. This method has its origins in the 2D bottom friction method which uses an increase in bottom friction to represent structures. This method was extended to 3D models by changing the bottom friction, however this may lead to simulation errors as the structure is only represented in the bottom sigma layer therefore misses out on some of the effects present higher in the water column. This led on to the structures being simulated as momentum sinks through the water column, which in most cases

simulated as land points unstructured grids. The bottom friction method does create an increase in turbulence, however this is focuses near the seabed and its effects are reduced up through the water column.

In this chapter, we apply the numerical model described in section 3.5 to a ROFI, Liverpool Bay and compare the numerical results to a momentum sink only model described in this chapter applied over the same domain. The objective of the work presented here is to assess the additional turbulence generation/dissipation effects impacts each method of simulation. We consider the numerical results obtained by simulating two wind farms, North Hoyle and Burbo Bank by using the structure model described in section 3.5 which applies the momentum and turbulence impact of a structure through the water column. We compare this to numerical data using the momentum sink model, which simulates offshore structures by modelling the momentum impact only.

This chapter contains a description of the mathematical equations used in the momentum sink model. Here we also provide a brief description of the hydrodynamics in Liverpool bay and the model set-up which is used to evaluate the impacts of OWF's. Reasons for the differences in the numerical results are discussed by considering near (defined as array radius plus 500 metres) and far-field effects and showing the change if impact due to the turbulence impact model (section 3.5).

Here we are using the momentum impact term discussed in section 3.2 to develop the momentum sink model used here.

$$G_d = \frac{1}{2} C_D a U \sqrt{u^2 + v^2} \tag{5.1}$$

$$where : a = \frac{N_s d}{A_{cell}} \tag{5.2}$$

Where G is total impact term, u and v are velocity components, east-west and

north-south respectively, U is the velocity component u or v. For multiple structures in one cell, equation 3.13 can be multiplied by the number of structures, N_s, d is the diameter of the structures and A_{cell} is the area of influence.

Equation 5.1 is the momentum impact equation derived in section 3.2 and is applied to the POLCOMS governing equations which leads to the momentum sink being applied through the water column. We use this application of the momentum equation which as momentum sink model and as such gain numerical results for comparison to the method described in section 3.2.

In this chapter, we compare two mathematical representations of structure representation to test the conceptual understanding that simulating structures using momentum and turbulence impacts is more accurate when compared to using only momentum impacts. We use model to model comparison to assess the differences on salinity, temperature and density.

5.1 Numerical Model Setup

We use the full impact model described in section 3.5 which uses POLCOMS-GOTM equations with added structure model as described in section 3.2 and use the built-in switch to turn off any numerical impact on the $k - \varepsilon$ equations in GOTM (hereafter known as M). We will also use a control model (hereafter known as C) as a comparison to assess the overall capability of the structure models to experimental data to assess the accuracy using skill values (Willmott 1981,[76]). We will also compare to observation field data (Polton et al, 2011 [57])used to valid the structure model (section 4.2) using the data at site A in Liverpool Bay.

We use the farm averaged method to represent the OWF in the domain (section 3.3), this is in line with the conclusions in Chapter 4 which is suitable for studying the far-scale effects of structures. This area represents the full spatial area of the OWF and uses an average method to apply the effects of

the structures. We use the 4m representative diameter to simulate the size of the cylindrical structure which is a typical size for an average offshore turbine. The drag coefficient is to be taken as 0.63, a cylindrical object in a water flow. The coefficient used in the turbulence closure scheme is set to 0.6 (section 3.2) as defined in Rennau et al, 2012 [59] as the high turbulence scheme which is justified for such strong tidal currents present in Liverpool Bay.

5.2 Yearly Time Series at Site A

Here we present results from M and F simulations and compare to assess the impact of the numerical simulation method. Table 5.1 uses the statistical skill values (Willmott 1981, [76]) to numerical compare the accuracy of the M and F compared to a control model for the yearly timeseries at site A.

Parameter	C	M	F
U	0.97	0.96	0.97
V	0.79	0.76	0.80
rho5	0.82	0.79	0.83
rho10	0.84	0.82	0.76
rhoB	0.76	0.79	0.76
T5	0.99	0.99	0.99
T10	0.99	0.99	0.99
TB	0.99	0.99	0.99
S5	0.54	0.43	0.55
S10	0.54	0.42	0.55
SB	0.47	0.37	0.49

TABLE 5.1: Skill Values (Willmott 1981, [76]) for C, M and F simulation runs at site A. U and V represent velocity components. rho5, rho10 and rhoB represent density at 5m below water level, 10m below water level and 0.5m above seabed respectively. T5, T10 and TB represent temperature at 5m below water level, 10m below water level and 0.5m above seabed respectively. S5, S10 and SB represent salinity at 5m below water level, 10m below water level and 0.5m above seabed respectively.

Table 5.1 shows that M has a lower skill value than F for most parameters. This suggests that using the momentum only approach to structure simulate in Liverpool tends to lead to a reduction in accuracy when comparing the observational data. We can also see looking at table 5.1 that M tends to incorrectly predict the salinity when compared to the control model. This shows that by using just momentum to simulate structures in Liverpool bay the overall prediction accuracy is reduced, where the full model (F) generally improves the numerical results. We can use this table to conclude that at in Liverpool Bay using the

momentum and turbulence to represent structures is slightly more accurate. We now move on to plot the yearly time series of salinity, temperature and density at site A at difference points in the water column.

Both simulation results are compared to observational data from site A at site A at 5m below surface, 10m below the surface and at the seabed. We show the hourly data for salinity, temperature and density and the 25 hour moving average of the density to remove the intra-tidal fluctuations.

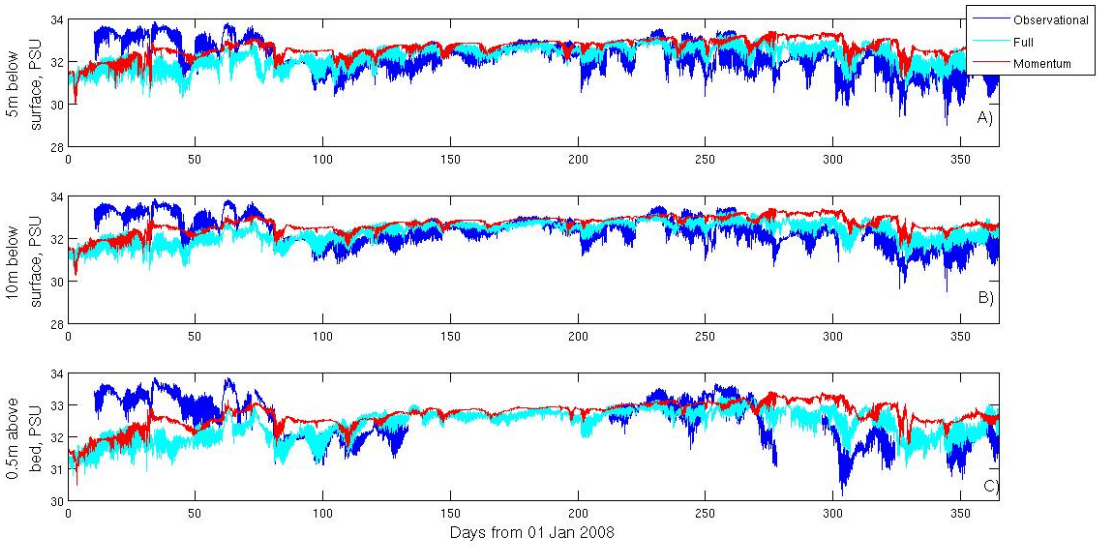

FIGURE 5.1: Salinity (PSU) yearly time series comparison at site A for F (light bule) and M (red) plotted against observational data Blue; A) 5m below sea level, B) 10m below sealevel, C) 0.5m above sea bed

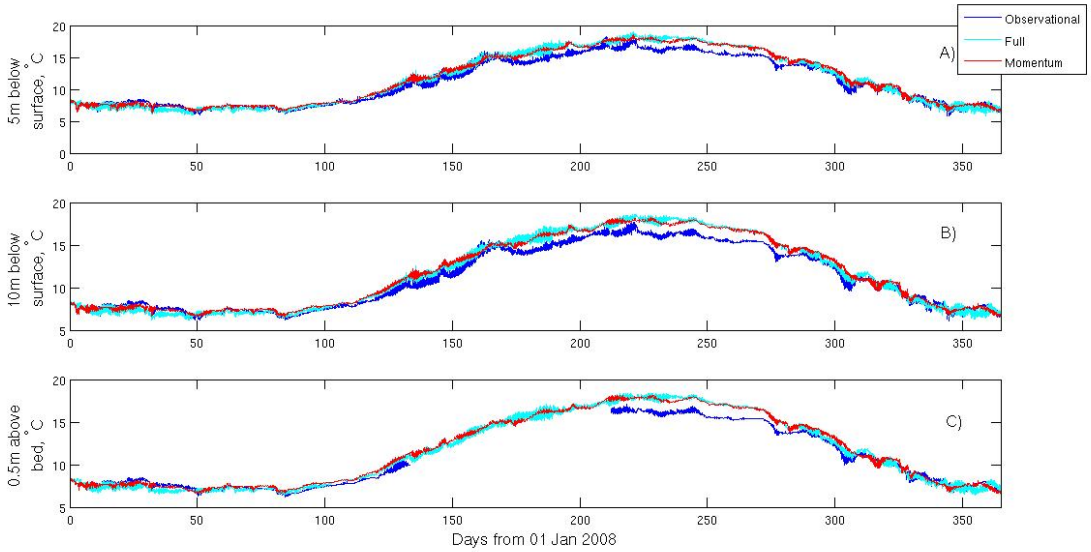

FIGURE 5.2: Temperature (°C); see Figure 5.1 for plot details

Figure 5.1 and 5.2 show the yearly timeseries at 5m below, 10m below and 0.5m above the seabed respectively. We plot the observational data as the dark blue line, red is the M model data and light blue is the F model data. In Figure 5.1, we can see the high frequency salinity fluctuations due to the tidal motion in Liverpool Bay, we can see M (red) tends to underestimate these fluctuations throughout the water column more than F does. We can see in the initial months the lack of accuracy which is in line with chapter 6.

M tends to generally over predict the salinity at site A, particularly in November and December where M fails to predict the fluctuations and is the salinity is larger than both observational data and F model data. This is consistent throughout the water column as shown in Figure 5.1 A), B) and C) which all show a lack of fluctuations predicted on the timeseries. These results for high frequency salinity data imply that the OWF effects are represented more accurately using momentum and turbulence. This also confirms the statistical metric values in table 5.1.

We can conclude that at site A in Liverpool bay 2008, structures are represented more accurately using both momentum and turbulence when considering the salinity through the water column.

In Figure 5.2 the temperature at site A for M is predicted well. The general overall pattern is simulated well throughout the year and the water column. There is a slight increase in simulated temperature in the summer months in both modelling methods, F and M however M results tend to under predict the tidal fluctuations in temperature when compared to both F and the observational data. This is again consistent through the water column (Figure 5.2 A), B) and C)). The reasons could be due to the lack of additional mixing caused by the turbulence.

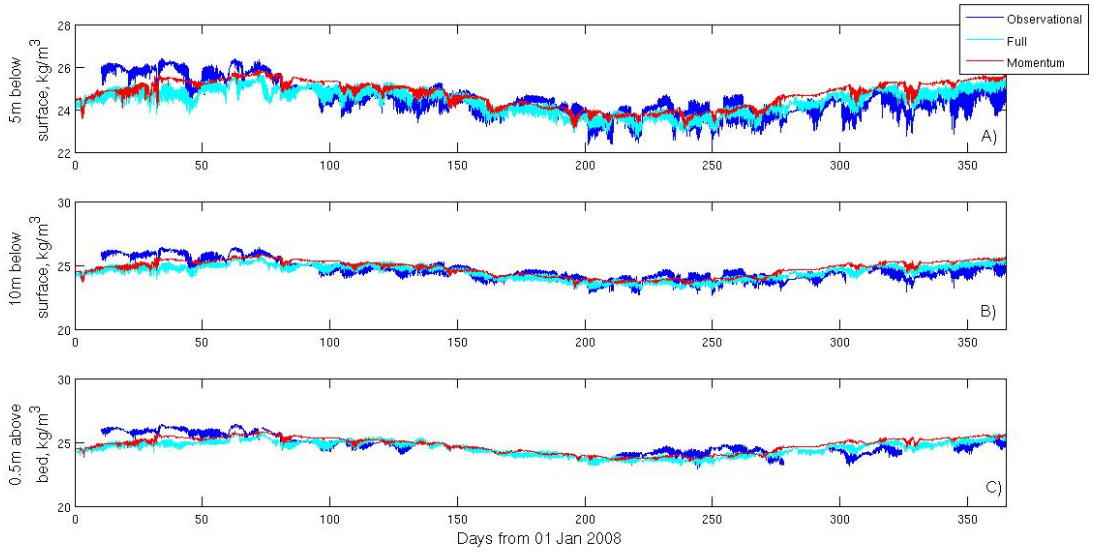

FIGURE 5.3: Density (kg/m^3), calculated using the UNESCO equation of state, (POLCOMS Documentation, [46]); see Figure 5.1 for plot details

Figure 5.3 shows the density yearly time series at 5m below, 10m below and 0.5m above the seabed respectively. We plot the observational data as the dark blue line, red is the M model data and light blue is the F model data. We can see the initial discrepancy mentioned previously (Chapter 4), however from March

onwards we can see the overall trend in density through the water column is simulated reasonably well. When we compare the M and F, it is clear that M fails to predict the intra-tidal fluctuations due to the salinity fluctuations. At the seabed, Figure 5.3 C) M completely fails to pick up any of the tidal fluctuations which are seen in the observational data and F model data.

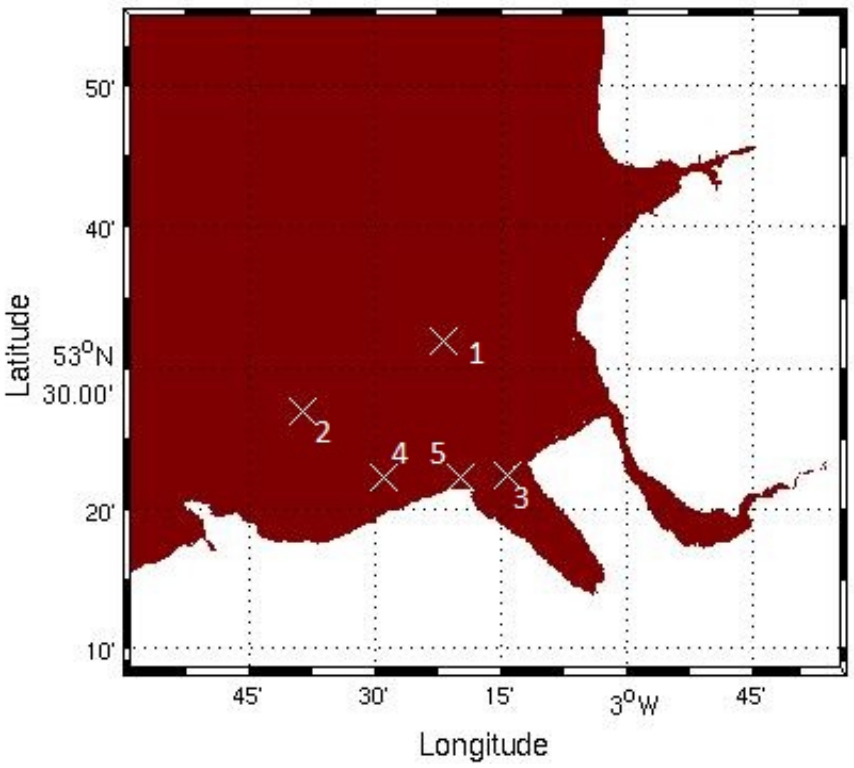

FIGURE 5.4: Locations of the investigation points

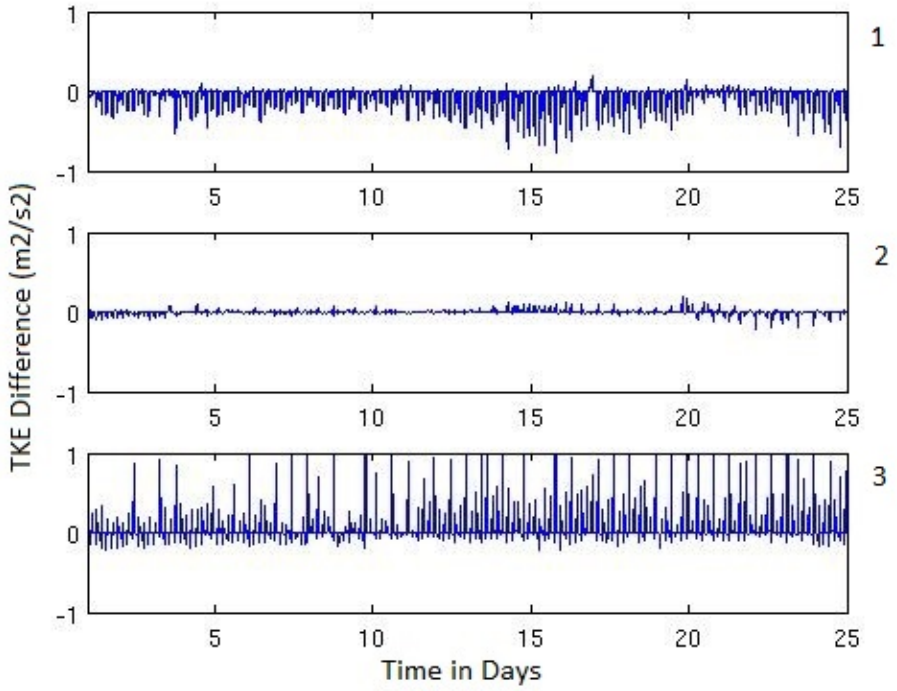

(a)

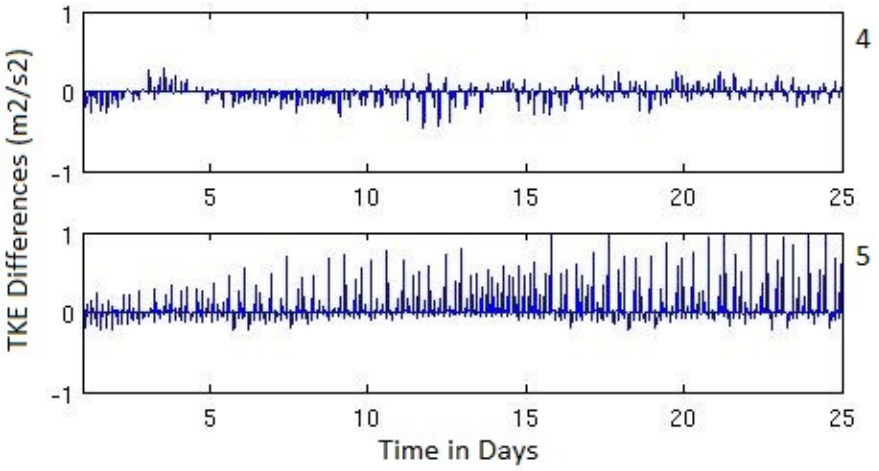

(b)

FIGURE 5.5: Surface tke differences (M-C) on the surface at 5 points within Liverpool Bay

Figure 5.5 shows the surface TKE differences for M-C at the locations in Figure 5.4. Line plot 1 shows that the momentum reduces the TKE at location 1, this shows that the momentum impacts extend into the Bay.

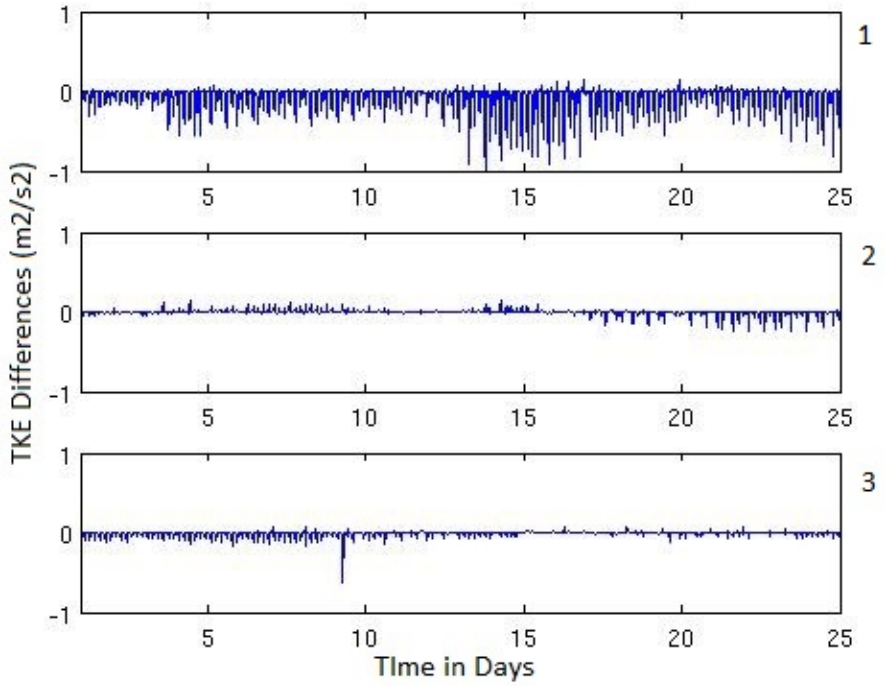

(a)

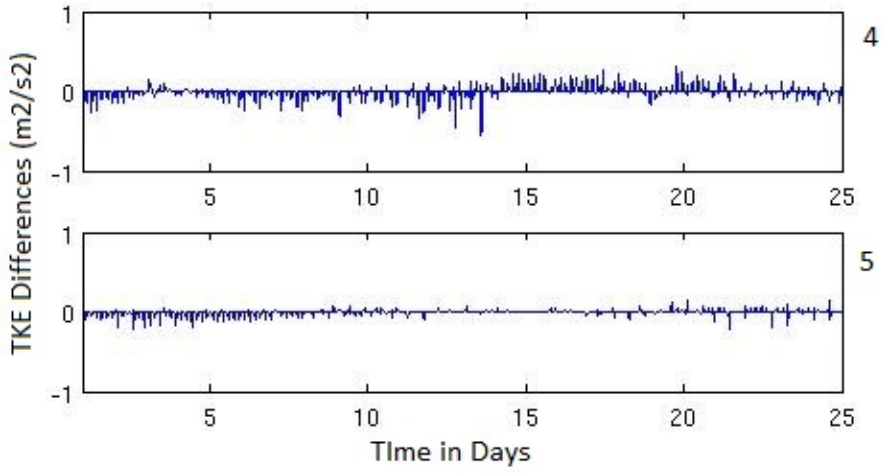

(b)

FIGURE 5.6: Surface tke differences (F-M) on the surface at 5 points within Liverpool Bay

Figure 5.6 shows the surface TKE differences for M-C at the locations in Figure 5.4. Comparing Figure 5.5 line 1 and Figure 5.6 Line 1 it is clear that the

use of both turbulence and momentum impacts reduces the impact at location 1. It is also clear that the momentum is the cause of the impacts at locations 3 and 5 near the freshwater outflow. A reason for this could be because the water column is unstable naturally in these areas as the freshwater is mixing with the saline water and adding an additional mixing term will create further instabilities.

The impacts on the momentum and turbulence could potentially cause a change in salinity and temperature. To that end, salinity and temperature are now considered.

5.2.1 Surface Salinity Comparison

We now consider the monthly surface average for December. We select December because it is an area of particularly large differences between M and F both in magnitude and fluctuations. We consider monthly averaged salinity calculated using equation 4.2 which sums the surface hourly output and divides by the number of hours in the month. This is done by comparing the F and M to the control simulation and shows the simulated impacts from each mathematical method.

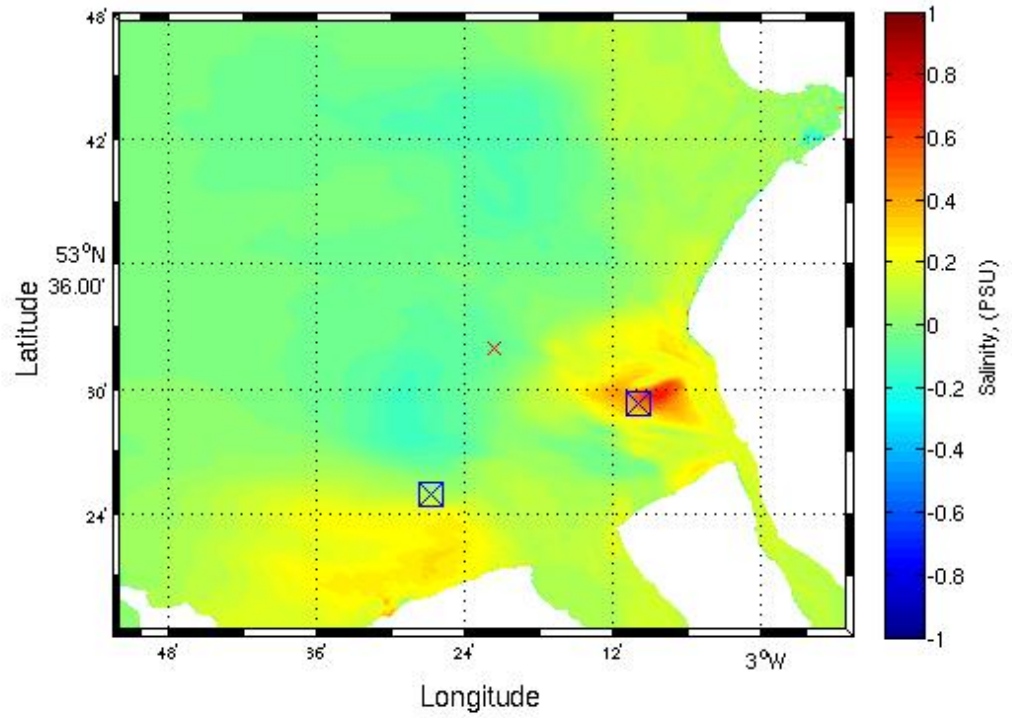

FIGURE 5.7: Surface Salinity difference, F - C. Plotted on a latitude/longitude domain with OWF centres represented with a blue box and site A represented by the red cross

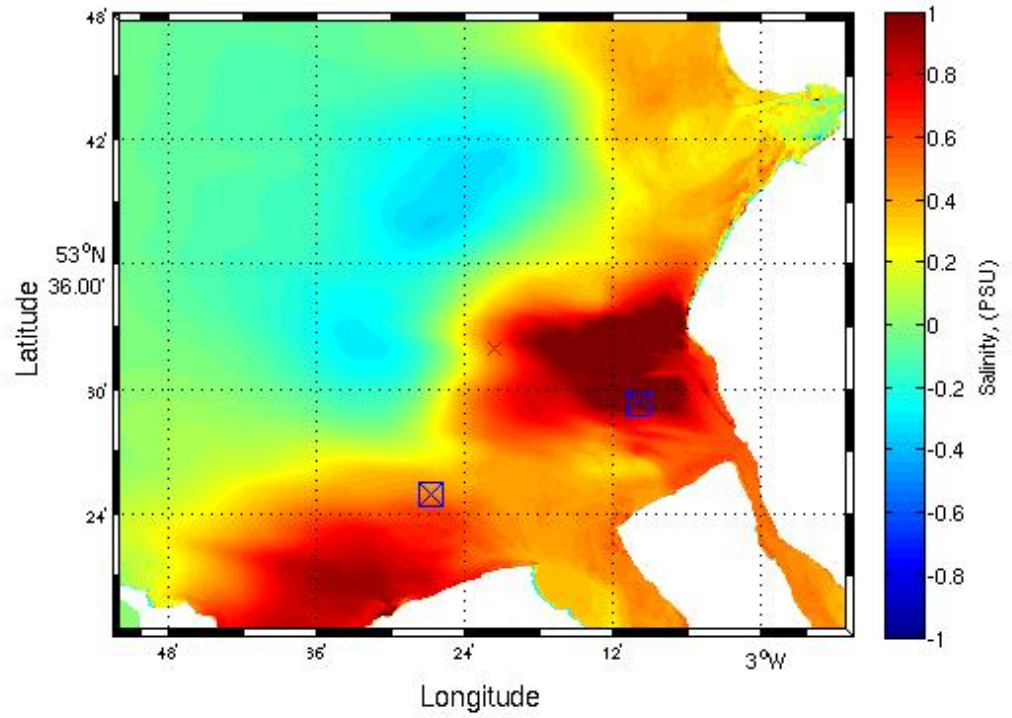

FIGURE 5.8: Surface Salinity difference, M - C. See Figure 5.7 for plot details

Figure 5.7 and 5.8 shows the impacts due to the F and M salinity respectively. The first major observation is that M (Figure 5.8)has a much larger change in surface salinity due to the OWF's. Figure 5.7 shows localised impacts which will be discussed in chapter 6. Figure 5.8 shows the change in surface salinity due to the momentum only representation. This shows the salinity increase across a large area in the bay. There is a clear increase of salinity in the area where the Ribble, Mersey and Dee freshwater inflows. This is likely due to the momentum blockage locally at the OWF sites which then prevents the salinity flushing out of the river estuaries. Burbo bank in both Figure 5.7 and 5.8 both show that the largest impacts are near Burbo Bank OWF (eastern OWF). As both models have the same momentum input, this effect is caused by the turbulence which is coupled together with the momentum. As this is also seen in Figure

5.8, we can conclude the localised impact is predominately due to the impacts on the momentum with the turbulence impacts having an opposing effect. Conceptually, such oppsoing effects between the two contributors (momentum and turbulence) is consistent with the physical representation in the governing equations (see chapter 3): a momentum sink reduces tidal energy and thus turbulent energy opposed to the extra turbulent production is introduced. Conversely, extra turbulence corresponds to more efficient transfer of momentum, opposed to the momentum sink.

5.2.2 Surface Temperature Comparison

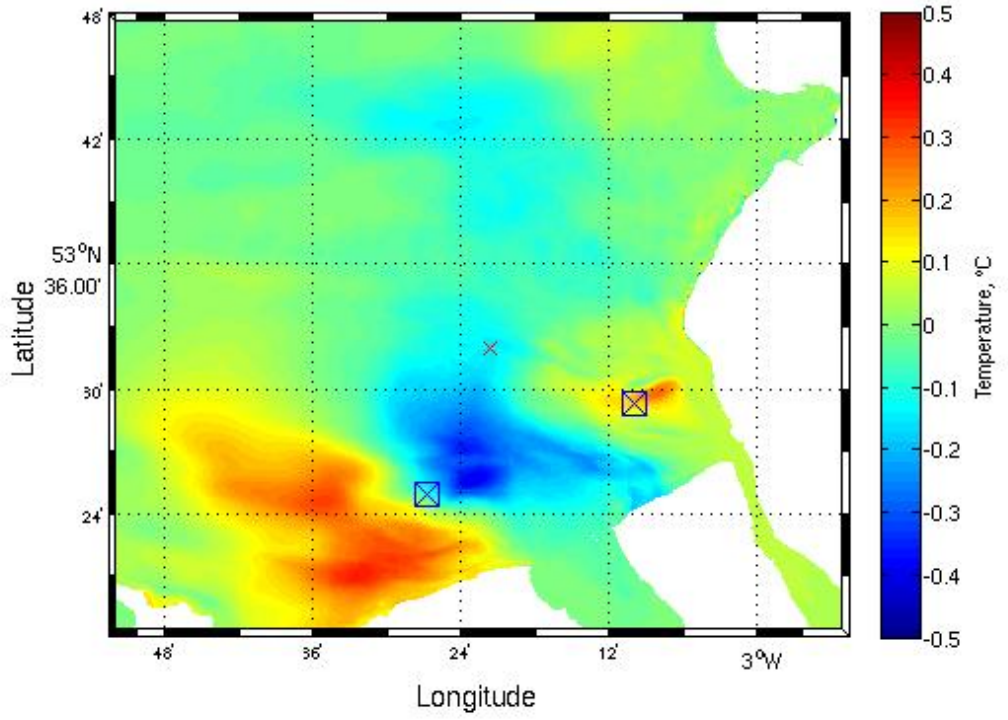

FIGURE 5.9: Temperature impacts due to Momentum and Turbulence model, M - C

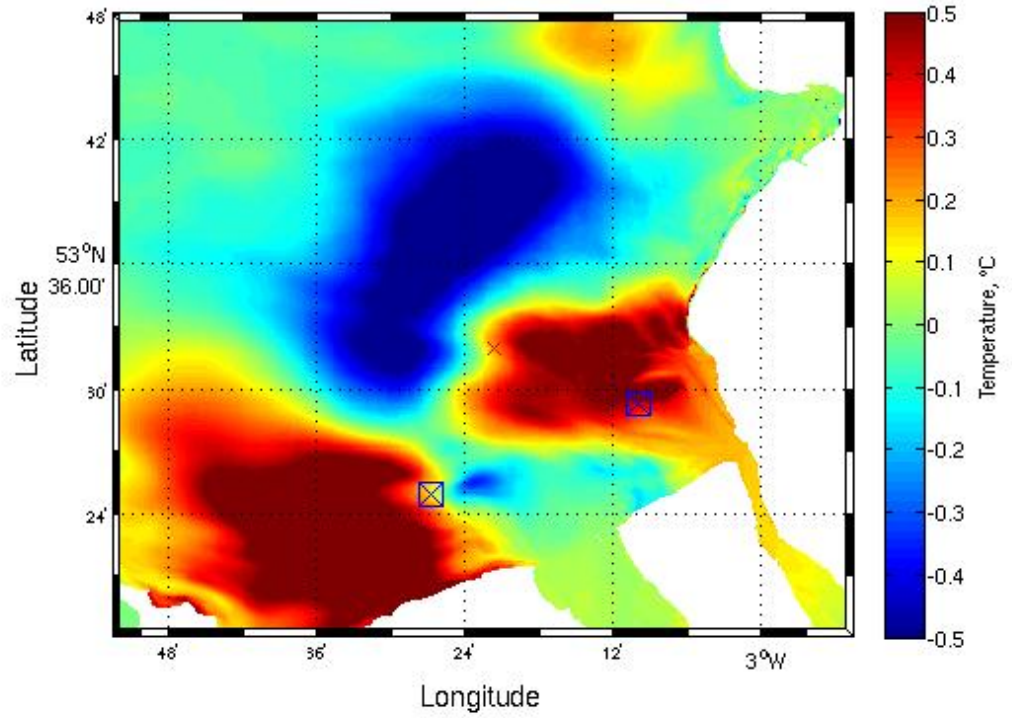

FIGURE 5.10: Temperature impacts due to the Momentum model, F - C.

In Figure 5.9 and 5.10 we present the surface temperature impacts due to the OWF's from F and M respectively. Figure 5.9 shows the impacts are far less when considering both momentum and turbulence impacts than when just considering momentum, Figure 5.10. When we look are M (Figure 5.10) we can see the effects of the OWF's can be seen throughout the domain, there are two large areas of increased surface temperature which are located near the OWF centres. This shows the warmer waters are staying in these areas instead of moving freely around the domain. There is also a large area of reduced temperature in the centre of the domain, suggesting that the colder waters emerging from the estuaries are being pooled in this area. When we consider the results from F, (Figure 5.9) we can see that the area between the OWF's that experiences a reducing in surface temperature. It can be assumed that the increased mixing due to the

OWF's allows the fresher, colder water to flush out of the estuaries where as in M this water is being blocked. This would again suggest that the increase in mixing that the turbulence impact equations introduces directly opposes the momentum impacts caused by the OWF's. To investigate this point further, we consider the momentum and turbulence contribution by plotting them individually.

Here we plot the turbulence impact contribution to F. We calculate it by subtracting M from F leaving the difference between the two models. This means the turbulence contribution we present is that from a model that also has momentum impacts simulated along side. As a result it represents the change in impact that are attributed to the P_d term in the impact equations (section 3.2). In the impact equations discussed in section 3.2 P_d and G_d have opposing signs which leads to the turbulence and momentum working against each other to balance the equations.

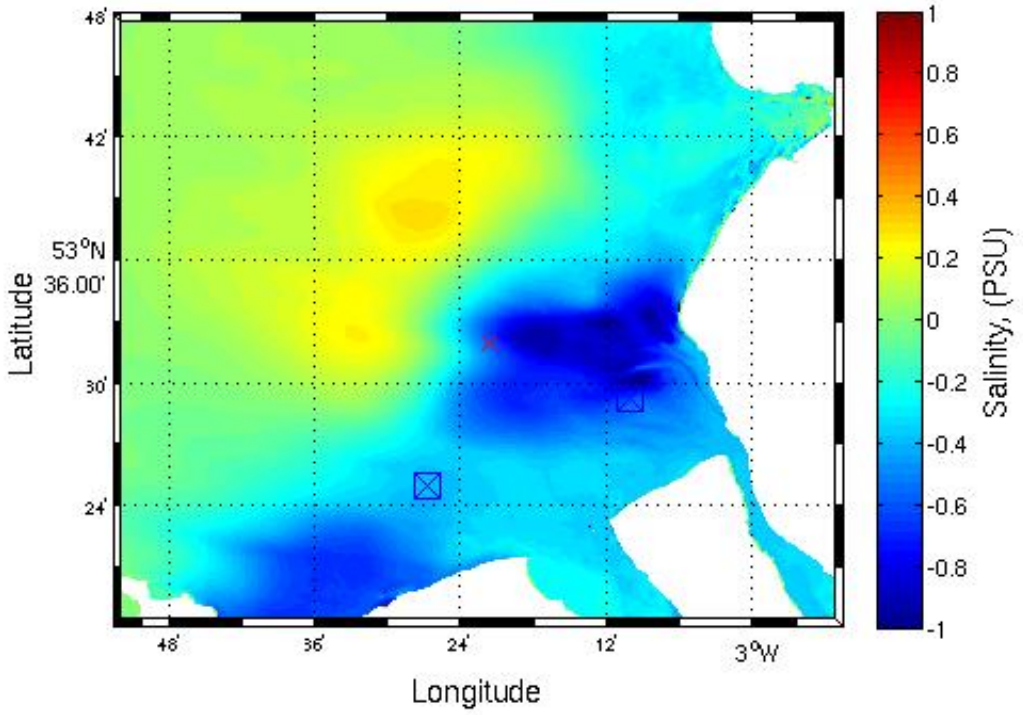

FIGURE 5.11: Salinity TKE impacts for December calculated by F - M, Latitude/Longitude Domain, Windfarms marked as squares, Site A and B marked as triangles

Figure 5.11 shows the surface salinity impacts due to the turbulence mixing. We can compare this with Figure 5.8 which shows the momentum contribution. As we predicted the turbulent impacts are opposing the momentum impacts. Figure 5.11 reduces the majority of the impact that is in the bay from which we can conclude that for the salinity in Liverpool bay, modelling structures with only momentum tends to over predict the impact on salinity. As Liverpool bay is a salinity driven ROFI this is likely to have a big effect on the density which is also supported by the differences seen in Figure 5.3

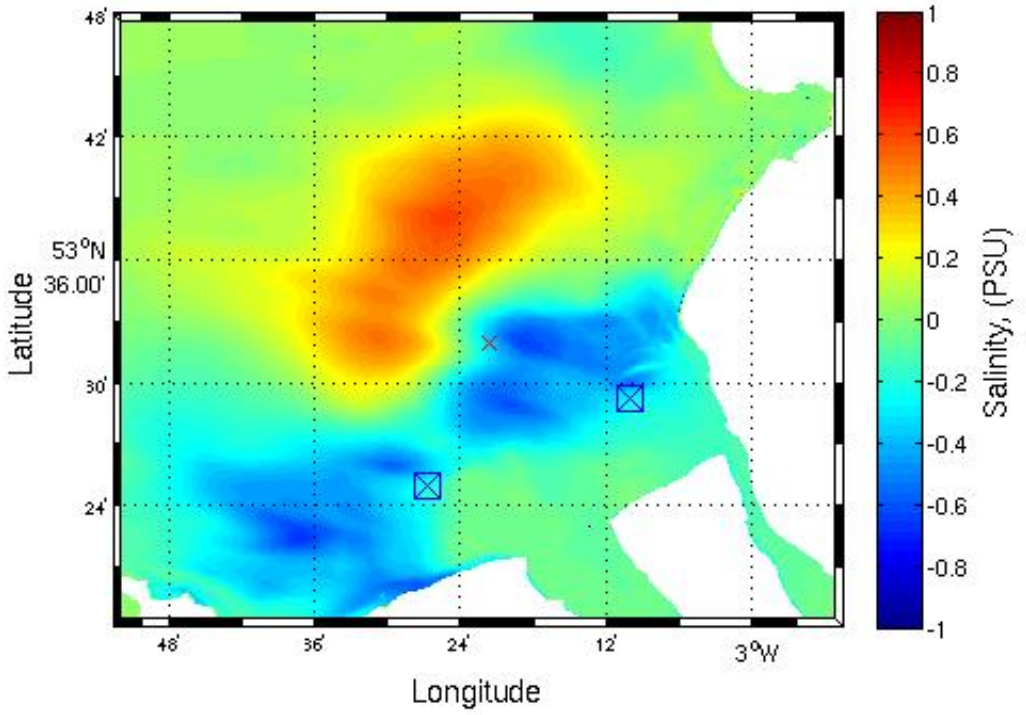

FIGURE 5.12: Temperature TKE impacts, see Figure 5.11 for details

Figure 5.12 shows the turbulent impacts on the surface temperature once again this shows the temperature change due to the turbulence is directly opposing that of momentum in Figure 5.10. The impacts are similar to the salinity discussed above in the sense that the major effects on the temperature tend to reduce the overall impact in the far field ranges of the OWF's. This backs up the fact that using only a momentum sink with over predict the impacts of the simulation.

5.3 Temperature Fronts

We use the 7°C temperature line to measure the effects due to M and F on the front in the ROFI. The 7°C temperature front can be used as a diagnostic variable

for freshwater inflows (Bricheno et al, 2014 [18]) which shows the position of a front in a ROFI. We present the data for C, F and M for December plotted on the latitude/longitude domain.

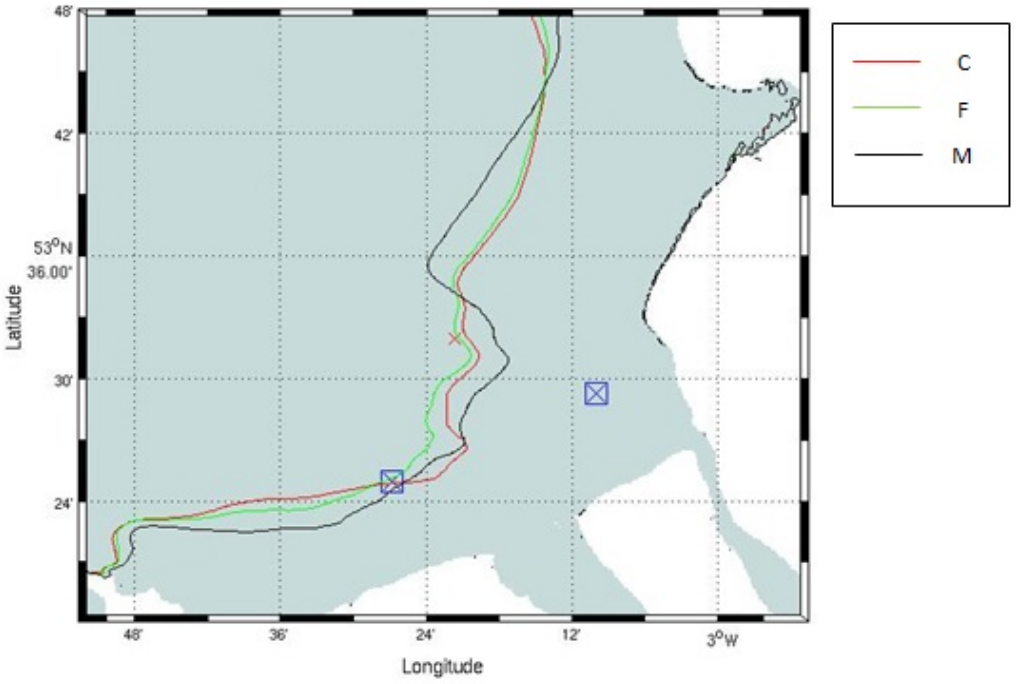

FIGURE 5.13: 7°C temperature front for December, Latitude/Longitude Domain, OWF's marked as squares

Figure 5.13 show the December 7°C for C, F and M respectively. There are very small differences in the fronts in F and C showing that the OWF's simulated using momentum and turbulence has limited effects on the temperature front. However, M shows a large effect near on the temperature front near the Ribble estuary. This is consistent with the decrease in temperature in Figure 5.10 which shows once again that representing structures are momentum sinks tends to change the hydrodynamics in the far field more than when using the momentum and turbulence method.

5.4 Conclusions

In this section we compared the results from a momentum sink structure simulation method and full turbulence and momentum structure simulation method. We use the parametrization technique which is applied to the POLCOMS-GOTM numerical model discussed in section 3.2. We use the setup We used field data measurements (Polton et al, 2011 [57]) at site A as a validation and use skill values to assess model accuracy. We found that for most hydraulic parameters F tends to preform better when simulating the hydrodynamics with structures in Liverpool Bay. This is shown in the skill values (table 5.1) which highlights a small increase in accuracy. On the intra tidal scale, M does not preform well when compared to F. It can be concluded that the assumptions made when using the momentum sink (ie no turbulence mixing)cause the model to not predict many of the fluctuations seen in density for observational data (Figure 5.3). F in comparison does manage to simulate them with better accuracy.

We have shown that using the momentum sink leads to over predictions for salinity and temperature is terms of absolute value change (Figures 5.10 and 5.10) and spatial extent of OWF influence. This moves the 7°C temperature creating additional areas of fresher water near the Ribble and higher salt intrusion near the Dee and Mersey. In the equations, the momentum and turbulence impact terms are numerically opposing. This is highlighted by the reduction in magnitude and area of influence of the full model compared to the momentum sink model.

This chapter shows that it is important to consider both the momentum and turbulence impacts when simulating structures in Liverpool bay otherwise the total impact on surface salinity and temperature is over estimated and the intra-tidal fluctuations are not modelled accurately. This has potential ramifications on impact studies for engineering purposes that could lead to under use of planned areas of commercial development.

Chapter 6

Impacts of OWF's on Liverpool Bay Dynamics

We now use the numerical model described in chapter 3 and apply it to a region of freshwater influence (ROFI) where OWF's have been deployed. The objective of the work presented hereafter is to assess the impacts of two wind farm deployments on the complex dynamics of Liverpool Bay in 2008 using the best model setup, as identified in the previous chapter.

This chapter contains a brief description of the hydrodynamics in Liverpool bay and the simulation set-up which is used to evaluate the impacts of OWF's on salinity, temperature and density at different spatio-temporal time scales; yearly, monthly and daily. Reasons are given for the changes by looking at inflow data and considering vertical mixing. Conclusions are drawn on the effects of the OWF's on the vertical profile of the water column at near and far spatial scales.

6.1 Numerical simulation

We use POLCOMS-GOTM coupled system (Holt and Umlauf, 2008 [33]) with the structure module described in section 3.2 and apply it to Liverpool Bay using the model described in section 3.5.

The OWF's are represented by applying a control area corresponding to full spatial area of the OWF (section 3.3), this is because the individual representation fails to predict the hydrodynamics (chapter 4) and the control method is representative of the method needed in large scale models where the horizontal resolution is greater than device scale. Also fully resolving the gradients and flow patterns within the OWF's is computationally more expensive and impractical using structured grid. A representative 4m diameter is used to simulate the cylindrical structure as their diameter ranges from 3m to 7m. The drag coefficient is taken to be 0.63, i.e. a cylindrical object in a water flow. The coefficient used in the turbulence closure scheme is set to 0.6 (section 3.5) as defined in Rennau et al, 2012 [59] for the high turbulence scheme which is justified for the strong tidal currents present in Liverpool Bay.

We present numerical results highlighting impacts of OWF's on complex dynamics of Liverpool Bay. The impacts of the OWF are determined by considering the difference between a control simulation (hereafter called C) containing no wind farms and a simulation including the full effects (hereafter called F) of OWF's in the domain.This will allow us to quantify any effects caused by the inclusion of structures and discuss what impacts these have on the near-field, here defined as array radius plus 500 metres (100 times diameter) and the far-field.

6.2 Results

We present and compare the numerical output from the model simulations to assess the impact of OWF's on the ROFI dynamics at different spatio-temporal scale. We will first focus on the year long time series at site A in Liverpool Bay. This specific site is chosen for two reasons, firstly extensive field data was collected as part of the Irish Sea Coastal Observatory program (Howarth and Palmer, 2011 [40]) and has been used for validation purposes (Polton et al, 2011 [57]), section 4.2). Secondly, the position of the site is such that we expect it to

be impacted by effects from both OWFs. We then select month averages where we consider the effects of surface dynamics due to the turbines. Finally, we zoom in both in space and time and study the inter-tidal response in the bay via a model-model comparison at site A.

6.2.1 Yearly Time series comparison

We present comparisons of yearly time series in order to assess the OWF impact over the 2008 full annual cycle and select months for closer analysis.

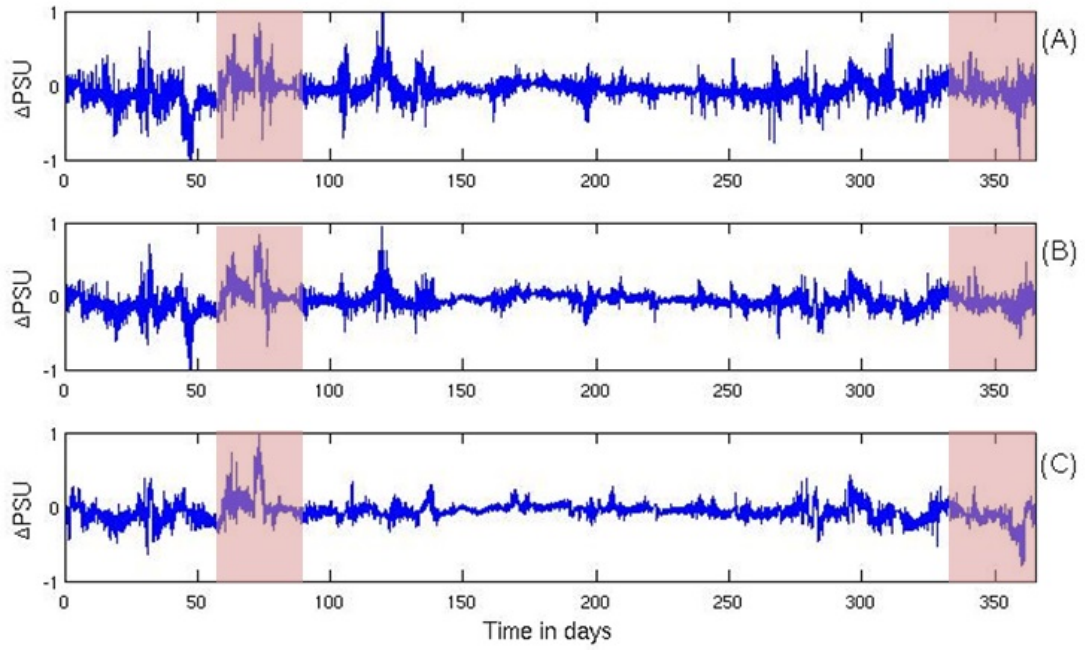

FIGURE 6.1: Time series of Salinity difference (PSU) between C and F, ($\Delta PSU = PSU_F - PSU_c$) at site A at different elevations in the water column a) 5m below surface, b) 10m below surface c) 0.5m above seabed. The shaded areas represent March and December which are the time periods used for the monthly averages.

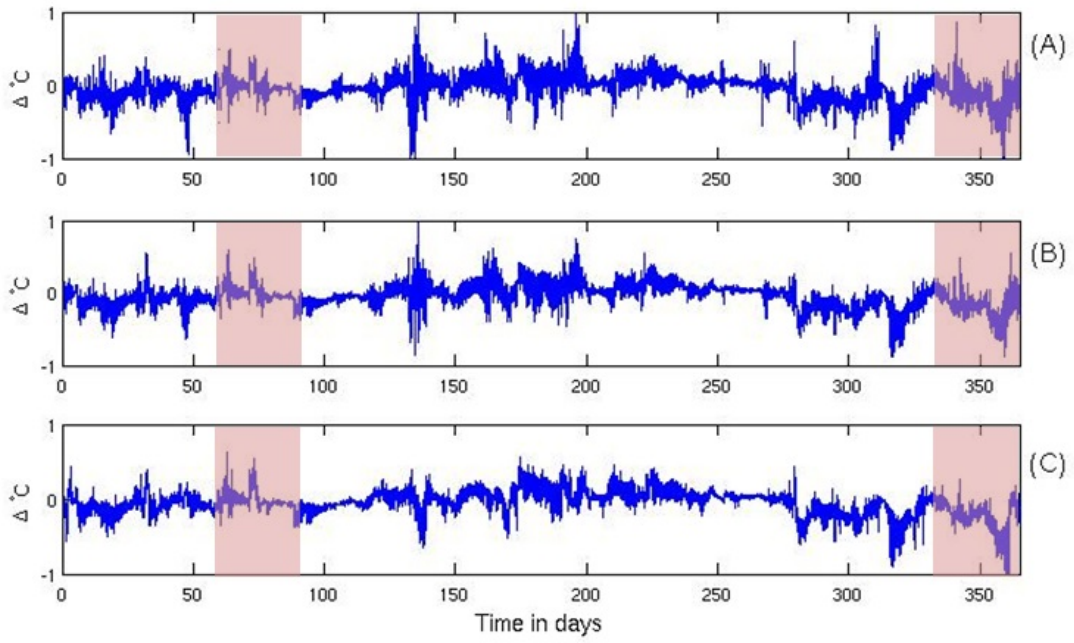

FIGURE 6.2: Time series of temperature difference, see Figure 6.1 for caption details

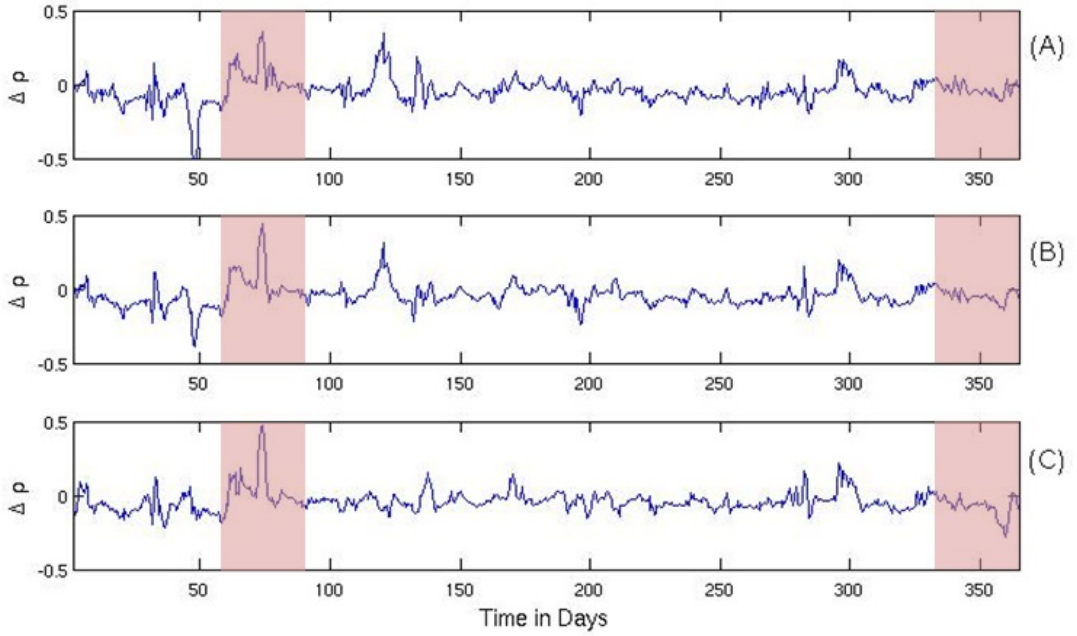

FIGURE 6.3: 25 hour filtered time series difference, Density. See Figure 6.1 for details

We use the model data (F) validated in section 4.2 (Figure 4.1, 4.2, 6.3) to compare the impacts of F for salinity (Figure 6.1), temperature (Figure 6.2) and 25-hour water density (Figure 6.3) at site A (Figure 3.10). Figure 6.1 shows the impact of OWF's on salinity and Figure 6.2 shows the OWF impacts on temperature by plotting the difference between F and C ($F - C$). Fluctuations are observed throughout the year with a few particular periods of strong impacts. However, we disregard the first two months (Jan-Feb) as the hydrodynamic predictions were significantly biased (Figure 4.1, 4.2) and discussed in section 4.2.

Figure 6.3 shows the 25 hour filtered density difference at various levels to remove intra-tidal fluctuations present in Figure 6.1 and 6.2. Once again the first two month are of little significance due to the poor quality of the numerical simulations (Figure 4.2, 4.2). We consider two time periods in this year for further analysis. March shown in Figures by the first red box shows the largest positive difference which extends throughout the water column. December, highlighted

in the second red box shows the largest negative difference (post February) at the seabed and can be seen at a decreasing rate up the water column. We intend focus the analysis on these periods of time to give reasons from these larger fluctuations. There are other areas where differences are present however they are either at one or two water levels or smaller in magnitude that the two areas selected.

Position	Density Average	Salinity Average	Temperature Average
-5m from surface	-0.041	-0.0590	-0.0413
-10m from surface	-0.039	-0.0567	-0.0424
-0.5m from seabed	-0.040	-0.0591	-0.0499

TABLE 6.1: Yearly average density difference, (F-C)

Table 6.1 shows the yearly average difference for the three positions in the water column at site A. The average effect on the density due to the OWF's appears to be a consistent reduction in average density through the water column of 0.04 kg/m^3. This could suggest the potential slight increase in fresher and cooler water (table 6.1).

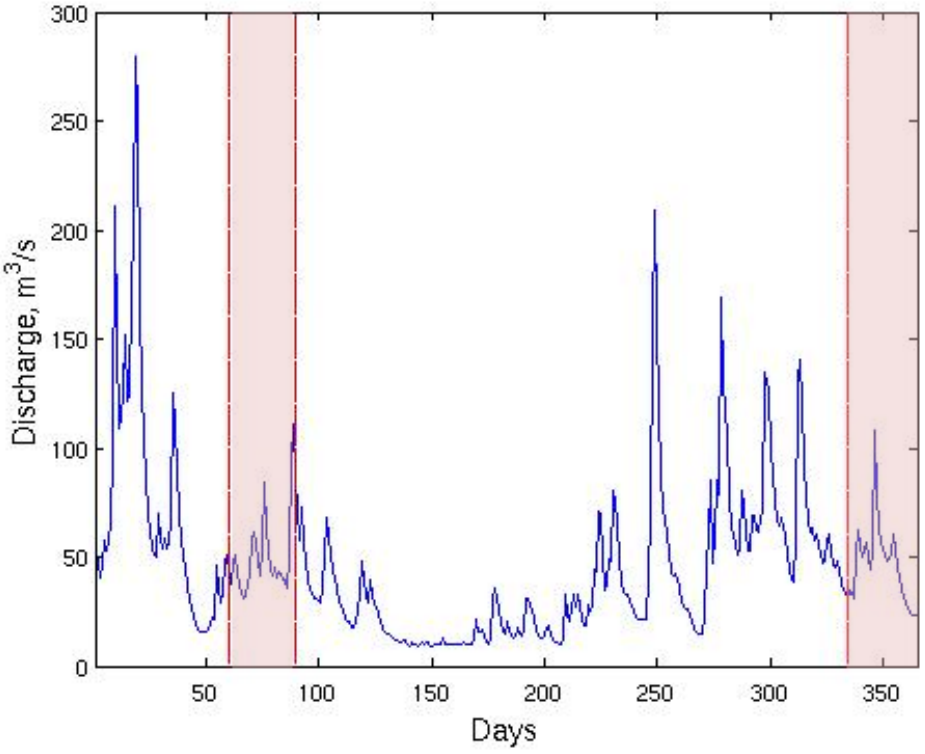

(a) River Dee

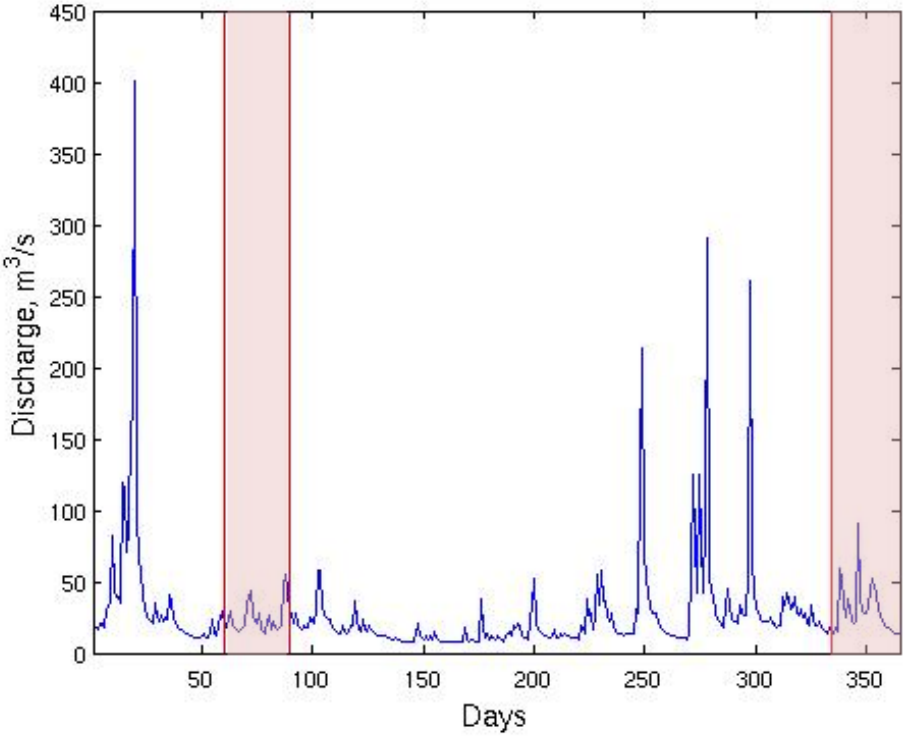

(b) River Mersey

FIGURE 6.4: River Input forcing for 2008 with highlighted March and December

River	March (m^3/s)	December(m^3/s)	Yearly average
The Dee	45.77	53.93	47.20
The Mersey	22.15	28.07	22.82

TABLE 6.2: Average River monthly discharge, ($\bar{x} = \frac{\sum_i x_i}{n}$)

Figure 6.4(a) and 6.4(b) show the yearly river inflow from the River Dee and Mersey (See Figure 3.6 for input location) with highlighted months for closer study. We look at shorter time periods to consider the monthly effects of the OWF's. March and December have been specifically chosen for a number of reasons. In the model validation plots (Figure 4.1, 4.2), the model starts to predict the overall trend well from March, it was important to investigate this time period to see the impacts as early in the year as possible. March was also chosen because the presence of a higher difference in the model comparison plots, Figure 6.3 which highlights the large difference in March which extends throughout the water column, which is the largest positive difference for the Year. Finally, Figure 6.4(a) shows the inflow is in gradual increase to a peak of over 100 m^3/s from the Dee river. Average flow rate from the Dee through March is $45.77m^3/s$ (table 6.2). The Mersey (Figure 6.4(b)) has an average discharge in March, $22.15m^3/s$ (table 6.2). We can use this month to make comments on the effects of OWF's in a month that experiences average freshwater discharge.

The reason December time period was chosen is two-fold, firstly we wanted to look for reasons for salinity and temperature (Figure 6.1, Figure 6.2) fluctuations seen through the water column. Fluctuations which are also be seen in the 25-hour density (Figure 6.3). Secondly, the outflow from the River Dee shows a rise in flow to a peak of over $100m^3/s$ and falls off at the end of the month. The Dee inflow shows an average of $53.93m^3/s$ and Mersey is $28.07m^3/s$ (table 6.2) which is consistently higher than both inflows in March. We can use December to view

the impacts of OWF's across Liverpool Bay in a month where the freshwater flow is greater than the yearly average.

We haven't focused on the late autumn months (September, October and November) where the inflow from the rivers tends to be much larger because there are no large visible effects when comparing the two different model's C and F (Figure 6.3). This could be due to a change in the dominant dynamics which are not affected by the OWF's.

6.2.2 Speed and Turbulent Kinetic Energy Comparison

We present the surface[1] speed plots for March 2008. Each chart represents the surface speed for C (Figure 6.5(a)), F (Figure 6.5(b)) and the difference (Figure 6.6(a)). The results are obtained using the surface U and V velocity monthly residuals to calculate the surface velocities for March. Monthly residuals are calculated by equation 4.2. All surface plots hereafter are plotted on latitude and longitude domain for Liverpool Bay with wind farm centres represented.

[1]All mentions of 'surface' refers to the surface sigma layer

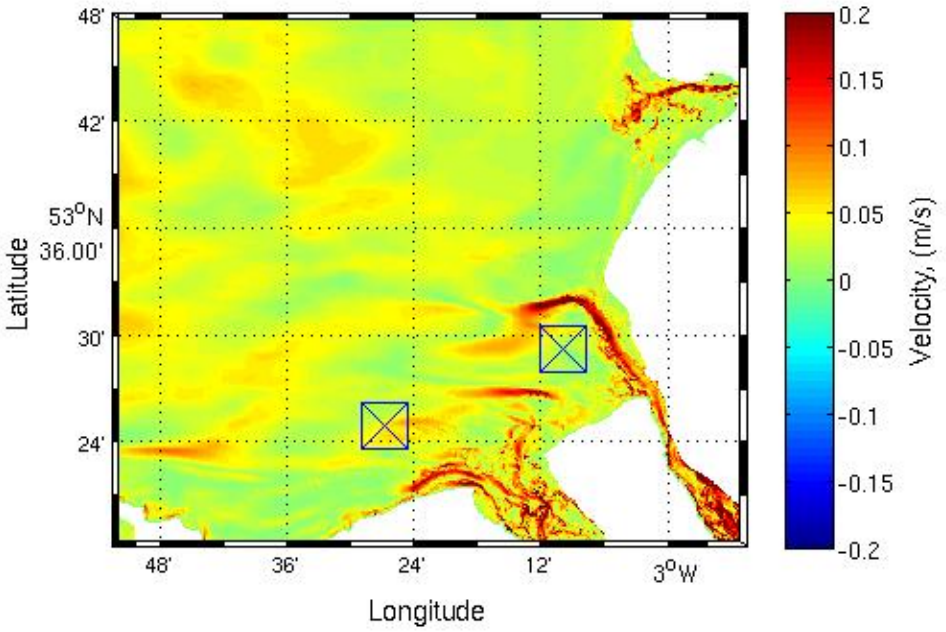

(a) March monthly residual for surface current speed from C simulation. The wind farm locations are indicated by the square crosses

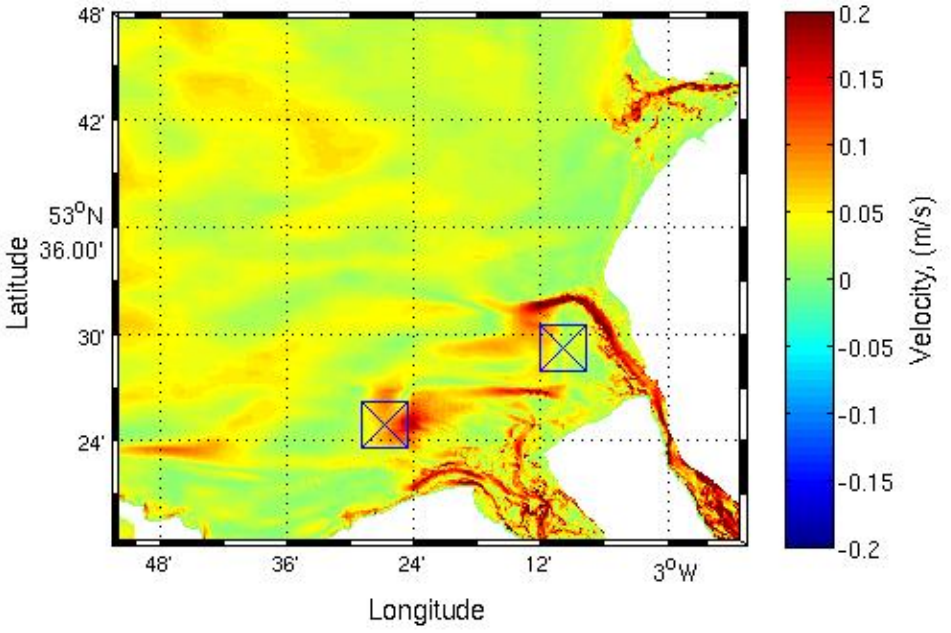

(b) March monthly residual for surface current speed for F simulation. The wind farm locations are indicated by the square crosses

FIGURE 6.5:

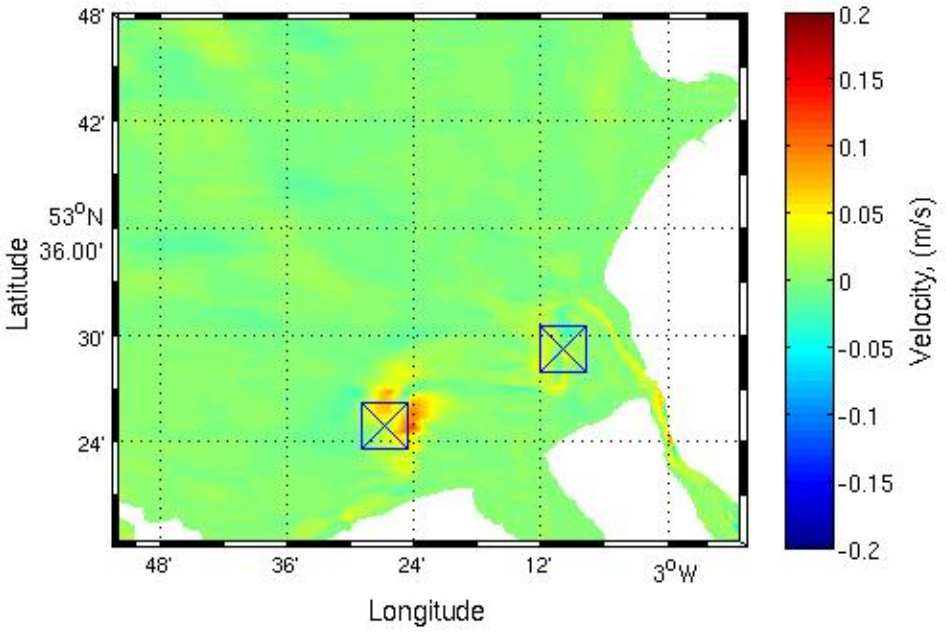

(a) Surface Speed Magnitude Difference $(C - F)$ in Liverpool bay for March 2008 with wind farm centres marked, $(\Delta U = U_F - U_C)$

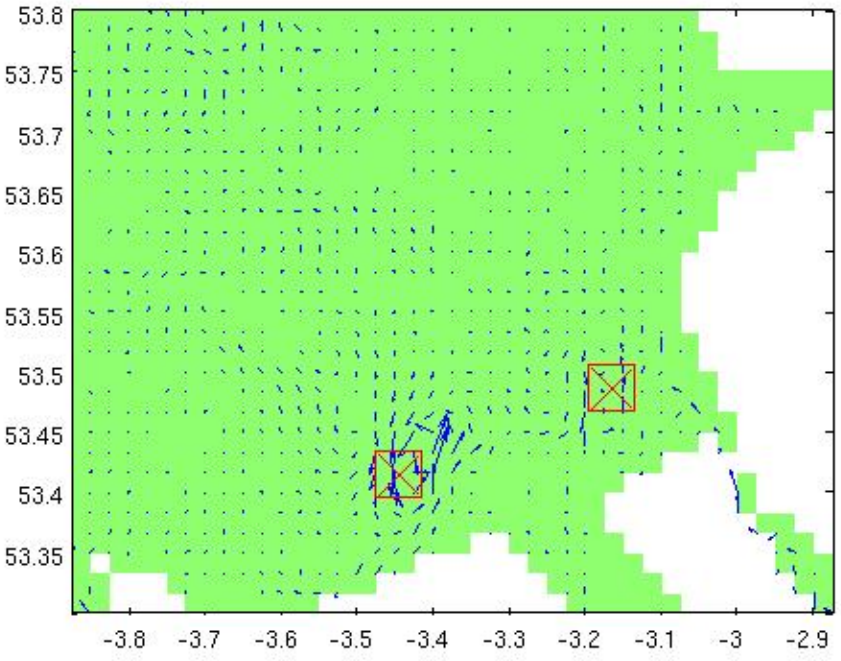

(b) Surface Speed Direction Difference $(C - F)$ in Liverpool bay for March 2008 with wind farm centres marked, $(\Delta U = U_F - U_C)$

FIGURE 6.6:

Figure 6.5(a) and 6.5(b) show the magnitude of the surface speed residual for the C and F model respectively. Both plots show similar spatial patterns, in particular the large values in the estuary channels of the Mersey, Dee and Ribble. We calculate the difference by taking of the speed plot for F from the speed plot for C ($Speed_F - Speed_C$) and plotting the directional difference, Figure 6.6(b).

The presence of the OWF's has a local (hereafter defined as 1km from the edge of the area of influence) effect in (Figure 6.6(a)). The largest impacts are caused by North Hoyle OWF (Western OWF with changes in residual speed of over 10 cm/s, which is similar in magnitude to the background residual (Figure 6.5(a)). Burbo Bank (eastern OWF) seems to have a weaker absolute impact, which may be due to its location in a region of weaker residual current. However, changes in residual speed of approximately 5 cm/s are still produced in the outer Mersey estuary channel. This corresponds to about 20 to 25% of the background residual and is likely that this effect is mostly due to the presence of Burbo Bank. The impact on the rest of the bay is small and mostly negligible. This confirms that the speed is principally affected locally and then recovers downstream as expected in wake behaviour (Neill et al, 2012 [52]).

The turbulent kinetic energy is one of the fundamental variables that cause the changes in salinity and temperature. Below are the surface line plots for tke at 5 locations in Liverpool Bay show on Figure 5.4. Two points are in the middle of the domain and three are along the coastline near the mouth of the Dee.

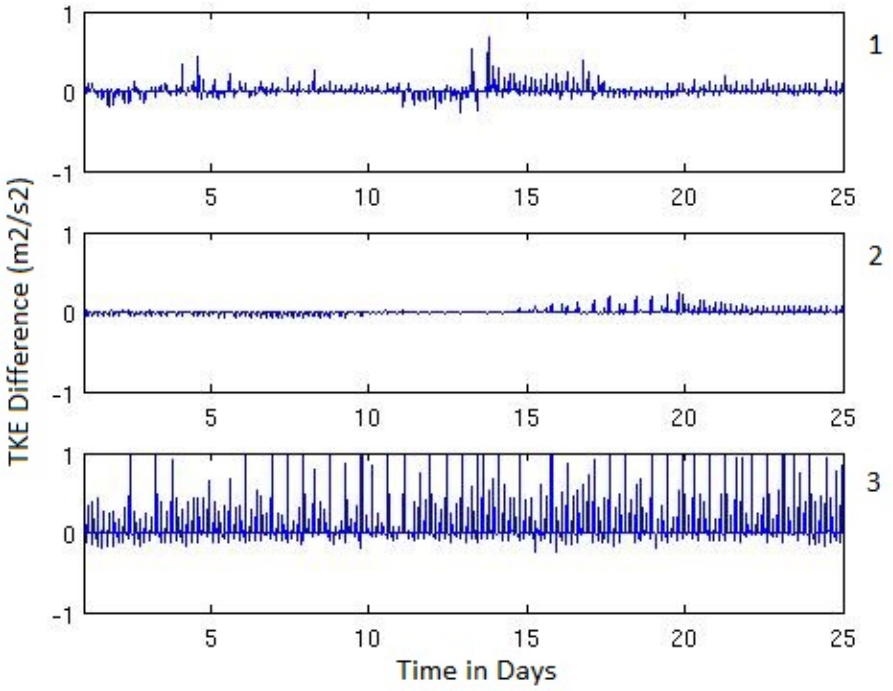

(a)

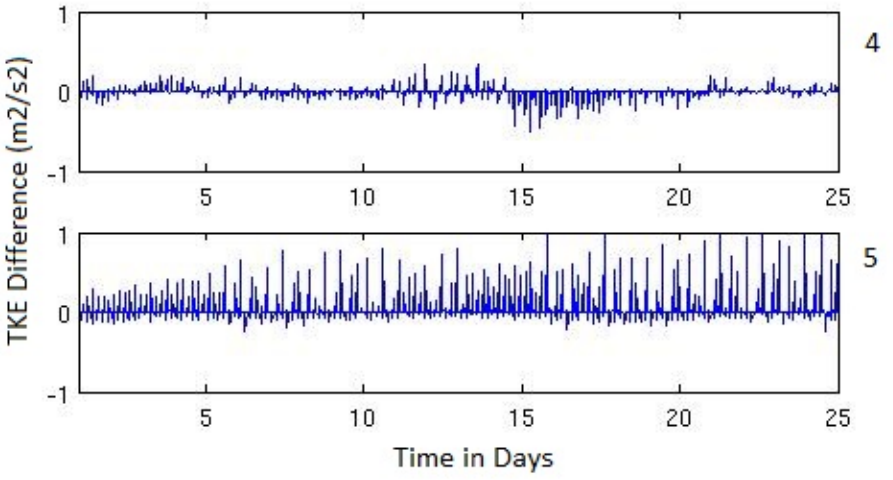

(b)

FIGURE 6.7: Surface tke differences (F-C) on the surface at 5 points within Liverpool Bay

Figure 6.7 shows the surface tke differences at the locations show in Figure 5.4. Line plot 1 and 2 shows that the model is sensitive to tke changes in the bay. These plots are outside of the area of significant influence of freshwater from the

rivers. The two line plots, 3 and 5 are located at the mouth of the Dee. There is a large change in tke at these locations. This shows that the OWF placements have a greater impact on the tke where the freshwater is discharging into the bay. All the line plots show that in most cases the tke is increased in the region of freshwater influence by the presence of the OWF.

6.2.3 Monthly Surface salinity

Monthly residuals of surface salinity for both March and December (Figures 6.8(a), 6.8(b), 6.11(a), 6.11(b)) are used to investigate the impact on the surface of the OWF's. March and December averages are plotted for C and F model results followed by an absolute difference and percentage difference plot calculated by F - C.

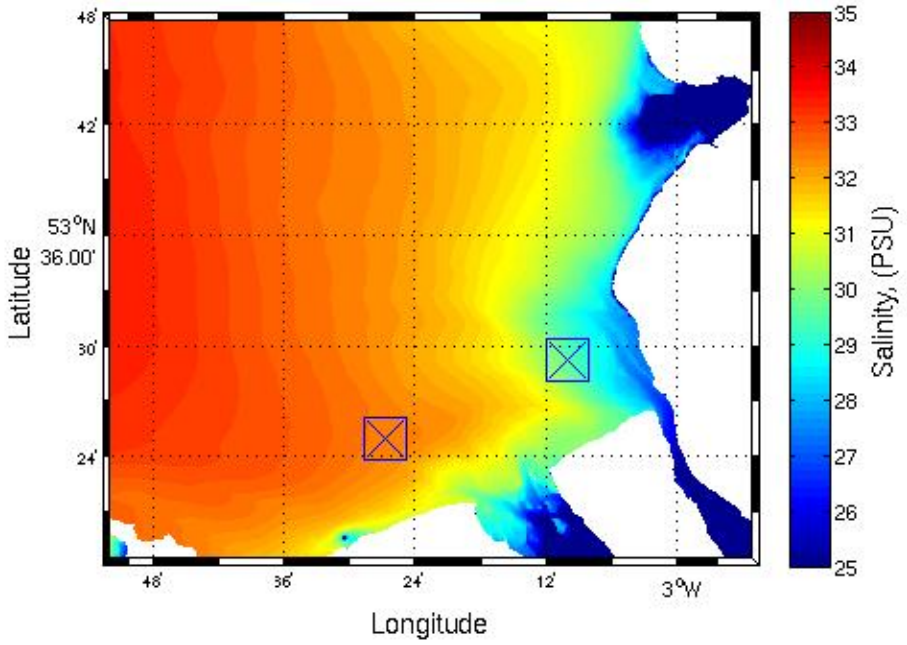

(a) C simulation

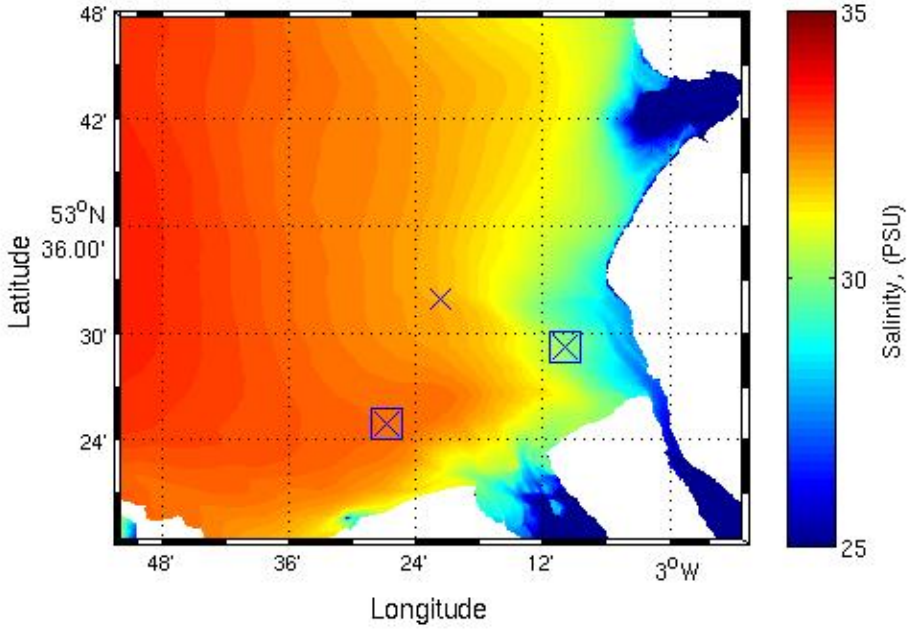

(b) F simulation

FIGURE 6.8: Surface Salinity Monthly residual for March, latitude/longitude Domain, OWF's marked as squares

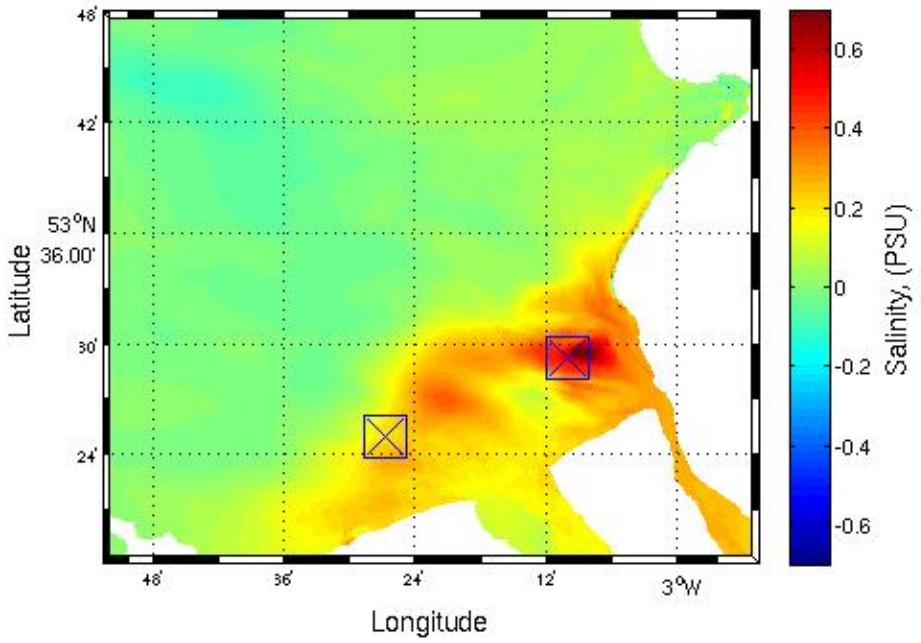

(a) $F - C$

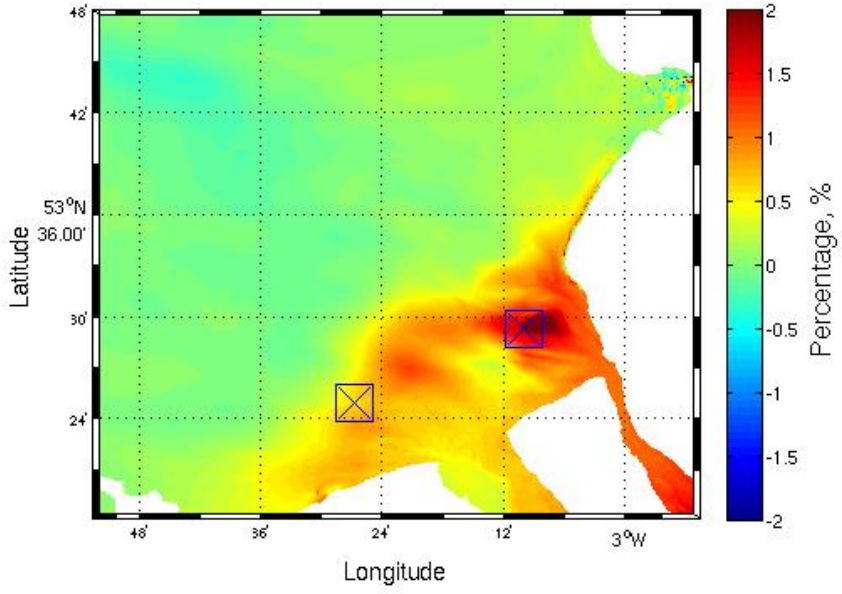

(b) Percentage difference $100 * ((F - C)/C)$

FIGURE 6.9: Surface Salinity Differences, latitude/longitude Domain. OWF's marked as squares, March

Figure 6.8(a) and 6.8(a) show the plotted monthly residual for C and F respectively. Both these plots show the positions of the wind farms modelled in this study. It is clear from these results that the Burbo Bank windfarm is located in the region of influence of the Mersey freshwater outflow. This has an effect on the impact on surface salinity as is shown in Figure 6.9(a) where the maximum impact on the monthly residual is in the near field of Burbo Bank with values of around 0.9 PSU (Figure 6.9(b): 3%) corresponding to a $0.6kg/m^3$ increase in density at the surface. The presence of Burbo bank in this area is likely to cause greater shear diffusion due to the proximity to the strong horizontal gradients near the Mersey freshwater plume.

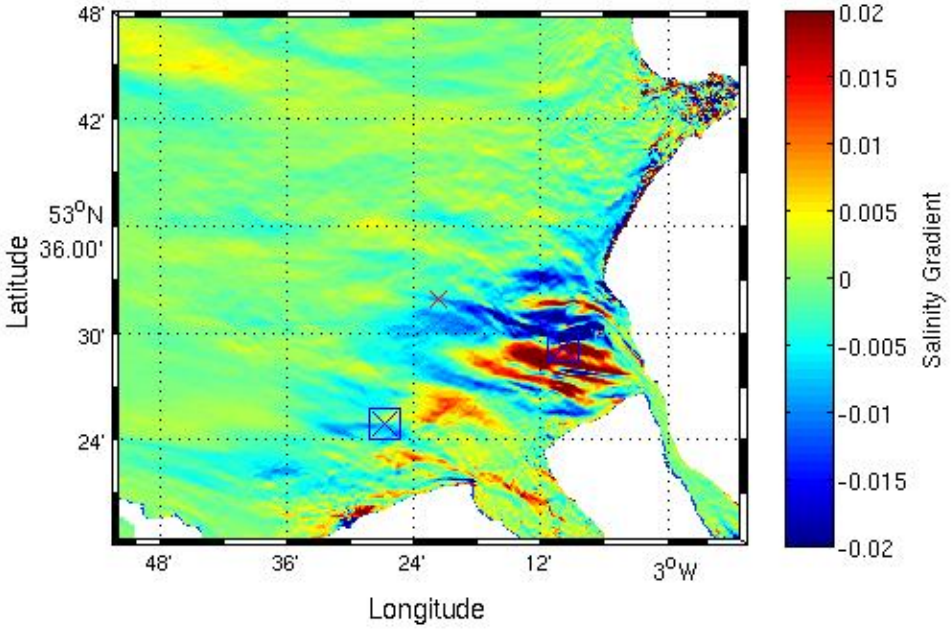

(a) East-West component

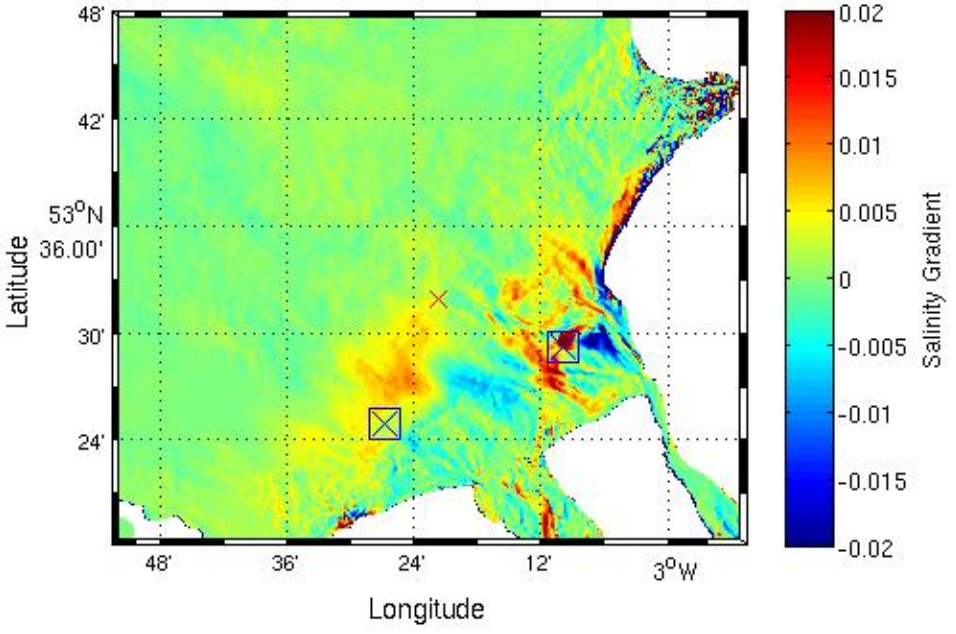

(b) North-south component.

FIGURE 6.10: Surface Salinity Gradient plotted on a Latitude/Longitude domain with OWFs marked as squares.

Figure 6.10(a) and 6.10(b) show the difference (F-C) in surface salinity gradients in the east-west and north-south directions. The gradients are calculated from the average surface salinity for March. Figure 6.10(a) shows that the impacts are spatially varying. The OWF appear to increase gradients locally (yellow/red areas) but decrease gradinets further away (Blue). This suggests (combination with Figure 6.6(a)) spatially varying changes to the balance between tidal mixing (changes to the currents) and buoyancy forcing (changes to the salinity gradients). For both, increases and decreases are observed and this has important implications for the dynamical behaviour of the Bay which is controlled by this balance.

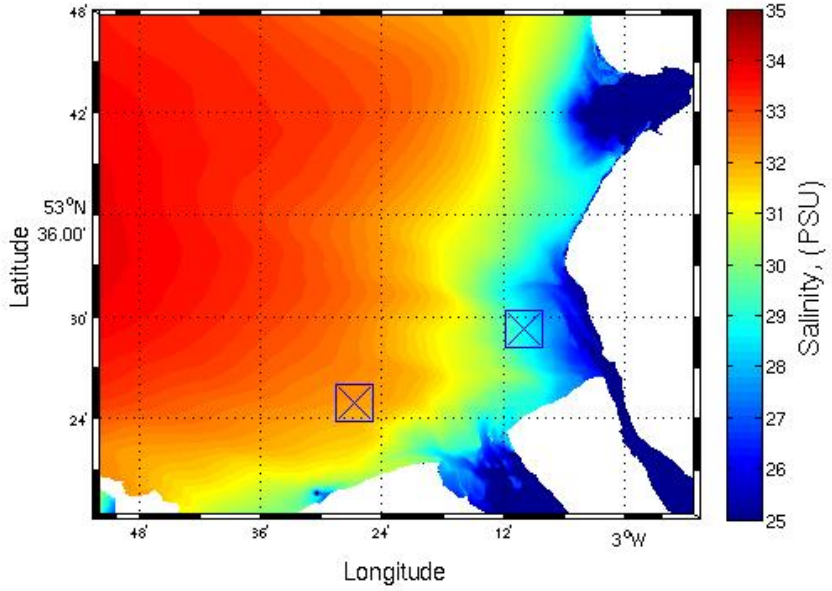

(a) C Simulation

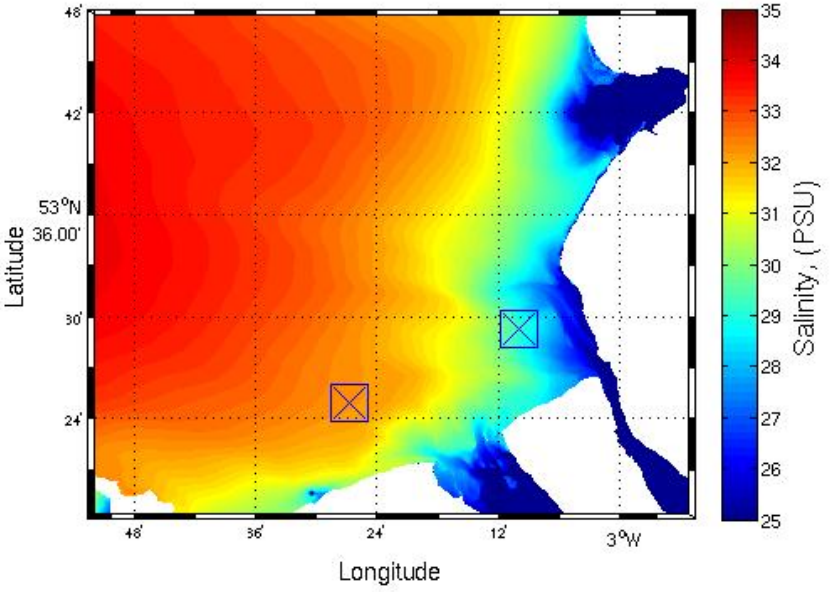

(b) F simulation

FIGURE 6.11: Surface salinity monthly residual for December, Latitude/Longitude Domain, OWFs marked as squares

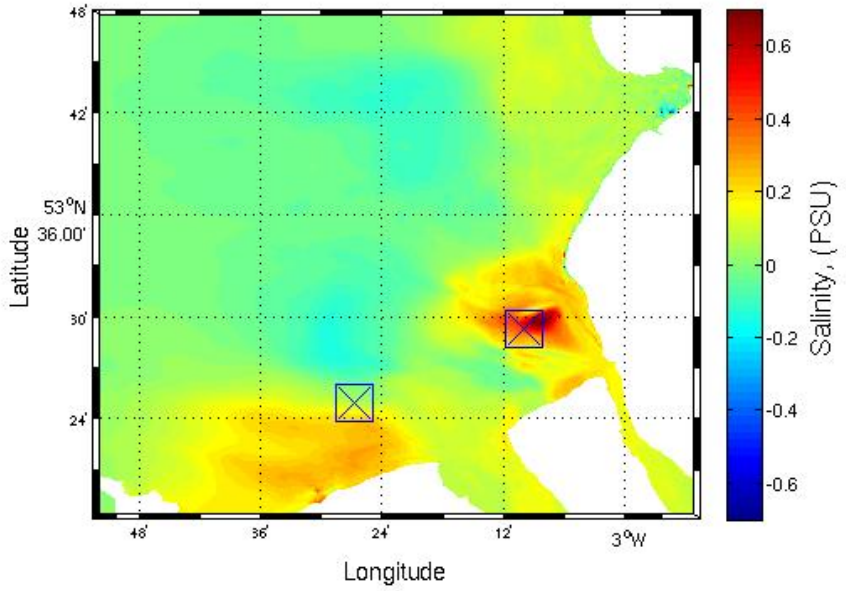

(a) $F - C$

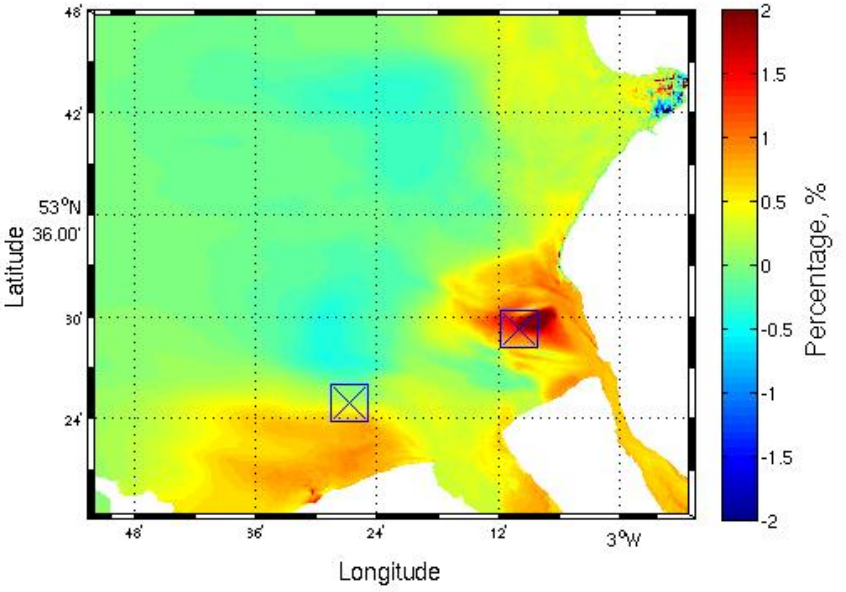

(b) Percentage difference $100 * ((F - C)/C)$

FIGURE 6.12: Surface salinity residual difference for December, latitude/longitude Domain. OWFs marked as squares

Figure 6.11(a) and 6.11(b) show the average surface salinity for C and F in December respectively. The Burbo Bank wind farm is in fresher water when compared to March (Figure 6.8(b)). One reason for this is the average flow rate

from the River Dee (Figure 6.4(a)) and the Mersey (Chapter 3) is greater in December.

Figure 6.12(a) and 6.12(b) show the absolute difference (F-C) and the percentage difference respectively. The Burbo Bank wind farm has the largest impact with values around 0.9 PSU (Figure 6.12(b): 3%) corresponding to a $0.6kg/m^3$ increase in density at the surface, this is in line with the largest impacts seen in March (Figure 6.9(a)). Effects in the estuaries of the Dee and Mersey are smaller in December than in March. However there are important difference between March and December. First, the freshwater plume extents slightly further offshore in December, likely due to the higher freshwater discharge. The spatial extent of the OWF effect in salinity (Figure 6.12(a) and Figure 6.12(a)) is also significantly different between March and December. Effects in the estuaries (Dee and Mersey) are smaller in December, which may be explained by higher freshwater discharge blocking propagation of effects up the estuary. December salinity plots overall, the numerical results suggest that the spatial extent of the impact of OWF on salinity is reduced under increased freshwater impact. This is, however, not entirely consistent with the year long comparison at Site a, where little change was observed (numerically) for the summer months (ie reduced freshwater impact). The consistently large spatial variability may help reconcile the time series at a single point and the spatial maps. Another possible explanation would be the effects are maximum where the competing forcings (tidal mixing and buoyancy) are near there average values, but that when buoyancy either decreases or increases significantly (due to changes in freshwater for example), either mechanism controls the overall dynamics and effects are reduced.

6.2.4 Monthly Surface Temperature

Monthly Temperature plots 6.13(a), 6.13(b), 6.15(a) and 6.15(b) show the surface temperature for March and December. All plots show the freshwater inflow is

cooler than the saline water. This is due to the assumption that the freshwater inflow is in equilibrium with the inland atmospheric temperature at the river source and as such a seasonal temperature can be included (Brown et al, 2015 [19].

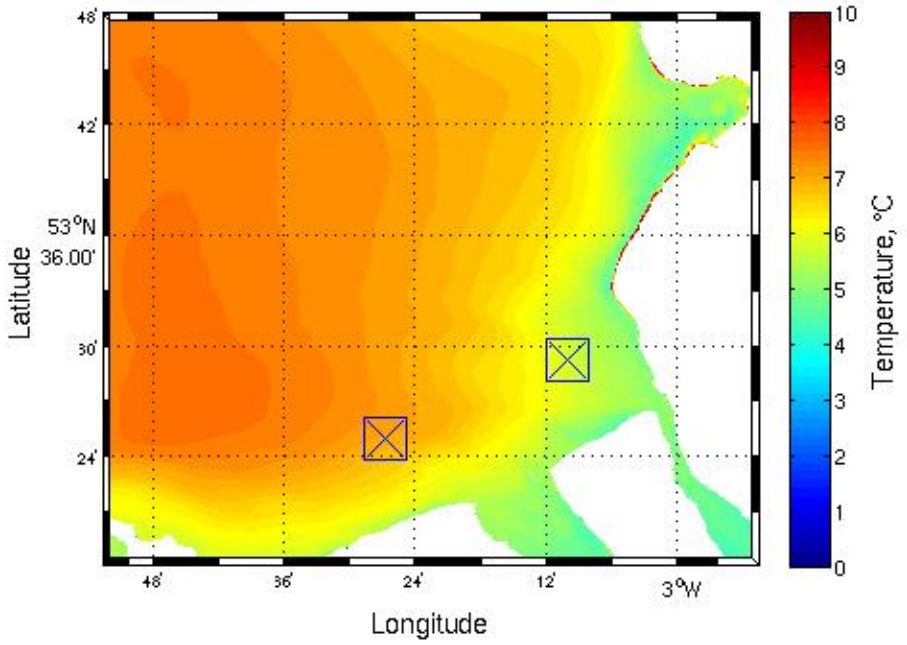

(a) C simulation

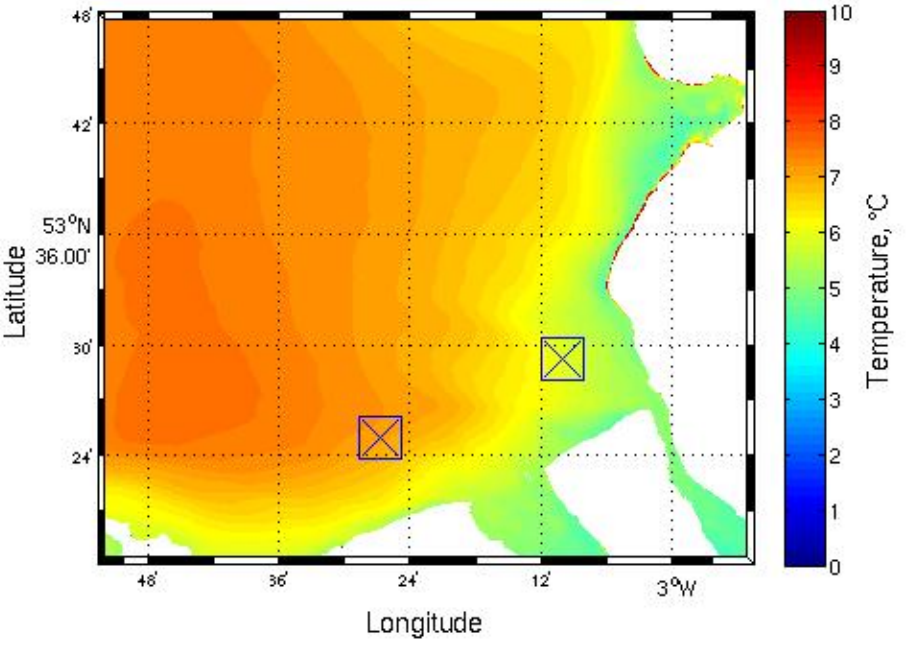

(b) F simulation

FIGURE 6.13: Surface temperature monthly residual for March. Latitude/-Longitude Domain, OWF's marked as squares

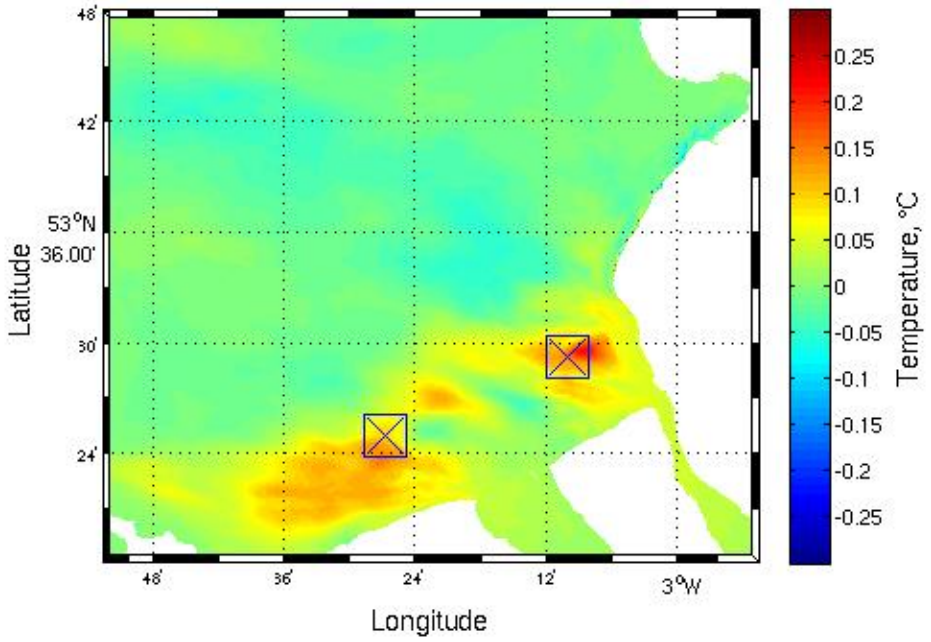

(a) $F - C$

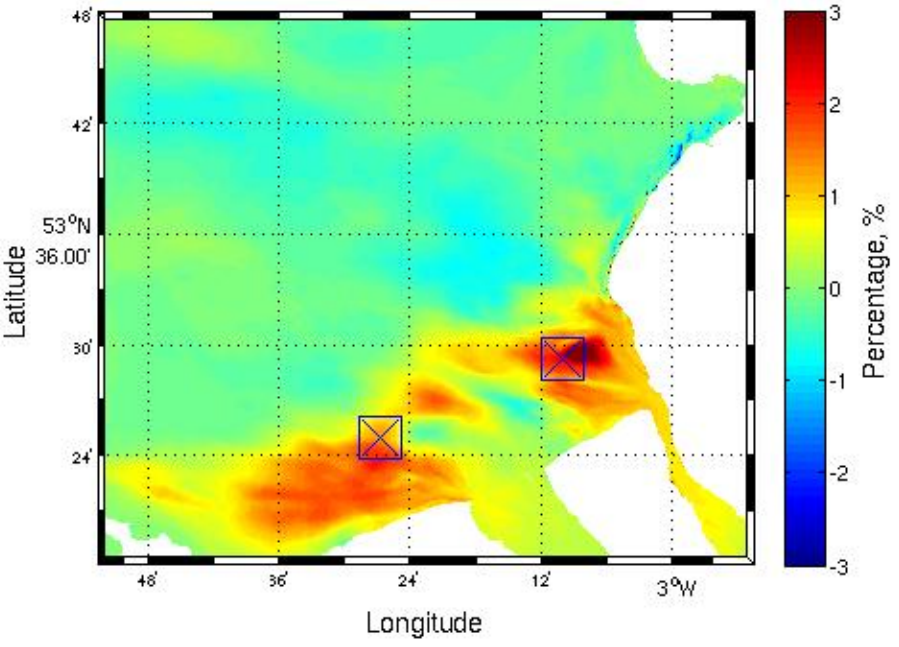

(b) Percentage difference $100 * ((F - C)/C)$

FIGURE 6.14: Surface temperature residual difference for March. Latitude/-Longitude Domain. OWF's marked as squares

Figure 6.13(a) and 6.13(b) show the average absolute temperatures for the full model and control model respectively. The temperature front is visible, showing the warmer saline water interacting with the cold, fresher water from major estuaries. Burbo Bank is situated in a sharp temperature gradient, to that end the OWF site produces a larger impact on the temperature locally.

Figure 6.14(a) and 6.14(b) show the absolute difference and the average percentage difference. Burbo Bank, with its position in the ROFI shows the high localised increased of temperature (3%). The effects are similar to that seen in salinity plots, with the localised impacts around the windfarm sites. However, Figure 6.14(a) shows a drop in temperature between the two sites. One further difference between temperature and salinity is the increase in temperature along the Welsh coast, this is most likely due to the blockage effect of the wind farm slowing the flow in the area.

The temperature appears of be more sensitive to change when compared to salinity. However, this difference is having a limited effect on the density, inline with a salinity driven system such as this.

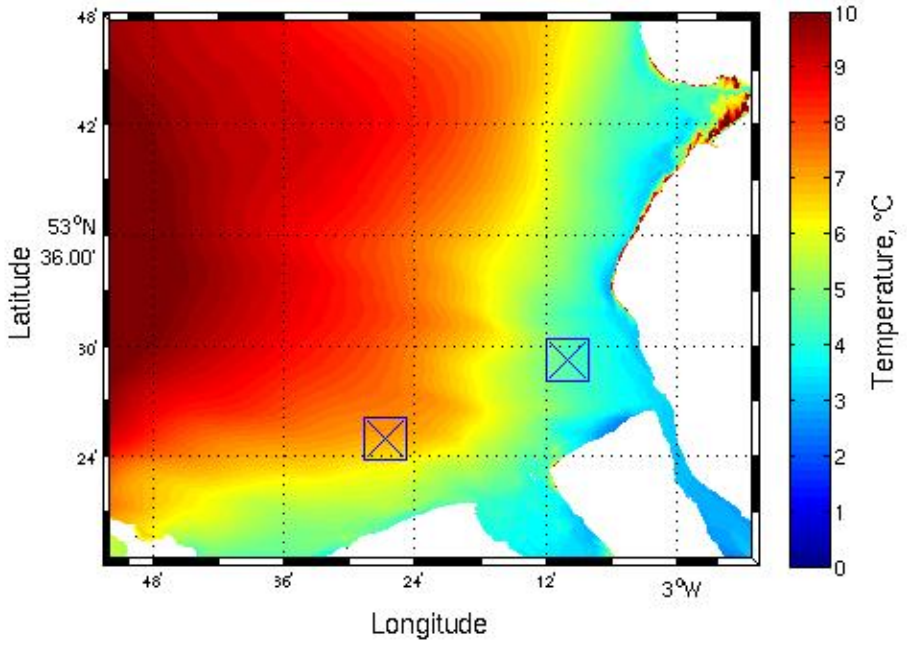

(a) C simulation

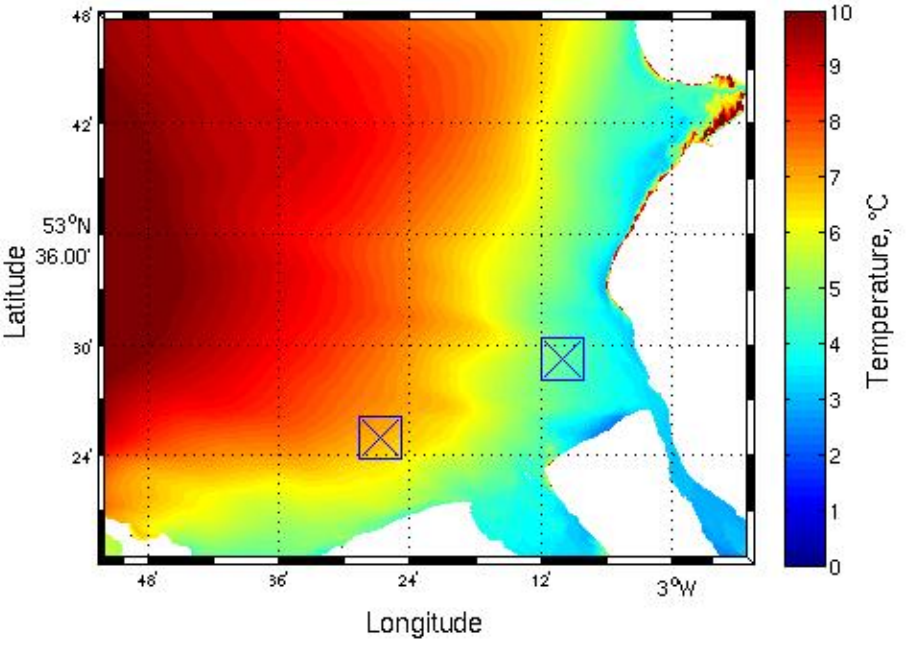

(b) F simulation

FIGURE 6.15: Surface temperature monthly residual for December.Latitude/Longitude Domain, OWFs marked as squares

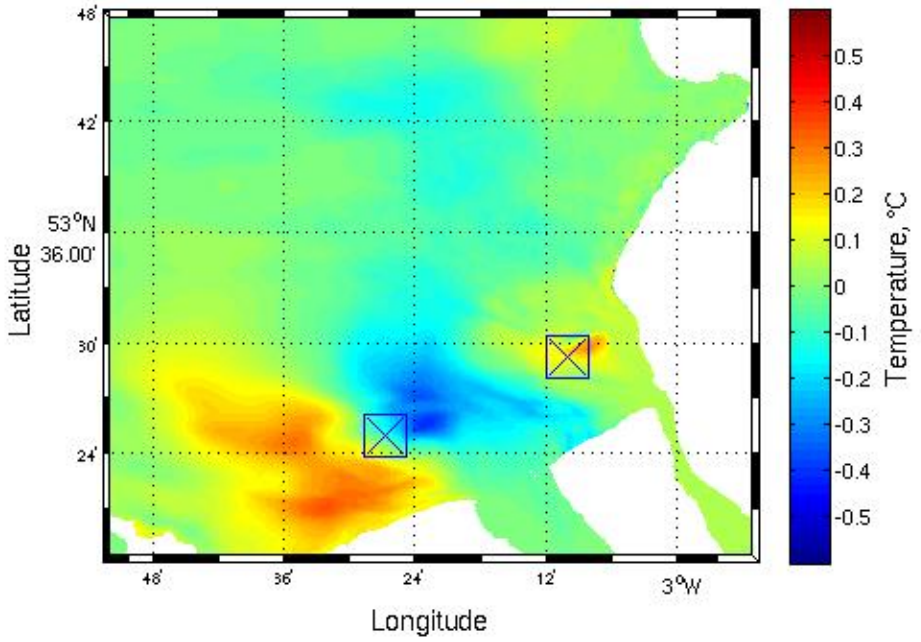

(a) $F - C$

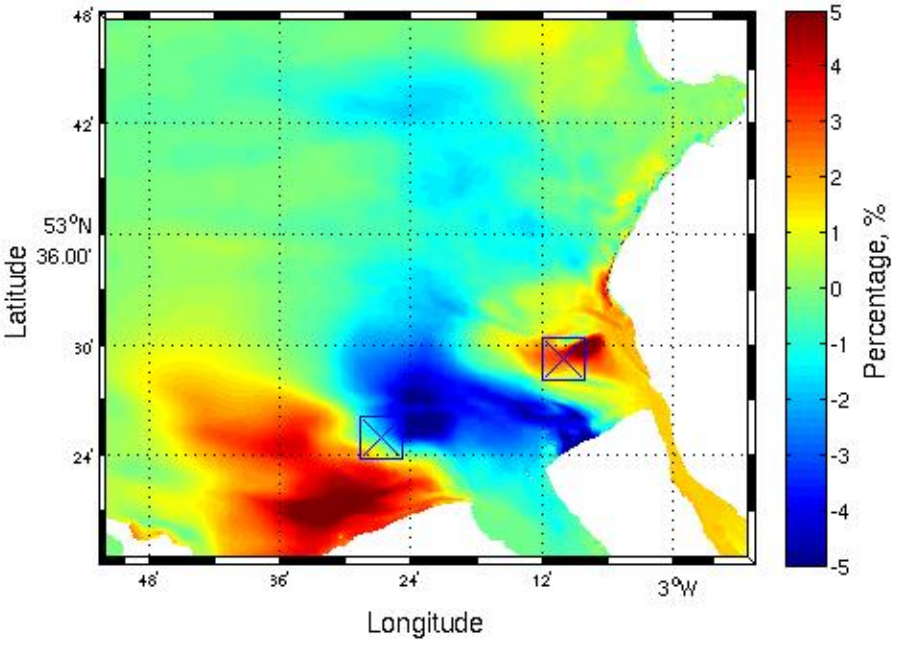

(b) Percentage difference $100 * ((F - C)/C)$

FIGURE 6.16: Surface temperature residual difference for December. Latitude/Longitude Domain. OWFs marked as squares

Figures 6.15(a) and 6.15(b) show the temperatures in Liverpool bay in December 2008 for C and F respectively. This shows the two OWF's in position in the bay, North Hoyle is near the temperature front, however the average temperature in Burbo Bank seems consistent across the full size of the OWF. This shows that the river discharges are pushing the freshwater further offshore past the OWF's as seen in the salinity maps. Figure 6.16(a) and 6.16(b) show the absolute difference and percentage difference between C and F. These Figures show the most dramatic differences in the study, what appears to happen is with the increase in river discharge from both the Dee an area of colder, freshwater is forcing its way into the bay. This shows a difference between the area to the left of North Hoyle where the surface water temperature has increased and the colder outflows in the Dee estuary. This creates differences of around $1°C$ or 10% between the two areas. This confirms that the surface temperature is very sensitive to the positions of the OWF's and leads to the possibility that the position of North Hoyle has a direct impact on the freshwater plume into the bay.

6.2.5 Monthly Temperature Fronts

Here we plot the 7° temperature front profiles to show the impact on the front due to the presence of wind farms over the same time periods, March and December.

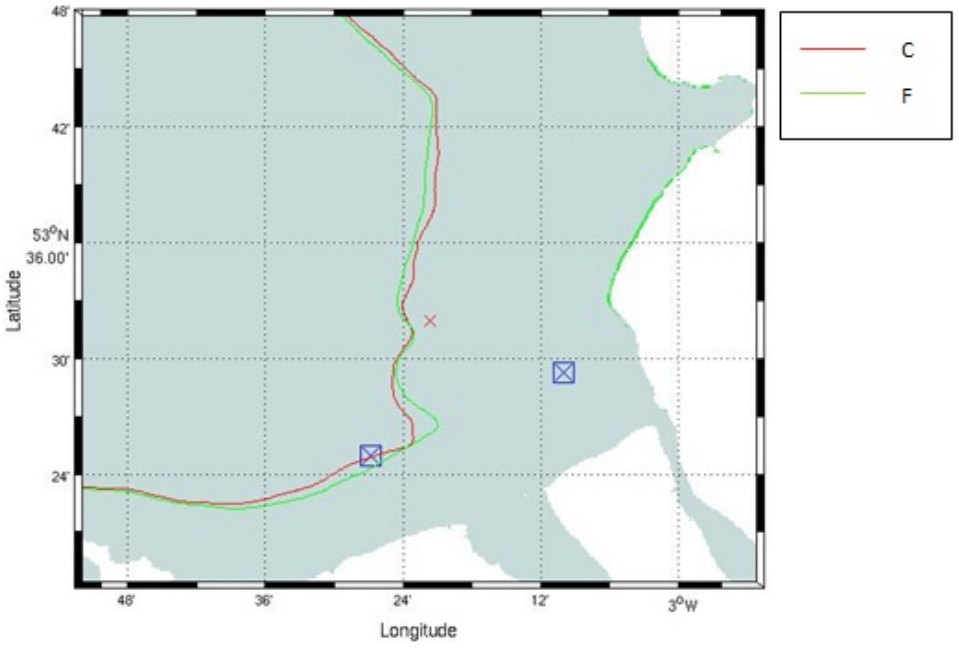

FIGURE 6.17: 7°C temperature front in March. OWFs marked as squares

Figures 6.2.5 shows for C and F in March. The majority of the front is unaffected as would be expected however the wind farms have caused the temperature front to move closer to the Dee estuary near North Hoyle. This means the freshwater is not intruding into the bay as far with the turbines present in F. This confirms the previous discussion that the fresh water is not penetrating the bay as far as is mentioned in the salinity and temperature plot sections.

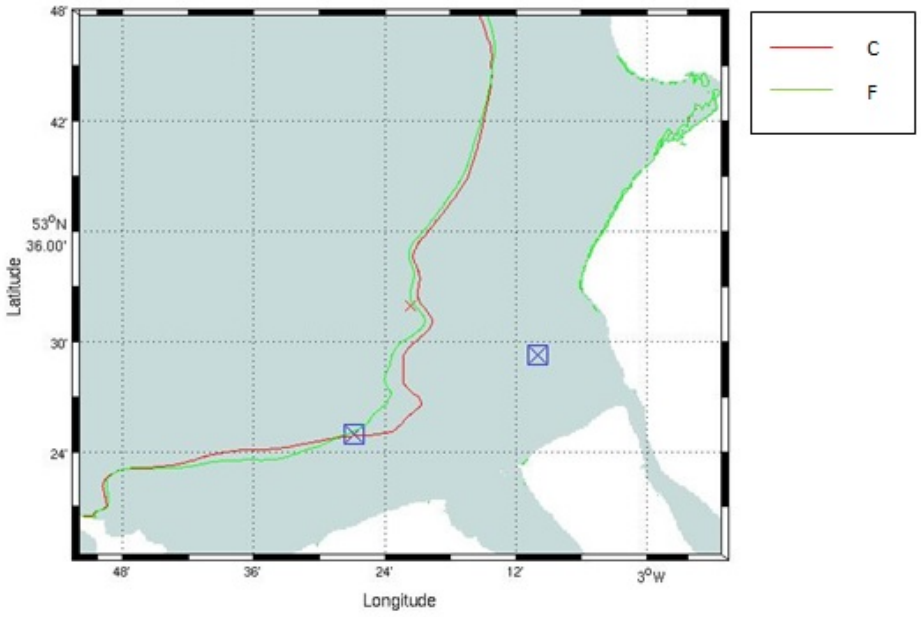

FIGURE 6.18: 7°C temperature front line for December, OWF's shown as squares

Figures 6.18 shows the temperature front for C and F 7°C temperature fronts in December. As in March, the front is relatively unaffected through most of the bay and a small effect showing around North Hoyle. In December F shows that the fresh water is penetrating through into the bay than C, and compared to March. This suggests that the increased average flow rate from the Dee has an effect on the position of the temperature front confirming that the temperature is very sensitive to the wind farm effects.

6.2.6 Site A comparison

We now focus on the intratidal dynamical processes that contribute to the overall residual behaviour in the Bay. To that end, we analyse numerical results for time dependent vertical profiles at site A. The aim is to determine the impact of OWF's on the intratidal processes which are otherwise averaged in the previous sections.

Here we present vertical timeseries at site A, to investigate the impacts of OWF's at Site A in Liverpool Bay (Figure 3.10) at a short 3 day timescale. Each plot contains Elevation in the top panel, timeseries for F in the second panel and timeseries of C in the third panel. A three day period in March after spring tides is chosen because it represents a particularly active time. The period includes approximately six tidal cycles of decreasing amplitude with time, as we move from spring tide to neap tide.

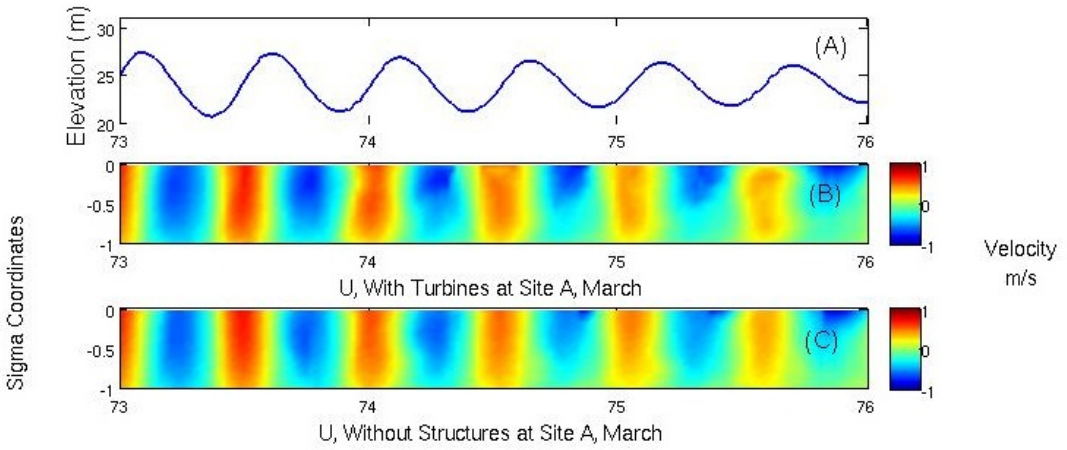

FIGURE 6.19: Site A, March U component comparison, top panel (A); Elevation, Second Panel (B); Model with turbine F, Third panel (C); Model without Turbines C

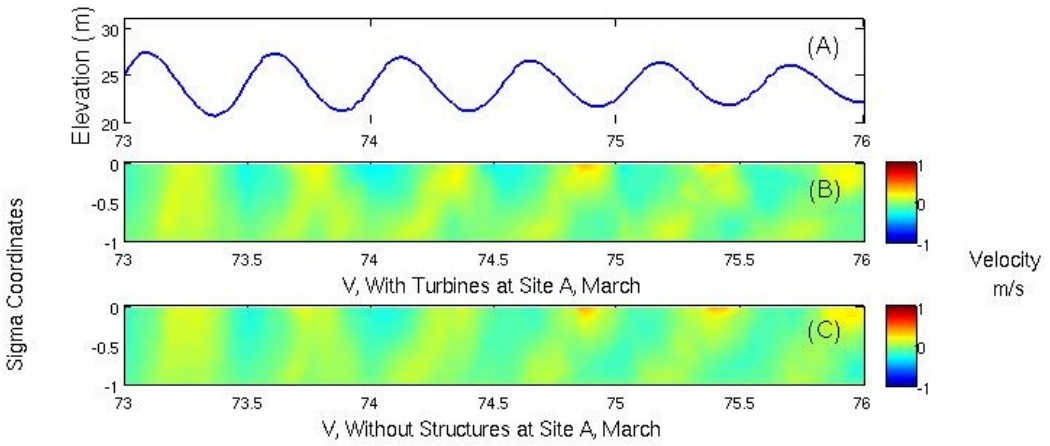

FIGURE 6.20: Site A, March V component comparison, top panel (A); Elevation, Second Panel (B); Model with turbine F, Third panel (C); Model without Turbines C

Figure 6.19 and 6.20 show the East-West (close to the major axis) and North-South velocity components through the water column at site A. Both theses plots highlight little distinguishable impacts at Site A which is consistent with the time-averaged results for surface velocity (Figure 6.6(a)). From these time averaged results, the impact on velocity remains localised around the OWF's and site A is located out of the zone of velocity influence. Even in regions of higher time-averaged impact, the effects at the intra-tidal scale would be very small in comparison to the dominant tidal currents (less than 1 m/s). When averaged over time, these very small effects can result in significant impacts for residual flow which is some cases can be in the order of cm/s (Figure 6.6(a).

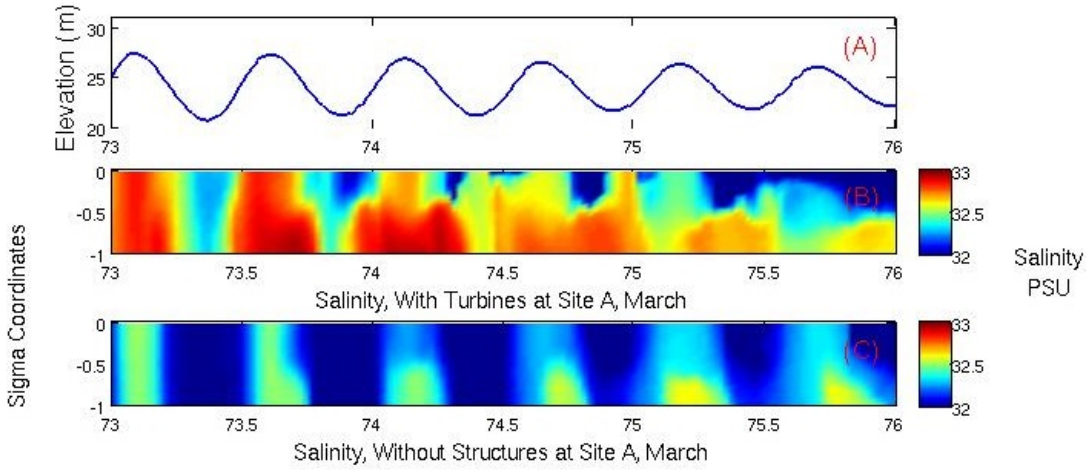

FIGURE 6.21: Salinity time series at Site A, top panel (A); Elevation, Second Panel (B); Model with turbine F, Third panel (C); Model without Turbines C

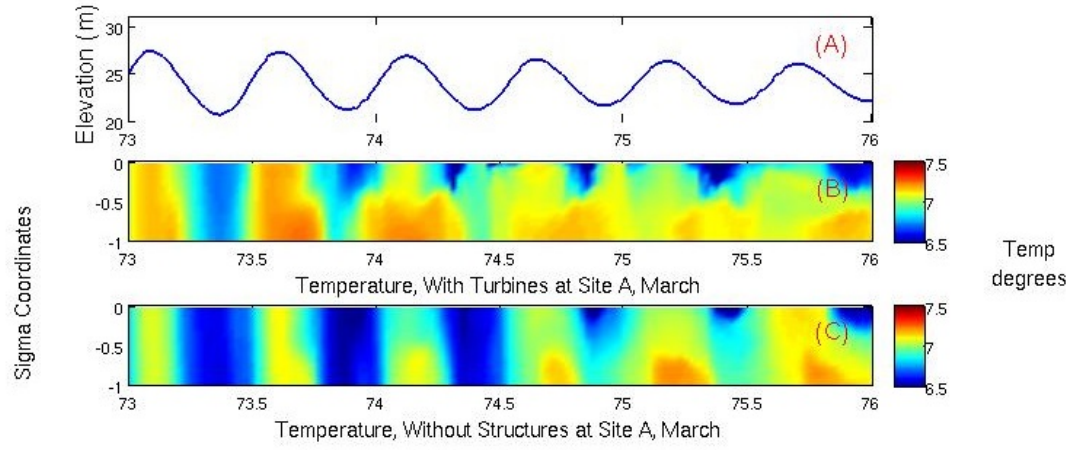

FIGURE 6.22: Temperature time series at Site A, top panel (A); Elevation, Second Panel (B); Model with turbine F, Third panel (C); Model without Turbines C

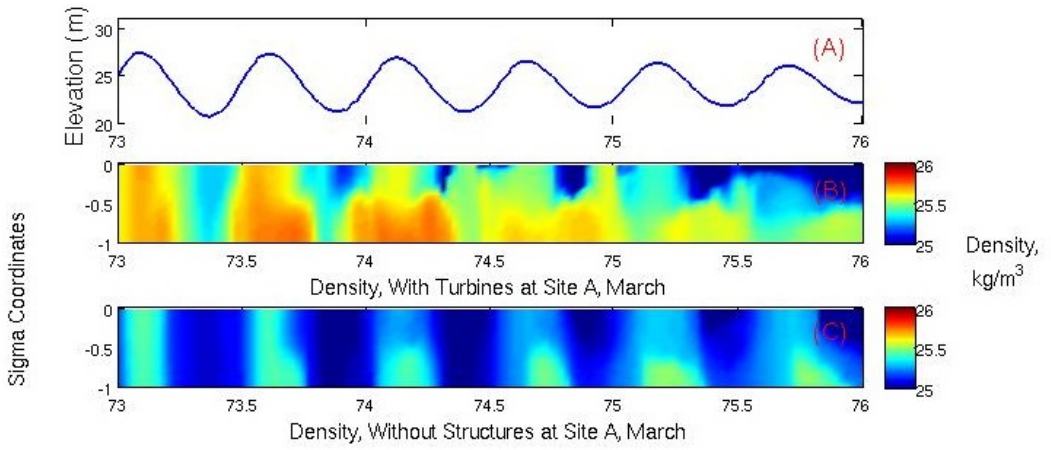

FIGURE 6.23: Density time series at Site A, top panel (A); Elevation, Second Panel (B); Model with turbine, Third panel (C); Model without Turbines

Figures 6.21, 6.22 and 6.23 show the impacts on the salinity, temperature and density respectively at Site A. Each shows that the OWF's have had an impact that can be seen through the water column. All three Figures show similar behaviour for this ROFI and we will focus our discussion on the density time-series. There is an overall increase in density, due to salter, warmer offshore waters. Without OWF structures (bottom panel) the numerical results indicate that, over the three day period the water column goes from permanently well mixed (first tide) to periodically stratified (SIPS) as tidal forcing reduces. This is consistent with previous studies in Liverpool Bay (eg Simpson et al, 1990 [67] and Palmer et al, 2010 [67]). During the SIPS periods, the water column is well mixed in later flood to high water and stratified during ebb and low water (last tidal cycle in Figures).

With the OWF (middle panels), the behaviour is significantly altered as numerical results indicate that over the three day period, the water column goes from already periodically stratified to permanently stratified. Early on during the time series, tidal straining and ebb stratification occur. In addition, flood

stratification is clearly visible. This is probably due to a salt wedge intrusion during flood. As tides diminish, the stratification intensifies and reaches a state of permanent stratification by the end of the timeseries.

Such a behaviour at Site A may not be directly intuitive given the changes in the governing equations, but reflects their coupled, non-linear behaviour. The overall increase in tidal mixing that could reasonably be expected for increases in current speed (Figure 6.6(a) and additional turbulence production competes with an increase in the horizontal density gradient.

Figure 6.23 shows a clear overall increase in Density over the entire period, this is attributed to the increase in salt water in the area. At the spring tide (day 73) the water column shows very little stratification having saline water through the entire water column. This pattern in consistent in F and C at day 73. F shows the clear salt intrusion effect on the density in the second tidal cycle, indicative of an intensified salt wedge through the site. As the plot tends towards the neap tide (day 76) the stratification becomes intensified, creating clear boundaries between salt and fresh water. This makes sense because the impact equations reduce the kinetic energy in the system close to the turbine sites. This gives rise to increased mixing due to the buoyancy which in turn sharpens the stratification.

6.2.7 Conclusions

This chapter has focused on the core study of this project where several conclusions have been drawn. Firstly, even a small number of OWF's with few turbine structures has a measurable impact on the hydrodynamics in a complex ROFI such as Liverpool Bay. Impacts of 3% in salinity and temperature can be seen locally due to increased shear dispersion which leads to change further into the bay of around 1%. This study has also shown that the impacts are sensitive to the ambient hydrodynamic parameters. This can be seen clearly when comparing

North Hoyle and Burbo Bank sites. At North Hoyle, the velocities are affected due to the increase in ambient flow which is in contrast Burbo Bank position as the affects the salinity and temperature are due to its position near the Mersey fresh water plume. Another conclusion that can be drawn from this study is the importance of the river inflows. When comparing the months of March and December where December has consistently higher freshwater inflow, the impacts are predominately around North Hoyle and the effects to the Dee estuary are reduced because the stresses caused by the estuary discharge. This shows that the OWF's impacts are heavily dependant on the freshwater inflow, particularly when considering the surface parameters. When considering inter tidal temporal scales in March, we can see the salt wedge intrusion and the strengthening of the stratification which in turn allows the 7°C temperature front to come closer to the coastline. This shows that the OWF's can have an impact of the structure of the water column caused by blockage of the freshwater out of the Dee. Altogether, even though the impacts indicated by the numerical results may not be very large, they remain large enough to fundamentally alter the complex behaviour of a ROFI, which is determined by the delicate balance between tidal mixing and buoyancy forcing. This assessment shows the model is sensitivity to velocity changes at the freshwater boundary where the flows are greater strength, this is in line with the impact equations which are dependant on the ambient. The model with OWF's is sensitivity to TKE at the mouth of the Dee where the freshwater enters the bay.

Finally, although the impacts shown and discussed here are relatively small (3-4%), it is important to bare in mind that the number of turbines simulated in this model is 1/5 of the total that are present in 2015 when the Gwent y Mor OWF(www.4coffshore.com, 2014 [1]) was fully commissioned. This shows that the impacts now can be assumed to be greater through the ROFI and does require further investigation beyond the scope of this project. This study has confirmed the basic conceptual understanding that a small number of structures

do have an impact on the hydrodynamics because it causes vertical instabilities mixing fresh and saline water through the water column.

Chapter 7

Conclusion

In this chapter we conclude the thesis by summarising the conclusions in each chapter ensuring we have met the initial objectives set out in the introduction (section 1.3.1). This will be completed in two sections; firstly we will discuss the effects on Liverpool Bay dynamics caused by the OWF structures. We will summarise our findings showing the effects on salinity, temperature and velocity due to the placement of the OWFs (chapter 6). We will discuss the need for this type of structure model which includes momentum and turbulence combined effects. The second part of this chapter will conclude the model development. We will discuss further development opportunities that could make use of the model.

7.1 Liverpool Bay Hydrodynamics

In this thesis we have conducted two separate studies to look at the impacts of OWF structures on Liverpool bay. In the 2008 setup, North Hoyle and Burbo Bank have been modelled in-situ (chapter 6). In the validation process we chose a site where field data had been recorded. This site is positioned close enough to both OWF sites, therefore it was considered an appropriate site of a model data-field data comparison study. This analysis showed the model predicts the

full year Salinity, temperature and water density pattern well. We discounted the results from January and February as the model fails to predict the salinity pattern. This is consistent with recently published studies in Liverpool Bay and is the subject of an investigation at NOC at the time of writing this thesis and is not in the scope of this project. The results for March to December show a good approximation of the dynamics through the site for salinity, temperature and density for 2008.

We found that the largest impacts on salinity and temperature were in the local area around Burbo Bank when we considered the monthly surface residuals. Increases of 3% were seen in the surface salinity in March, and 3% in December. One observation we make when comparing December and March is that the peak impact is very similar in magnitude. However the spatial range of impacts changes significantly between the two months, December shows a larger area of influence which extends along the Welsh coast.

When comparing sites of the two OWFs, we can see that the highest impacts on salinity and temperature are near Burbo Bank. We have attributed this to the increase in vertical mixing caused by the structure which is added to the ambient instabilities due to the freshwater flow from of the Mersey. North Hoyle in contrast is in an area that has greater ambient vertical stability, as it is out of the main fresh water plume from the Dee is directed to the East of the OWF. The increased mixing causes warmer-saline water to mix up through the water column. The major conclusion we have drawn from this is that the position of the OWFs are important to the total impacts on the hydrodynamics in the near and far-scale ranges in this area where freshwater input is important.

When we compare the surface velocities we can see a change in the velocity residual near the North Hoyle OWF. In comparison, Burbo Bank shows very little in the way of impacts on velocity residual. This is likely due to the ambient velocity residuals in the North Hoyle area is much higher therefore the impacts are greater, this can be attributed to the momentum equation dependant on the

velocity of the water. This is around 100% increase in surface velocity residual close to the OWF's. The blockage has caused a large eddy flow pattern to form north of the North Hoyle OWF.

We also focused on intra-tidal dynamics at the mooring site in the Bay via plotting a 3 day time period showing the hydrodynamics in the water column to access intra-tidal and sub-tidal time scales. There is a clear impact on the vertical structure through the water column. The density structure shows a Strain-Induced Periodic Stratification (SIPS) pattern that is creating a stratified environment at low tide. This shows that the structures have increased the density through the site and intensified stratification by tidal straining and salt wedge intrusion.

One of the most important objectives of this thesis was to show the impacts on the momentum and turbulence caused by any structure. To test this theory we conducted a study to compare the momentum sink method to the full momentum-turbulence representation method. We concluded that the full representation method does provide a better approximation, which we showed numerically by using skill values as a comparison across 2008. When looking at the monthly surface hydrodynamic plots, we can conclude that when using only momentum or only turbulence the total impact is significantly over-estimated. This is due to the turbulence/momentum balance within the governing equations. The decrease in momentum locally is countered by the increase in mixing. This is an important conclusion that shows the use of momentum and turbulence reduces the total impact shown therefore using the method is beneficial to many applications and therefore should be used in all future studies through the Liverpool bay area and other areas.

This work has focused on the impacts on salinity, temperature, density and velocity. We have shown that the structures do have a measurable impact of the surface hydrodynamics and shown that the structures cause an increase in tidal

straining and considering both momentum and turbulence impacts is beneficial within a salinity driven ROFI.

7.2 Structure Module

The main aim of this project was to develop a structure impact model capable of simulating any man-made structure in a structured grid coastal ocean model. We have developed a module which simulates the impacts in the momentum and turbulence governing equations. This has been accomplished by using a modified drag equation which applies an impact of a structure to the fixed grid. This allows the user to simulate structures that are several orders of magnitude smaller than the smallest resolution of the fixed grid model. Using this approach is beneficial because it is most suited to large spatial resolution models without causing the assumptions made in the governing equations to become flawed or increased computational time by having to increase the resolution. These relatively course models are still needed, in particular to investigate cumulative large scale (up to whole UK waters and NW European shelf) impacts. We have applied an averaged drag force to the momentum equation and the impact equation used for the turbulence comes from the momentum impact terms when the k equation is derived. This is then directly applied to the k-ε turbulence equation to simulate the increased mixing. In this thesis, we have coded the module to be as generic as possible. This means that the user can have as much flexibility as required for the study. We conducted several sensitivity studies to assess the best set up. Firstly we did a sensitivity study to assess the method we used to simulate the OWFs. There were two options to test, farm-averaged and intra-farm resolving, each method has benefits and are discussed in this thesis. The Farm-Averaged method simulates the OWF as one area that has the complete influence of all the structures averaged across the footprint. The Intra-farm resolving method

individually picks out the structures and simulates the impacts on a cell by cell basis.

In the study we found that the farm-averaged method provided the best approximation when compared to the hydrodynamics at site A. In comparison, the intra-farm resolving method fails to predict the tidal variations through the year. This is likely due to the assumptions made in the derivation of the impact equations that mean the resolution is at the same time too high and too low, as it does not properly resolve the length scales withing the OWF and thus causes numerical errors. The farm-averaged method is also the most valid for any larger scale model therefore using this method to validate the model is appropriate and this is the conclusion we can draw from the results.

7.3 Further Work

As part of this thesis we tested a 2015 set up which included the four OWF's which are currently in position in Liverpool Bay. Figure 7.1 shows the positions and sizes of the OWF set up used in 2015. The number of turbine structures has increased dramatically in the 7 years between the 2008 and 2015, increasing from 55 to 240 due to the large site at Gwynt y Mor which has 160 turbines.

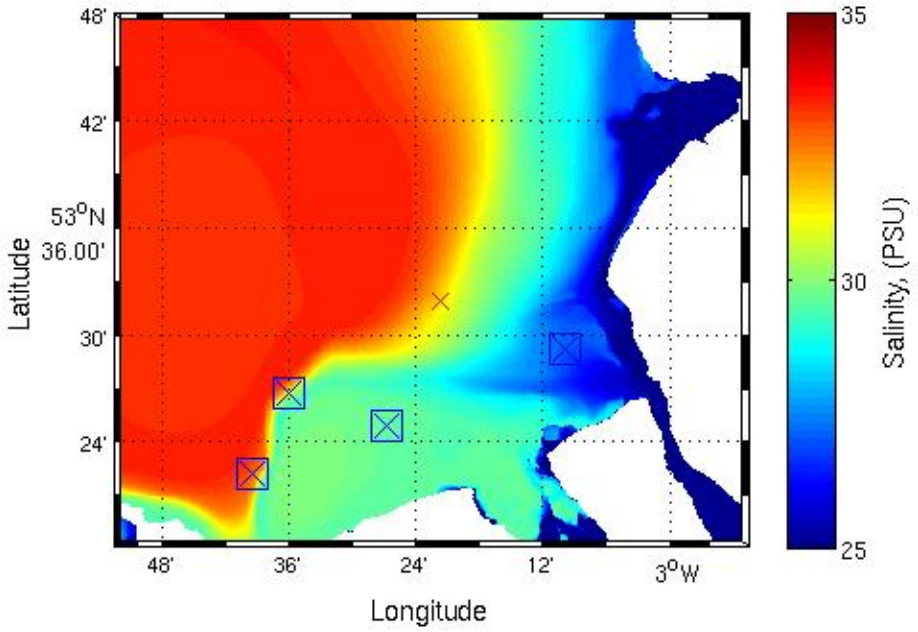

FIGURE 7.1: 2015 surface salinity, Liverpool Bay showing site A (small red cross) and centre of four wind farms, represented by the blue squares. from left to right; Rhyl Flats, 25 structures, Gwynt y Mor, 160 structures, North Hoyle, 30 structures, Burbo Bank, 25 structures

We tested the 2015 set up using the 2008 initial conditions as described in this thesis to see if the module can cope with the greater shock imposed by the larger number of structures in its current state described in 3.5. Figure 7.1 show the surface salinity impact simulated by the module.

It is possible that the proximity of the OWF to the boundary has caused numerical errors. This shows that the Liverpool domain is too restricted to simulate the 2015 set up correctly. This is where further work would be necessary to simulate this setup correctly. Several options could be investigated, firstly increasing the size of the domain. This can be achieved by using the POLCOMS Irish Sea domain and applying the structure module at the correct places. Another potential method is to create a two way coupling at the boundary of Liverpool

Bay. This will show Liverpool Bay effects in detail however it is likely to cause a significant increase in computing time.

The module lends itself to being scaled to larger domains, for example to simulate the OWF's on the continental shelf model domain POLCOMS used. This could be achieved by applying the average impacts from all the OWF's and the number of structures averaged across the footprint of each farm. This would show the far-scale impacts across the continent shelf on the hydrodynamics.

When creating the module we intentionally coded in a framework that can be used to simulate each layer independent of the others, this means with further work it is possible applied different drag coefficients to difference layers. This would create a situation where the structure is not the same through the water column. This framework will also allow for tidal turbines to be included which could apply a drag force at the specified layer.

In conclusion, this project has developed a highly flexible working module that utilises the hydrodynamic solver POLCOMS and turbulence model k-ε from GOTM to simulate any man-made structure with a fixed grid domain. We have intentionally created a frame-work that can be modified in the future to create a varied structure impact module. We have validated the module using the 2008 offshore wind farm set up in Liverpool Bay in 2008, this consisted of 2 OWF's containing 55 structures simulated as cylindrical pylons extending through the water column. We compared the numerical results with field data at site A and have shown that the module can improve the accuracy of the Liverpool Bay model pre-structures. We conducted a study on the method of representation, 'farm-averaged' and 'intra-farm resolving' which has shown the farm-averaged method provides the best approximation. We compared the full momentum and turbulence impacts to a momentum sink model. This has shown the full impact model improves the overall accuracy of the simulation when compared to the momentum sink model and we recommend using the full impact method is appropriate when simulating structures in Liverpool Bay. Finally we investigated

the 2008 set up in Liverpool Bay and have seen the local increase in surface salinity and temperature monthly residual and effects can be seen further away along the Welsh coast. The position of the OWF is important in the effects because of the positions of the freshwater fronts.

References

[1] *www.4coffshore.com*, 2014, accessed 2016.

[2] *www.renewableuk.com-Offshore wind*, 2015, accessed 2016.

[3] International Energy Agency, *Internation Energy outlook*, 2016.

[4] Laurent O. Amoudry, Rafael Ramirez-Mendoza, Alejandro J. Souza, and Jennifer M. Brown, *Modelling-based assessment of suspended sediment dynamics in a hypertidal estuarine channel*, Ocean Dynamics **64** (2014), no. 5, 707–722.

[5] Laurent O. Amoudry and Alejandro J. Souza, *Impact of sediment-induced stratification and turbulence closures on sediment transport and morphological modelling*, Continental Shelf Research **31** (2011), no. 9, 912–928.

[6] AKIO ARAKAWA and VIVIAN R. LAMB, *Computational design of the basic dynamical processes of the UCLA general circulation model*, Methods in Computational Physics: Advances in Research and Applications, vol. Volume 17, pp. 173–265, Elsevier.

[7] Mike Ashworth, Jason T. Holt, and Roger Proctor, *Optimization of the POLCOMS hydrodynamic code for terascale high-performance computers*, Parallel and Distributed Processing Symposium, 2004. Proceedings. 18th International, IEEE, 2004, p. 8.

[8] World Nuclear Association, *Safety of nuclear power reactors*, 2016.

[9] Joel F. Atwater, Gregory A. Lawrence, Joel F. Atwater, and Gregory A. Lawrence, *Regulatory, design and methodological impacts in determining tidal-in-stream power resource potential*, Energy Policy **39** (2011), no. 3, 1694.

[10] Matthias Baeye and Michael Fettweis, *In situ observations of suspended particulate matter plumes at an offshore wind farm, southern north sea*, Geo-Marine Letters **35** (2015), no. 4, 247–255.

[11] R. J. Barthelmie, K. Hansen, S. T. Frandsen, O. Rathmann, J. G. Schepers, W. Schlez, J. Phillips, K. Rados, A. Zervos, E. S. Politis, and P. K. Chaviaropoulos, *Modelling and measuring flow and wind turbine wakes in large wind farms offshore*, Wind Energy **12** (2009), no. 5, 431–444.

[12] Rebecca Jane Barthelmie and LE Jensen, *Evaluation of wind farm efficiency and wind turbine wakes at the Nysted offshore wind farm*, Wind Energy **13** (2010), no. 6, 573–586.

[13] W. M. Batten, M. E. Harrison, and A. S. Bahaj, *Accuracy of the actuator disc-rans approach for predicting the performance and wake of tidal turbines*, Philosophical transactions.Series A, Mathematical, physical, and engineering sciences **371** (2013), no. 1985, 20120293 (eng), LR: 20130424; JID: 101133385; 2013 [ppublish]; epublish.

[14] Leslie C. Bender, *Modification of the physics and numerics in a third-generation ocean wave model*, Journal of Atmospheric and Oceanic Technology **13** (1996), no. 3, 726–750.

[15] Gerben J. De Boer, Julie D. Pietrzak, and Johan C. Winterwerp, *On the vertical structure of the Rhine region of freshwater influence*, Ocean dynamics **56** (2006), no. 3-4, 198–216.

[16] R. Bolanos, JM Brown, and A. Souza, *Three dimensional circulation modeling in the Dee estuary*, J Coast Res SI **64** (2011), 1457–1461.

[17] R. Bolanos and A. Souza, *Measuring hydrodynamics and sediment transport processes in the Dee estuary*, Earth System Science Data **1** (2010), no. 2, 157.

[18] Lucy M. Bricheno, Judith M. Wolf, and Jennifer M. Brown, *Impacts of high resolution model downscaling in coastal regions*, Continental Shelf Research **87** (2014), 7–16.

[19] Jennifer M. Brown, Laurent O. Amoudry, Alejandro J. Souza, and Jon Rees, *Fate and pathways of dredged estuarine sediment spoil in response to variable sediment size and baroclinic coastal circulation*, Journal of environmental management **149** (2015), 209–221.

[20] Jennifer M. Brown, Rodolfo Bolanos, and Judith Wolf, *Impact assessment of advanced coupling features in a tidesurgewave model, POLCOMS-WAM, in a shallow water application*, Journal of Marine Systems **87** (2011), no. 1, 13–24.

[21] Hans Burchard, *Combined effects of wind, tide, and horizontal density gradients on stratification in estuaries and coastal seas*, Journal of Physical Oceanography **39** (2009), no. 9, 2117.

[22] Changsheng Chen, Hedong Liu, and Robert C. Beardsley, *An unstructured grid, finite-volume, three-dimensional, primitive equations ocean model: application to coastal ocean and estuaries*, Journal of Atmospheric and Oceanic Technology **20** (2003), no. 1, 159–186.

[23] Andrea Copping, Hoyt Battey, Jocelyn Brown-Saracino, Meghan Massaua, and Courtney Smith, *An international assessment of the environmental effects of marine energy development*, Ocean and Coastal Management (2014), no. 0.

[24] The Crown Estate, *Offshore wind energy, tech, report*, 2016.

[25] Benoit Cushman-Roisin and Jean-Marie Beckers, *Chapter 4 - equations governing geophysical flows*, International Geophysics, vol. Volume 101, pp. 99–129, Academic Press.

[26] US Energy Administration Department, *International Energy Outlook - 2013*, Tech. Report DOE/EIA-0484(2013), EIA, 2013.

[27] M. Fischetti, *Offshore wind farms could knock down hurricanes*, 2014.

[28] Department for Energy and Climate Change, *Energy roadmap, update 2013, tech. report*, Tech. report, 2013.

[29] B. Galperin, LH Kantha, S. Hassid, and A. Rosati, *A quasi-equilibrium turbulent energy model for geophysical flows*, Journal of the Atmospheric Sciences **45** (1988), no. 1, 55–62.

[30] Louise Gray, *Doha: Latest figures show global co2 emissions are rising*, 2012.

[31] K. Bolding H. Burchard and L. Umlauf, *Gotm.net*, 2014, accessed 2016.

[32] J. M. Harris, R. J. S. Whitehouse, and T. Benson, *The time evolution of scour around offshore structures*, Proceedings of the Institution of Civil Engineers.Maritime Engineering **163** (2010), no. 1; 1, 3–17.

[33] Jason Holt and Lars Umlauf, *Modelling the tidal mixing fronts and seasonal stratification of the northwest European continental shelf*, Continental Shelf Research **28** (2008), no. 7, 887–903.

[34] Jason Holt, Lars Umlauf, Jason Holt, and Lars Umlauf, *Modelling the tidal mixing fronts and seasonal stratification of the northwest European continental shelf*, Continental Shelf Research **28** (2008), no. 7, 887.

[35] Jason T. Holt and Ian D. James, *An s coordinate density evolving model of the northwest European continental shelf: 1. model description and density structure*, Journal of Geophysical Research: Oceans **106** (2001), no. C7, 14015–14034.

[36] Martin Holt, Zhihong Li, and Jeff Osborne, *Real-time forecast modelling for the nw european shelf seas*, Elsevier Oceanography Series **69** (2003), no. 0, 484–489.

[37] Thomas Holtz, *Examining the perils of climate change*, 2011.

[38] Joanne Hopkins and Jeffrey A. Polton, *Scales and structure of frontal adjustment and freshwater export in a region of freshwater influence*, Ocean Dynamics **62** (2012), no. 1, 45–62.

[39] Michael John Howarth, Roger Proctor, MJ Smithson, R. Player, and PJ Knight, *The liverpool bay coastal observatory*, Current Measurement Technology, 2005. Proceedings of the IEEE/OES Eighth Working Conference on, IEEE, 2005, pp. 132–136.

[40] MJ Howarth and R. Proctor, *The POL coastal observatory in the eastern irish sea*, EGS-AGU-EUG Joint Assembly, vol. 1, 2003, p. 1522.

[41] IMCS, *Regional ocean modeling system (roms)*, 2016.

[42] I. D. James, *A front-resolving sigma coordinate sea model with a simple hybrid advection scheme*, Applied Mathematical Modelling **10** (1986), no. 2, 87–92.

[43] ID. James, *Advection schemes for shelf sea models*, Journal of Marine Systems **8** (1996), no. 34, 237–254.

[44] jorn Bruggeman, Karsten Bolding, and Hans Burchard, *Framework for aquatic biogeochemical models (FABM)*, Tech. report, 2011.

[45] Andrew Kusiak and Zhe Song, *Design of wind farm layout for maximum wind energy capture*, Renewable Energy **35** (2010), no. 3, 685–694.

[46] Proudman Oceanography Laboratory, *Polcoms documentation, tech. report.*

[47] BMT Group Ltd, *Tuflow, flood and coastal simulation software*, 2015.

[48] David J. C. MacKay, *Sustainable energy [electronic book] : without the hot air / [david jc mackay]*, Cambridge : UIT Cambridge, 2008; version 3.5.2], 2008.

[49] George L. Mellor and Tetsuji Yamada, *A hierarchy of turbulence closure models for planetary boundary layers*, Journal of the Atmospheric Sciences **31** (1974), no. 7, 1791–1806, doi: 10.1175/1520-0469(1974)0312.0.CO;2; M3: doi: 10.1175/1520-0469(1974)0312.0.CO;2; 17.

[50] Matthias: Fettweis Baeye Micheal, *AGU on tumblr, tech. report*, 2015.

[51] SG Monismith, JR Burau, and M. Stacey, *Stratification dynamics and gravitational circulation in northern san Francisco Bay*, San Francisco Bay: The Ecosystem (1996), 123–153.

[52] Simon P. Neill, Emmer J. Litt, Scott J. Couch, and Alan G. Davies, *The impact of tidal stream turbines on large-scale sediment dynamics*, Renewable Energy **34** (2009), no. 12, 2803–2812.

[53] NOAA, *In the wake of a wind turbine*, 2011.

[54] D. L. Norman, J. M. Brown, L. O. Amoudry, and A. J. Souza, *Was 2008 a typical year in Liverpool Bay?*, Tech. report, National Oceanography Centre, 2014.

[55] C. K. O'Neill, J. A. Polton, J. T. Holt, and E. J. O'Dea, *Modelling temperature and salinity in Liverpool Bay and the Irish Sea: Sensitivity to model type and surface forcing*, Ocean Science **8** (2012), no. 5, 903–913 (English).

[56] Matthew Robert Palmer, *The modification of current ellipses by stratification in the Liverpool Bay ROFI*, Ocean Dynamics **60** (2010), no. 2, 219.

[57] Jeffrey A. Polton, Matthew Robert Palmer, and Michael John Howarth, *Physical and dynamical oceanography of Liverpool Bay*, Ocean Dynamics **61** (2011), no. 9, 1421–1439.

[58] R. Proctor, L. D. James, R. Proctor, and I. D. James, *A fine-resolution 3d model of the southern north sea*, Journal of Marine Systems **8** (1996), no. 3-4, 285.

[59] Hannes Rennau, Stefan Schimmels, and Hans Burchard, *On the effect of structure-induced resistance and mixing on inflows into the baltic sea: A numerical model study*, pp. 53–68.

[60] T. P. Rippeth, N. R. Fisher, and J. H. Simpson, *The cycle of turbulent dissipation in the presence of tidal straining*, Journal of Physical Oceanography **31** (2001), no. 8, 2458–2471 (English).

[61] Wolfgang Rodi, *Turbulence models and their application in hydraulics*, CRC Press, 1993.

[62] David P. Roy, MA Wulder, TR Loveland, CE Woodcock, RG Allen, MC Anderson, D. Helder, JR Irons, DM Johnson, and R. Kennedy, *Landsat-8: Science and product vision for terrestrial global change research*, Remote Sensing of Environment **145** (2014), 154–172.

[63] Pierre-Elouan Rthor, *Wind turbine wake in atmospheric turbulence, Ph.d thesis*, (2009).

[64] Jonathan Sharples and John H. Simpson, *Semi-diurnal and longer period stability cycles in the Liverpool Bay region of freshwater influence*, Continental Shelf Research **15** (1995), no. 2, 295–313.

[65] JH Simpson, E. Williams, LH Brasseur, and JM Brubaker, *The impact of tidal straining on the cycle of turbulence in a partially stratified estuary*, Continental Shelf Research **25** (2005), no. 1, 51–64.

[66] John H. Simpson, Wim G. Bos, Florian Schirmer, Alejandro J. Souza, Thomas P. Rippeth, Sarah E. Jones, and David Hydes, *Periodic stratification in the Rhine ROFI in the north sea*, Oceanologica Acta **16** (1993), no. 1, 23–32.

[67] John H. Simpson, Juan Brown, John Matthews, and Graham Allen, *Tidal straining, density currents, and stirring in the control of estuarine stratification*, Estuaries **13** (1990), no. 2, 125–132.

[68] Timothy Stovall, Gary Pawlas, and PJ Moriarty, *Wind farm wake simulations in OpenFOAM*, AIAA Paper **825** (2010), 2010.

[69] G. Sutherland, M. Foreman, C. Garrett, G. Sutherland, M. Foreman, and C. Garrett, *Tidal current energy assessment for Johnstone Strait, Vancouver Island*, Proceedings of the Institution of Mechanical Engineers Part A Journal of Power and Energy **221** (2007), no. 2, 147.

[70] Graig Sutherland, Chris Garrett, Mike Foreman, Graig Sutherland, Chris Garrett, Mike Foreman, Graig GS Sutherland, Chris CG Garrett, Mike MF Foreman, Graig Sutherland, Chris Garrett, and Mike Foreman, *Tidal resonance in Juan de Fuca Strait and the Strait of Georgia*, Journal of Physical Oceanography **35** (2005), no. 7, 1279.

[71] David Toke, *The UK offshore wind power programme: A sea-change in UK energy policy?*, Energy Policy **39** (2011), no. 2, 526–534.

[72] Lars Umlauf and Hans Burchard, *Second-order turbulence closure models for geophysical boundary layers. a review of recent work*, Continental Shelf Research **25** (2005), 795–827.

[73] Johan van der Molen, Helen C. M. Smith, Paul Lepper, Sian Limpenny, and Jon Rees, *Predicting the large-scale consequences of offshore wind turbine array development on a North Sea ecosystem*, Continental Shelf Research **85** (2014), 60–72.

[74] Quinten Vanhellemont and Kevin Ruddick, *Turbid wakes associated with offshore wind turbines observed with Landsat 8*, Remote Sensing of Environment **145** (2014), 105–115.

[75] Frank Mangrem White, *Fluid mechanics*, New York, NY : McGraw-Hill, 2011; 7th ed, 2011.

[76] Cort J. Willmott, *On the validation of models*, Physical geography **2** (1981), no. 2, 184–194.

[77] www.bbc.co.uk, *History, james watt*, 2014, accessed 2015.

[78] www.dongenergy.com, *Anholt wind farm, demark, tech. report*, 2012.

[79] www.floodmodeler.com, 2016, accessed 2016.

[80] www.fvcom.smast.umassd.edu, *The unstructured grid finite volume community ocean model (FVCOM)*, 2013, accessed 2016.

[81] www.mikepoweredbydhi.com, *Mike modelling systems*, 2016, accessed 2016.

[82] Z. Yang and T. Wang, *Assessment of tidal energy removal impacts on physical systems: Development of MHK module and analysis of effects on hydrodynamics*, Tech. Report PNNL-20804, US Department of Energy, 2011.

[83] Zhaoqing Yang, Taiping Wang, and Andrea E. Copping, *Modeling tidal stream energy extraction and its effects on transport processes in a tidal channel and bay system using a three-dimensional coastal ocean model*, Renewable Energy **50** (2013), 605–613.